Respiratory chain deficiency alters cellular proteostasis and triggers Alzheimer's disease-like tau alterations

By

Ian Walter Weidling

Submitted to the graduate degree program in Neuroscience and the Graduate Faculty of the University of Kansas in partial fulfillment of the requirements for the degree of Doctor of Philosophy.

_____

Co-Chair: Russell Swerdlow, MD

_____

Co-Chair: Douglas E. Wright, PhD

_____

Hao Zhu, PhD

_____

Wen-Xing Ding, PhD

_____

T. Christopher Gamblin, PhD

Date Defended: 6 December 2019

The dissertation committee for Ian Walter Weidling certifies that this is the approved version of the following dissertation:

Respiratory chain deficiency alters cellular proteostasis and triggers Alzheimer's disease-like tau alterations

Co-Chair: Russell Swerdlow, MD

Co-Chair: Douglas E. Wright, PhD

Date Approved: 6 December 2019

Abstract

Sporadic Alzheimer's disease (AD) is defined clinically as a progressive brain disorder resulting in memory loss and, eventually, an inability to perform simple tasks. Pathologically, AD brains accumulate insoluble protein aggregates known as neurofibrillary tangles (NFTs) and amyloid plaques. Definitive diagnosis of AD requires the presence of NFTs and amyloid plaques. Furthermore, variants in genes coding for amyloid associate with early onset forms of the disease. For these reasons and more, removing amyloid plaques from sporadic AD patient brains has been the field's major therapeutic target for decades. Unfortunately, clinical trials focused on treating AD through amyloid reduction continue to fail. The current standard of care for AD typically extends patient lifespan for months rather than years. The field needs new therapeutic targets and rescuing brain energy production represents a reasonable strategy.

Reduced glucose utilization occurs early in AD brains and correlates fairly well with disease progression. Widespread mitochondrial dysfunction accompanies decreased glucose consumption. AD mitochondria display changes in number, ultrastructure, and enzyme activity. The evidence for mitochondrial dysfunction in AD is clear, however, the notion that defective mitochondria could initiate pathological cascades remains controversial. Thus, therapies aimed at mitochondrial function have been slow to reach clinical trials. The following studies examine the relationship between mitochondrial defects and AD pathology and provide evidence that mitochondrial dysfunction leads to AD-relevant retrograde responses.

Retrograde responses maintain cellular homeostasis by adapting nuclear gene expression and cytosolic signaling pathways to changes in mitochondrial function. AD mitochondrial dysfunction likely initiates numerous retrograde responses, yet few studies examine defective mitochondria's influence on AD pathology. Here, we provide evidence that reduced

mitochondrial respiratory flux leads to AD-like tau alterations, including changes in splicing, conformation and oligomerization. Alzheimer's disease cybrids recapitulate disease relevant tau alterations. Further experiments suggest mitochondrial function affects cellular proteostasis pathways including the mitochondrial unfolded protein response (mtUPR), integrated stress response (ISR), autophagy/mitophagy, and proteasome function. Although initial studies in *C. elegans* and rat hepatoma cells established a link between mtDNA depletion and mtUPR activation, we find mammalian cells downregulate the mtUPR upon mtDNA depletion. Instead, mtDNA depleted human cells activate the ISR, a pathway which alters cellular metabolism and halts general protein translation to preserve proteostasis during stress.

Finally, we examine how mtDNA depletion affects cytochrome oxidase (COX) and complex I activity. AD tissue displays decreased COX activity, while complex I activity does not change. The reason for specific reductions in COX activity remain unclear. We found COX activity decreases proportionally to declines in mtDNA levels. Whether complex I activity follows the same pattern will give insight into potential mechanisms for reduced COX activity in AD.

Acknowledgments

First and foremost, I would like to thank Dr. Russell Swerdlow and my committee members, Dr. Doug Wright, Dr. Hao Zhu, Dr. Wen-Xing Ding, and Dr. Chris Gamblin. Any successes that I had during my time at University of Kansas Medical Center are due to this group of mentors. Dr. Swerdlow was kind enough to take me in for the second half of my final IGPBS rotation when the original lab I was rotating through was not working out. Since then, he has been a fantastic mentor, always guiding me in the proper direction while giving me the freedom to make mistakes and learn from them. I will always be grateful for the chance I had to work in Dr. Swerdlow's lab and learn from him. It is easy to see that he truly cares about and values his students. Dr. Zhu gave me my first chance by hiring me as a research assistant at KUMC. My time in his laboratory was as good an introduction to research as I could have hoped for. Dr. Zhu continues to be a positive influence on my career and is always willing to help me with anything I need. Dr. Wright has been great as the neuroscience program director, cultivating a positive environment which people want to be a part of. He always helped me stay on track and I am grateful for his guidance. Dr. Ding's expertise and willingness to help have greatly assisted my progression. I really enjoyed the time I got to spend in his lab and learned a lot in a short time. I owe Dr. Gamblin a large debt for the help he provided in my studies. He shared valuable reagents with me time and again which helped me immensely. Beyond reagents, he was always willing to answer my questions and provide valuable feedback on my research. I also want to thank him for driving to Kansas City from Lawrence for every committee meeting. Thank you all for the guidance you gave me during my time here. Also, thank you to Dr. Nicholas Kanaan and Dr. Christopher Gamblin for their kind antibody gifts. TOC1 antibody was a gift from Nicholas Kanaan at Michigan State University (originally created by Lester Binder at Northwestern

University). Tau12 antibody was a gift from Christopher Gamblin at the University of Kansas (originally created by Lester Binder at Northwestern University). Thanks to the Library of Science and Medical Illustrations for illustrations that were incorporated into the figures. Free access to the Library of Science and Medical Illustrations can be found at http://www.somersault1824.com/science-illustrations/.

I also want to thank all the Swerdlow lab members who helped me constantly and made the lab enjoyable. I am very grateful to Madison and Lila Self, for the funding and skills development they generously provided me. They had a clear vision for the legacy they wanted to leave and I am extremely fortunate to have benefited from their kindness. Finally, I want to thank my wife, Perry, and my family for their constant support. I never could have done this without them.

Table of Contents

List of Figures

List of Tables

Chapter 1: Introduction

This chapter has previously been published as an open access article and is reprinted here with adaptations from Weidling, Ian, and Russell H. Swerdlow. "Mitochondrial dysfunction and stress responses in Alzheimer's disease." Biology 8.2 (2019): 39. https://www.mdpi.com/460770

AD Diagnosis and Biomarkers

Alzheimer's disease (AD) accounts for ~80% of all cases of dementia, making AD the most common form of dementia. The AD death rate in the United States continues to rise, while the percentage of deaths due to strokes and heart disease decline. Current AD treatments improve cognitive ability but do not slow the rate of cognitive decline [1]. Clinically, AD is defined by cognitive impairment interfering with a person's ability to work or complete daily activities. Definitive AD diagnosis requires post-mortem brain analysis and the discovery of amyloid plaques and neurofibrillary tangles (NFTs). AD biomarkers exist, however, clinicians rarely utilize these diagnostically. Decreased cerebrospinal fluid (CSF) Aβ42 levels and positive positron emission tomography (PET) amyloid scans correlate with brain amyloid deposition. Biomarkers of neuronal degeneration include increased total and phosphorylated CSF tau, decreased 18-fluorodeoxglucose uptake in temporo-parietal cortex, and brain atrophy in the temporal lobe and medial parietal cortex [2].

While all of these biomarkers display fairly strong specificity for differentiating non-demented from demented patients, some possess superior AD specificity. Increasing CSF tau phosphorylated at threonine 181 displays strong AD specificity, whereas increasing CSF total tau occurs in numerous forms of dementia. Decreased CSF Aβ42 also fails to discriminate between AD and other forms of dementia, however, lower CSF Aβ42 appears earlier in disease progression than increases in CSF phosphorylated and total tau. This makes CSF Aβ42 attractive for early disease detection and intervention. Currently, some clinical trials utilize CSF Aβ42 levels to sort participants into non demented and AD groups [3]. Unfortunately, early AD detection means little to the average patient if the current standard of care does not improve drastically.

Current AD Treatments

Current AD treatments achieve modest cognitive improvements but fail to slow disease progression. Treatment regimens usually begin with one of three approved acetylcholinesterase inhibitors. If symptoms continue to worsen despite treatment, then patients may be switched to another cholinesterase inhibitor or the N-methyl-D-aspartate receptor antagonist, memantine, may be prescribed concurrently [4]. Although rarely prescribed, the Food and Drug Administration (FDA) approved a medium chain triglyceride (MCT) formulation named Axona® as a medical food treatment for AD. Clinical trials suggest MCTs can improve cognition in AD patients lacking an apolipoprotein E4 (ApoE) allele [5]. Reduced brain glucose utilization occurs early in AD and MCTs provide alternative energy sources to the brain in the form of ketone bodies. A recent study supports this idea, showing MCT supplements increase brain ketone consumption in AD patients without inhibiting glucose uptake. Furthermore, AD patient brains showed the same ability to utilize ketone bodies as healthy young adults [6]. Unfortunately, clinicians usually do not know a patient's ApoE status, making it hard to prescribe MCTs in typical settings [5].

A number of promising therapeutic targets have come and gone, yielding very little return. Numerous case reports and small studies suggest statins, the low density lipoprotein (LDL)-cholesterol lowering drugs, can reduce Alzheimer's disease risk. Interest in the link between statins and AD increased when multiple epidemiological studies reported decreased dementia risk in statin users [7, 8]. Further studies found similar decreases in AD rates among statin users. Statins quickly became viewed as a promising therapy to slow AD progression. However, comprehensive studies with large data sets show no difference in dementia rates with statin use and no delay of AD progression. Furthermore, statin use has been associated with

reversible cognitive decline. Numerous studies refute this idea at the population level but case reports describing altered cognition with statin use persist, suggesting some portion of the population may be sensitive [9]. Currently, there is not sufficient evidence to suggest statins can decrease AD risk.

Similar to statins, several epidemiological studies suggest an association between using NSAIDs and reduced AD risk. This idea fit well with theories on AD pathogenesis suggesting brain inflammation contributes to disease progression. Multiple meta-analyses of observational studies suggest NSAID usage may reduce AD risk by nearly 20% [10, 11]. Activated microglia and numerous other inflammatory markers associate with AD pathology. Furthermore, studies in transgenic AD models showed reductions in AD pathology with NSAID treatment [12]. However, a recent meta-analysis study found no significant difference in AD risk between NSAID users and non-users. The use of non-aspirin NSAIDs displayed a trend toward significance in terms of AD risk reduction [13]. Clinical trials investigating NSAIDs as a treatment for AD have failed to show positive effects for NSAID usage in patients with mild cognitive impairment (MCI) or AD and have been plagued by high drop-out rates suggesting AD patients may not tolerate NSAID usage well. The ADAPT trial gave patients naproxen, celecoxib, or placebo and was planned to last seven years. The study was stopped early (most participants underwent 2 years of treatment) but the results suggest NSAID usage in AD patients actually increases cognitive decline while NSAID usage prior to disease onset may reduce risk. Other clinical trials also suggest NSAID usage in AD patients accelerates disease progression [14]. Clearly, treating AD with NSAIDs does not appear to be a viable approach and, again, a once-promising solution to AD has fallen flat.

The Amyloid Cascade Hypothesis of Sporadic AD

While statins and NSAIDs had their moments as potential AD treatments, most therapeutic interventions have targeted the signature AD pathology, amyloid plaques. For many reasons, amyloid plaques have long been the preferred causative agent in AD. This view gained steam following a 1992 article outlining the amyloid cascade hypothesis of sporadic AD. The amyloid cascade hypothesis proposes amyloid beta (Aβ), the main constituent of AD's extraneuronal plaques, initiates the disease process and precipitates subsequent phenomena including neurofibrillary tangles, cell loss, vascular damage, and dementia. To support this notion, the authors point to high rates of AD in Down syndrome, as chromosome 21 contains the amyloid precursor protein (APP) gene. The authors of the amyloid cascade hypothesis speculate that increased amyloid production occurs from the additional APP gene, causing AD [15].

Genetic data also seems to support the amyloid cascade hypothesis. Just prior to the advent of the amyloid cascade hypothesis, genetic studies identified three APP mutations as causative variants in familial AD cases [16, 17]. Genetic studies also discovered causative AD mutations in the presenilin 1 gene, which encodes a subunit of gamma secretase. Gamma secretase, an intramembrane protease, cleaves multiple targets including APP. The association between presenilin 1 and APP furthered the argument that amyloid causes sporadic AD [18]. Follow up studies showed increased plasma Aβ in patients harboring presenilin mutations. These findings were taken as further proof of Aβ's primary role in AD [19]. Although extraordinarily rare, the field viewed disease-causing APP mutations as a major piece of evidence supporting amyloid's toxicity.

The authors of the amyloid cascade hypothesis believed Aβ to be the primary toxin responsible for AD, and the final pieces of evidence supporting their hypothesis came from

studies in cultured neurons treated with amyloid beta fragments and animal models of amyloidosis. Initial studies suggested neuronal cultures exposed to high concentrations of amyloid beta fragments experience toxicity. *In vivo* experiments showed amyloid deposition in rat cortex causes cell loss and AD-relevant tau alterations [20, 21]. The amyloid cascade hypothesis fails to note, however, findings from cell culture studies suggesting amyloid fragments exert neurotrophic effects on undifferentiated hippocampal neurons [20]. Furthermore, some studies suggest amyloid beta is not inherently toxic, although these studies show that Aβ sensitizes cultured neurons to excitotoxic damage [22, 23]. Another study noted no toxicity upon monomeric Aβ treatment, instead describing neurite promotion. This study did observe neuronal toxicity following treatment with aggregated Aβ [24]. Aβ's inherent toxicity remains open to debate, especially given the results of recent clinical trials centered on removing amyloid plaques.

AD Clinical Trials

The continued failures in AD clinical trials raise many questions. Current trials focus on a variety of therapeutic targets from neuroplasticity modulators or growth factors to oxidative stress, metabolism and inflammation. Amyloid-centric therapies continue to dominate the landscape, though. The most common treatment strategy involves anti-amyloid antibodies intended to reduce brain amyloid burden. Another popular strategy focuses on inhibiting gamma secretase activity [25]. While amyloid antibodies and gamma secretase inhibitors produce favorable results in transgenic animals with plaque and tangle pathology, positive results in clinical trials remain elusive. Trials of semagacestat, a gamma secretase inhibitor, found decreased cognitive performance, leading to a cancellation of the study. Attempts to immunize

patients with human Aβ aggregates had no effect on cognition and led to autoimmune encephalopathy in some participants. Early amyloid based clinical trial failures did little to slow future amyloid therapies from advancing to clinical trials.

Following these disappointments, numerous studies attempted to explain the failures. Close examination uncovered numerous defects, including issues in pharmacokinetics, dosing and outcome measures, leading many to contend the issue lay with study design and execution rather than flaws inherent to the amyloid cascade hypothesis [26]. Recently, additional amyloid based clinical trials have concluded with disappointing results. As of 2018, six amyloid targeted therapeutics had reached phase III clinical trials and all failed to meet their primary endpoints. Aducanumab is the latest therapy to stall in phase III trials. This anti-amyloid monoclonal antibody reduced amyloid fibrils in patients with prodromal and mild AD during phase I trials and, initially, demonstrated a beneficial effect on cognition between 6 and 12 months among a small sample size [27]. After reaching phase III trials, however, Biogen halted the aducanumab trial, citing insufficient evidence of the drug's efficacy in treating AD [28]. BAN2401 – an anti-oligomeric Aβ monoclonal antibody- showed promise at its highest dose in phase II clinical trials. The results may have been skewed, unfortunately, by the necessary removal of ApoE4 carriers from the high dose group. The possibility of brain swelling excluded ApoE4 carrier participation. However, preferentially removing ApoE4 carriers from the treatment group could artificially decrease the group's cognitive decline in the absence of beneficial drug effects. Other concerns have arisen around this study regarding the statistical analyses employed [27]. The drug currently remains in phase III trials. Some hope remains that anti-amyloid therapies will find success in clinical trials.

Brain hypometabolism in AD

Amyloid levels correlate fairly poorly with cognitive decline. Furthermore, many cognitively intact brains possess amyloid plaque burdens on par with those in AD brains. Amyloid cascade hypothesis proponents explain this apparent paradox by hypothesizing that cognitively intact brains containing high amyloid burden represent patients in the prodromal phase of AD. Indeed, amyloid plaques typically appear long before clinical symptoms. Amyloid cascade hypothesis detractors argue against amyloid's primary role in AD by pointing to this delay between amyloid plaque deposition and subsequent cognitive decline [29, 30]. Furthermore, meta-analysis of triple transgenic (3xTg-AD) mouse studies shows a weak, but significant, relationship between high Aβ load and Morris water maze and novel object recognition performance. The analysis suggests a stronger relationship between increased phosphorylated tau levels and cognitive decline in AD mouse models [31]. Generally, brain tau accumulation correlates better with cognitive decline than amyloid load [32]. Studies in aged rhesus monkeys found no correlation between plaque levels and cognition [33]. As referenced earlier, other AD biomarkers exist.

Synaptic loss and brain atrophy display the strongest correlation with cognitive decline in AD [34]. In fact, brain volume measurements may predict disease progression and differentiate potential AD subtypes [35]. Brain glucose utilization also correlates with cognitive decline. MCI and AD patients display regional hypometabolism via (18F)-2-fluoro-deoxy-D-glucose positron emission tomography (FDG-PET). Early studies describe reduced temporo-parietal glucose uptake as an AD hallmark [36]. FDG-PET combined with magnetic resonance imaging provides superior anatomical resolution. A study utilizing these techniques found severe metabolic defects throughout the limbic system in MCI and AD groups. The AD group displayed additional

metabolic deficiency in the amygdala, tempoparietal cortex, and frontal cortex [37]. Longitudinal FDG PET studies, which confirm AD diagnoses post-mortem, uncovered additional AD specific changes in brain metabolism [38].

Evidence suggests brain hypometabolism may be useful in early AD detection and diagnosis, as well as differential dementia diagnoses [39, 40]. Further studies have attempted to use FDG-PET to predict disease progression. A recent systematic review, however, determined current FDG-PET studies have not achieved high enough accuracy to predict conversion from MCI to AD. FDG PET studies utilizing computer aided visual read metrics seem to show improved accuracy and consistency in predicting disease progression [41]. Regardless, brain hypometabolism occurs early in AD and worsens as the disease progresses. Brain hypometabolism often occurs in regions devoid of AD pathology, indicating tau tangles and plaques need not be present for reduced glucose utilization to happen [42]. These findings led many to wonder whether metabolic disturbances play a primary role in AD.

Systemic metabolic defects in AD

Metabolic defects occur systemically and in the brain during AD. Metabolic disorders including diabetes, hypertension and hypercholesterolemia correlate with AD [43, 44]. Furthermore, obesity during middle age increases AD risk three times, while being overweight increases AD risk two times [45]. Insulin receptor levels increase in the AD brain compared to age-matched controls, which may represent a compensatory response to the decreased glucose uptake observed via FDG-PET [46]. AD treatments targeting insulin pathways may be viable based on these findings [47]. Brain derived neurotrophic factor (BDNF), an important regulator of neuronal development, survival, and metabolism, is altered in the AD brain [48]. Evidence

suggests BDNF deficiency can cause metabolic impairments [49]. AD brains also display reduced glucose transporter levels, even after correcting for neuronal loss. The decrease in glucose transporters is thought to contribute to AD brain hypometabolism [50]. The alterations in glucose uptake and insulin signaling in AD suggest broad metabolic deficiencies occur in AD.

Metabolomics studies provide more specific information regarding AD metabolic deficiencies. AD metabolomics studies have identified metabolic signatures of neurodegeneration, although differences in the tissues examined and the disease cohorts make direct comparisons across studies difficult. Studies utilizing nuclear magnetic resonance spectroscopy to assay metabolites consistently associate reduced *N*-acetylaspartate (NAA) with neurodegeneration [51]. NAA's biological function in the brain is not well described, although it is interesting to note that neuronal mitochondria synthesize NAA [52]. NAA may contribute to lipid conversion to myelin, aspartate storage, or osmoregulation, although these roles remain speculative [53]. NAA levels decrease in the AD brain, although NAA reduction does not differentiate AD from other neurodegenerative diseases. AD brains also display increases in *myo*-inositol (mI). Little is known about the biological importance of mI changes. NMR and magnetic resonance spectroscopy studies provide some evidence to support their use in differentiating AD from MCI and possibly in predicting conversion from MCI to AD [54, 55]. Measuring metabolite levels through MRS or brain volume through MRI may provide important information during clinical trials regarding drug efficacy [56]. Additional techniques monitoring AD metabolite levels provide more information.

Liquid chromatography (LC) can be used for targeted metabolomics studies. LC-electrochemistry array metabolomics platform (LCECA), a variant of LC, has been used to interrogate neurotransmitter pathways and oxidative stress in AD CSF, discovering decreased

serotonin in AD CSF [57]. A study utilizing LCECA to analyze post-mortem ventricular CSF found decreased norepinephrine levels [58]. Combining metabolomics techniques ca provide further power and a study using this strategy found that coincident decreases in uridine and increases in cysteine best differentiated between AD and control subjects [59, 60]. A recent study performed metabolomics on AD brain and blood tissue to identify systemic disease correlates. Their analyses showed a consistent correlation between sphingolipids and AD progression and severity [61]. Ceramide accumulates in AD brains, providing another example of sphingolipid changes in AD. Ceramide accumulation can stimulate apoptosis, making this a potentially disease relevant alteration [62]. Lipid changes in AD blood or CSF may serve as biomarkers [63]. Extensive evidence of AD metabolic dysfunction exists but the underlying causes remain unclear.

Cytochrome Oxidase Defects in AD

Systemic mitochondrial defects occur in AD, likely contributing to metabolic dysfunction. The enzymes of the mitochondrial electron transport chain (ETC) allow cells to convert cellular energy into adenosine triphosphate (ATP). However, mitochondria perform many crucial tasks beyond ATP production. Mitochondrial function contributes to diverse cellular processes including apoptosis, cell growth and division, calcium storage and lipid metabolism [64]. Deficient mitochondrial function is associated with numerous diseases [65]. In fact, mitochondrial dysfunction directly causes multiple diseases, known as primary mitochondrial disorders [66]. Primary mitochondrial disorders preferentially affect the brain and heart, organs known for having high energy demands. Based on these observations, the brain and heart are thought to have a lower threshold for tolerating mitochondrial dysfunction relative to

other tissues [67]. Therefore, the systemic mitochondrial defects observed in AD may manifest in cognitive impairment prior to the deterioration of other organs.

Changes in mitochondrial enzyme activity occur in AD. Reduced cytochrome oxidase (COX) activity has consistently been observed across numerous tissues. Initial studies describe decreased COX activity in AD patient brains and platelets. The discovery of COX deficiency in non-degenerating tissues such as platelets suggests mitochondrial dysfunction occurs independently of neurodegenerative processes. The study also examined other ETC enzyme activities in AD platelets, finding no change in their function. Therefore, this study established two important points: 1) systemic COX defects occur in AD and 2) COX defects do not reflect a general electron transport chain failure. The authors speculated at the time of publication that mitochondrial DNA (mtDNA) may contribute to COX deficiency [68]. Further studies purifying COX from AD and control brains observed anomalous kinetic behavior in AD COX enzyme. The altered enzyme kinetics were thought to stem from structural abnormalities and the authors proposed this contributes to AD bioenergetics defects [69]. Another study discovered similar AD COX deficiencies absent changes in mitochondrial complex I and II-III activities [70]. The cause of AD COX defects remains unknown, however, studies utilizing cytoplasmic hybrids (cybrids) furthered our understanding of this phenomena.

Cybrids provide insight into the cellular effects of mtDNA mutations. Generating cybrids involves repopulating mtDNA depleted cells (ρ0) with exogenous mtDNA, often from patient platelets. Thus, it is possible to generate cybrid lines containing mtDNA from AD and age-matched control subjects. AD cybrids effectively model AD mitochondrial function on a stable nuclear background. As referenced earlier, Parker et al. hypothesized that mtDNA likely contributed to the AD COX defect. Cybrids provided an elegant model to test this hypothesis

and, indeed, AD cybrids recapitulate the COX defect. Later studies discovered decreased mitochondrial oxygen consumption between control cybrids and grouped MCI and AD cybrids. AD and MCI cybrids also have decreased NAD+/NADH and increased ADP/ATP ratios [71]. This is strong evidence that mtDNA contributes to AD mitochondrial dysfunction [72, 73].

AD brains display additional COX abnormalities. Post-mortem analysis of AD brain tissue reveals decreases in COX subunits with disease progression. COX levels have been analyzed in AD brain regions which are relatively preserved compared to healthy controls. AD cerebellar Purkinje neurons were found to have reduced COXIV and COXII subunit levels. Furthermore, aged control subjects displayed decreased COX protein relative to young control subjects. These findings suggest that COX levels decline with age and increased rates of COX decline contribute to AD [74]. COX levels have also been examined in the AD hippocampus. Interestingly, the AD hippocampus contains increased numbers of “COX deficient” neurons. A study using immunohistochemistry concurrently labeled COX and mitochondrial complex II. In order to qualify as COX deficient, neurons needed to lack COX staining while maintaining complex II levels. COX deficient neurons, therefore, selectively deplete COX subunits. This suggests mitochondrial mass is maintained [75]. Later studies attempted to find a correlation between COX deficiency and AD pathology. The study suggested a correlation between COX deficiency and decreased tau tangles, while finding no relationship between amyloid and COX levels [76]. The reason for AD’s COX specific defects remains unclear. Answering this question may provide great insight into the nature of AD’s origin.

AD Mitochondrial Defects

Beyond COX defects, AD mitochondria undergo numerous changes. Mitochondrial morphology becomes disrupted during the disease process. Mitochondrial surface area decreases, while cristae structure is altered and increased variability in mitochondrial shape occurs [77]. Some of these changes may be precipitated through changes in the mitochondrial fission and fusion machinery. In fact, alterations in fission and fusion occur early in AD. One study found changes in fusion and fission proteins along with defective mitochondrial localization in AD neurons. Furthermore, the authors found that recapitulating AD relevant fission/fusion protein alterations in neuronal cultures led to similar changes in mitochondrial localization [78]. Three-dimensional electron microscopy (3D EM) studies found a novel mitochondrial morphology in AD brains. This new morphological feature resembled beads on a string, leading to the term "mitochondria on a string" (MOAS). The authors propose MOAS formation occurs in response to AD bioenergetic stress. MOAS formation may inhibit mitophagy, thereby preserving a low level of mitochondrial function under extreme stress. The findings suggest MOAS result from arrest of mitochondrial fission. Previous EM studies could not detect this feature, likely categorizing MOAS as fragmented mitochondria [79]. Changes in mitochondrial morphology provide further evidence of mitochondrial dysfunction in AD.

Lysosomal alterations may also contribute to AD mitochondrial defects. AD neurons attempt to increase lysosomal proteins early in disease progression, specifically upregulating cathepsin D mRNA and protein levels with concomitant increases in lysosomal structures [80]. Dystrophic AD neurons experience disrupted axonal and dendritic autophagy, precipitating in the accumulation of partially digested cellular components [81]. Along these lines, AD neurons often possess increased COX and mtDNA levels despite morphometric analyses showing reduced

mitochondrial mass. Rather than signaling an increase in functional mitochondria, therefore, increased COX and mtDNA may stem from deficient mitochondrial degradation. In AD neurons containing increased mitochondrial components, said components tend to colocalize with lysosomal structures [82]. Mitophagy impairment also occurs in the AD brain. A recent study found reductions in numerous elements of the mitophagy program in AD hippocampus, in induced pluripotent stem cell-derived human AD neurons, and in AD animal models. The authors conclude that impaired mitophagy may contribute to AD and enhancing mitochondrial clearance may prove therapeutically useful [83]. Mitochondrial function declines during AD, but whether these deficits contribute to or result from disease progression remains unclear.

The root cause for AD mitochondrial dysfunction remains controversial. Initially, researchers assumed mitochondrial defects represented a consequence of neuronal degeneration. Strong evidence, outlined above, argues against this assumption. Namely, the presence of mitochondrial dysfunction in non-degenerating tissues and the ability of AD mtDNA to recapitulate mitochondrial dysfunction in cancer cells refutes the hypothesis that mitochondrial issues occur secondary to neurodegenerative processes. However, many groups propose AD pathology, including amyloid β and NFTs, trigger mitochondrial failures [84, 85]. Others view mtDNA as the primary cause for AD bioenergetic defects. Numerous lines of evidence suggest mtDNA plays an important role in AD pathogenesis.

Role of Mitochondrial DNA in AD

mtDNA inheritance and the accumulation of somatic mtDNA mutations influence mitochondrial function. However, mtDNA's interaction with the nuclear genome complicates interpretations of the mitochondrial genome's cellular effects. Regardless, studies implicate

somatic mtDNA mutations in aging and AD progression. The “common deletion”, a 4997 base pair deletion, increases in the brain during normal aging. Brain areas with the highest metabolic activity display the heaviest common deletion burden. Groups speculate that somatic mtDNA deletions increase the risk of neurodegeneration [86]. As referenced earlier, AD brains accumulate COX-deficient neurons. Further studies on AD COX-deficient neurons found an association between COX deficiency and increased mtDNA deletions associated with aging [87]. This suggests that mtDNA deletions may contribute to AD bioenergetic defects. Early AD brains display increased common deletion burden compared to age-matched controls. Around age 75, though, common deletion rates decline in the AD brain. This is in contrast to age-matched control brains, which accumulate the common deletion at a greater rate beyond age 75 [88, 89].

Oxidative damage often associates with mitochondrial dysfunction and may contribute to mtDNA damage. Levels of oxidative damage increase in the AD brain, especially in the parietal lobe. A study found three-fold increases in oxidized nucleoside levels among AD mtDNA, while AD nuclear DNA displayed a small increase in oxidative damage. This established that mtDNA experiences increased oxidative damage in AD and suggests mtDNA is more prone to damage by this mechanism than nuclear DNA. It is interesting to note that the region displaying the most mtDNA oxidative damage, the parietal lobe, also exhibits early reductions in glucose consumption during AD. This suggests a possible relationship between mitochondrial dysfunction and brain hypometabolism [90]. Based on these findings, researchers hypothesized that AD oxidative damage leads to mtDNA mutations. In line with this hypothesis, mtDNA control region mutations accumulate at a greater rate in the AD brain. Mutations in this mtDNA region correlate with disrupted transcription and replication. Furthermore, AD brains had around a 50% reduction in the mtDNA/nuclear DNA ratio. Control region mutations may contribute to

AD mitochondrial dysfunction [91]. More recent studies, utilizing next generation sequencing, discovered increased somatic mtDNA mutations in the AD hippocampus. This study examined mutation burden in early stage AD patients and used techniques to determine the likely cause for mutations. The authors found evidence that AD mtDNA mutations largely stem from replication errors rather than oxidative damage [92].

mtDNA inheritance also influences AD risk. Numerous studies suggest AD follows a maternal inheritance pattern [93]. However, some groups suggest that AD's apparent preference toward maternal transmission is merely an artifact stemming from women's superior longevity [94]. Other studies show a maternal AD history also associates with brain hypometabolism, and suggest this could contribute to increased AD risk. Patients with a maternal AD history experience progressive brain hypometabolism in the same brain regions as AD patients [95]. This indicates that maternal genes may provide a link between brain bioenergetics and AD risk. Although the maternal genes that mediate this susceptibility to bioenergetics defects and possibly AD remain unknown, it is interesting to note that mtDNA is largely inherited from the mother. These findings support the idea that mtDNA influences AD risk.

Further studies in AD cybrids also suggest mtDNA contributes to AD pathogenesis. As mentioned earlier, AD cybrids display reduced COX activity, while maintaining activity of other respiratory chain complexes [72]. Beyond COX deficiency, AD cybrids produce more reactive oxygen species (ROS), have swollen mitochondria with reduced membrane potential, and recapitulate AD-like pathological alterations [73, 96]. AD cybrids have elevated intracellular Aβ and secrete Aβ into the media at a greater rate. Concomitantly, AD cybrids increase caspase-3 activity and cytochrome c release. These apoptotic responses may facilitate Aβ accumulation in AD cybrids [97]. Aβ treatment in AD cybrids caused greater apoptotic responses compared to

age-matched control cybrids [98]. Numerous lines of evidence suggest mtDNA contributes to AD, leading some to hypothesize mtDNA alterations play a primary role in AD.

The Mitochondrial Cascade Hypothesis of Sporadic AD

The amyloid cascade hypothesis has guided the AD field since its publication in 1992. Alternative hypotheses of sporadic AD's etiology have been posited. The mitochondrial cascade hypothesis of sporadic AD challenges the notion that AD neuropathology, namely amyloid plaques and tau tangles, causes cognitive decline. Instead, the mitochondrial cascade hypothesis argues AD neuropathology occurs secondary to mitochondrial dysfunction [99]. This view of AD does not attempt to discount the detrimental effects of aggregating proteins completely. Under this paradigm, AD neuropathology represents a downstream consequence of failing energy production but is still viewed as a contributor to disease progression and an important AD biomarker.

The mitochondrial cascade hypothesis proposes that an individual's mtDNA and nuclear DNA inheritance determine their baseline mitochondrial function and durability. As the individual ages, their mitochondrial dysfunction declines due to somatic mtDNA mutations and deletions. Compensatory responses maintain adequate mitochondrial function in the face of normal declines in mitochondrial energy production. At some point, mitochondrial function declines to an extent that exceeds compensation and disease processes ensue. This theory posits that insoluble protein aggregates accumulate in response to changing mitochondrial function [100].

Threshold effects are an important concept at the core of the mitochondrial cascade hypothesis. Each organ likely possesses its own threshold for tolerating mitochondrial dysfunction, beyond which normal function becomes impaired. The brain requires high levels of

energy production relative to other organs, making it particularly susceptible to bioenergetic lesions [67, 101]. This could explain why mitochondrial dysfunction presents systemically in AD, yet preferentially affects cognition.

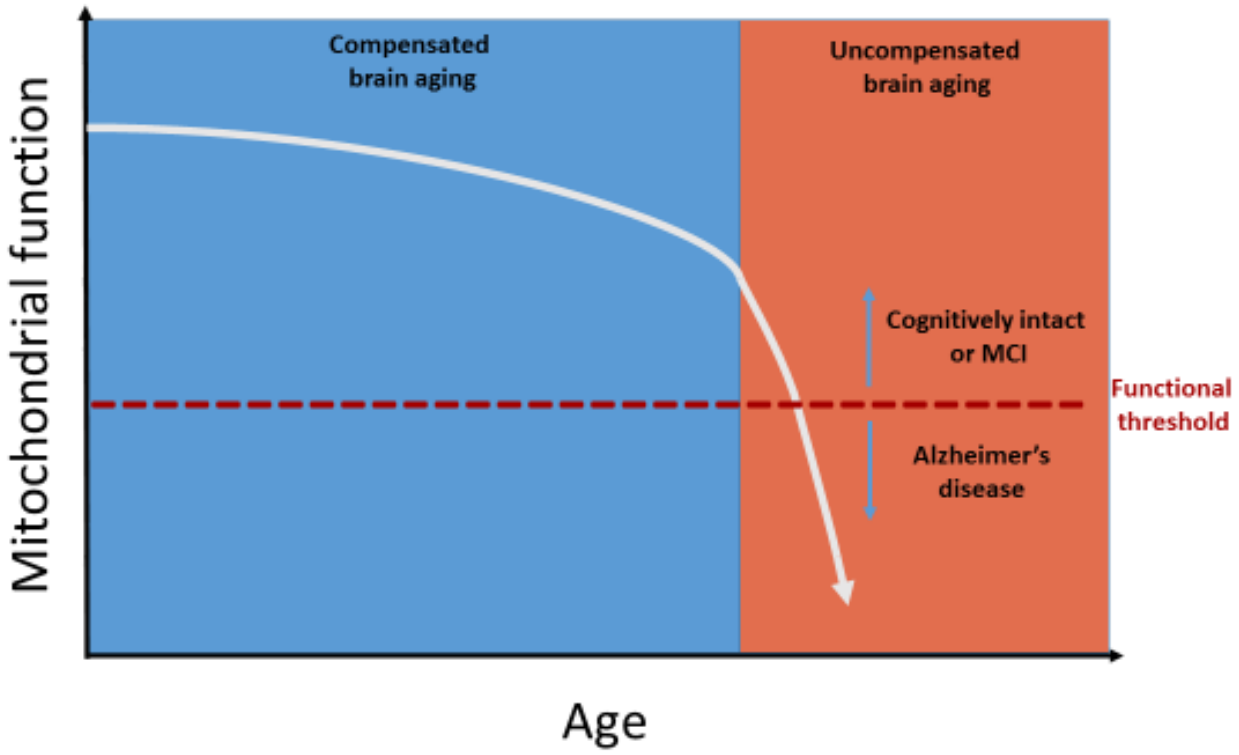
Mitochondrial function
Compensated brain aging
Uncompensated brain aging
Cognitively intact or MCI
Functional threshold
Alzheimer's disease
Age

Figure 1.1. Graphical representation of the mitochondrial cascade hypothesis. The mitochondrial cascade hypothesis of sporadic AD posits that mitochondrial dysfunction declines during normal aging, but the brain compensates for this dysfunction (compensated brain aging). At some point, compensatory responses fail (uncompensated brain aging) and mitochondrial dysfunction declines beyond a functional threshold. From here, disease rapidly ensues.

The mitochondrial cascade hypothesis may well prove wrong. Regardless, the theory raises important questions around sporadic, late onset AD etiology. Reduced brain energy metabolism also provides a new therapeutic target for treating AD. After numerous clinical trial failures pursuing other treatment strategies, it is important to diversify therapeutic targets. Growing evidence implicates mitochondria in AD's pathogenesis and, while it remains unclear whether mitochondrial dysfunction is a primary or secondary event in disease progression, mitochondrial function is increasingly viewed as a reasonable therapeutic target in AD.

Relationship Between Mitochondrial Energy Production and AD Pathology

Many studies have examined the effects of various amyloid and tau species on mitochondrial function. Cell culture treatment with Aβ disrupts numerous mitochondrial endpoints, including mitochondrial polarization, respiratory chain activity and oxygen consumption [102]. The Aβ treatment caused non-specific respiratory chain deficits, including decreased complex I, III and IV activity. AD brains display specific reductions in complex IV (COX) activity. Studies in which researchers exposed isolated mitochondria to Aβ found decreases in COX, alpha-ketoglutarate, and pyruvate dehydrogenase activities. The activity of these enzymes all decline in AD [103]. Studies observe APP accumulation in mitochondrial translocases of the AD brain. This may disrupt mitochondrial function [85]. Aβ also enters mitochondria under some conditions and interacts with a mitochondrial matrix alcohol dehydrogenase, known as Aβ-binding alcohol dehydrogenase (ABAD). ABAD contributes to proper mitochondrial function and Aβ's binding inhibits ABAD activity [104]. Further studies observe Aβ associated with the mitochondria in mouse cell lines and and transgenic mice expressing human APP. Mutant APP expression also stimulated free radical production and

oxidative DNA damage in these studies, suggesting a relationship between APP and mitochondria [105].

Evidence suggests AD-like tau protein alterations can impact mitochondrial function. Since tau contributes to microtubule stability, tau alterations may influence mitochondrial function by disrupting mitochondrial transport along microtubules. Studies in AD brain tissue suggest disturbed mitochondrial transport occurs in AD neurons. For example, studies find fewer mitochondria localized to synapses in AD neurons [106]. This could stem from microtubule stability defects or a number of other mitochondrial transport issues. AD tau alterations have the potential to disrupt microtubules leading to changes in mitochondrial localization. Direct interactions between tau and mitochondria have also been observed. Low-capacity runner (LCR) rats display metabolic defects along with hippocampal neurodegeneration. LCR rats also accumulate hyperphosphorylated tau within their mitochondria. This finding is especially interesting, as these rats do not overexpress human tau. The implications of this study extend beyond tau alterations, however, as the authors suggest mitochondrial dysfunction potentially causes neurodegeneration in LCR rats [107]. Additional studies observe mitochondrial localized tau protein. In AD brains, hyperphosphorylated tau accumulates in voltage dependent anion channel 1 (VDAC1). Phosphorylated tau also interacts with VDAC1 in APP, APP/PS1, and triple transgenic AD mice. The authors propose that phosphorylated tau inhibits VDAC1 function. Furthermore, they suggest clearing pathologic tau from mitochondria may improve cognitive function by improving mitochondrial function [108].

Truncated tau species increase in AD neurons and these tau derivatives also appear to influence mitochondrial function. Tau cleaved at aspartate 421 (Asp-421) increases in AD brains and evidence suggests Aβ enhances cleavage at this site independently of cellular apoptosis

[109] . Overexpressing this tau fragment in neuronal cell culture causes oxidative stress and mitochondrial fragmentation [110]. Overexpressing a different tau fragment, NH2-26-44, causes primary neuron death. N-terminal tau fragments cause mitochondrial dysfunction by disrupting adenine nucleotide transporter (ANT) function [111]. Although it is not known whether this tau fragment increases in AD brains, the study provides additional evidence of tau-mitochondrial interactions.

Another AD relevant protein, apolipoprotein E (apoE), interacts with mitochondria. The ApoE ε4 (apoE4) allele is the only known genetic risk factor for sporadic AD. The apoE4 protein builds up in endosomal compartments and poorly stimulates cholesterol efflux relative to the apoE2 and apoE3 isoforms [112]. ApoE fragments can be found in NFTs from the AD brain. ApoE4 appears particularly susceptible to c-terminal protease cleavage. Neuronal cells transfected with truncated apoE4 display increased NFT formation, suggesting apoE4 fragments are sufficient to induce NFT formation [113]. Subsequent studies discovered associations between apoE fragments and mitochondrial proteins. ApoE4 binds to mitochondrial complex III and complex IV subunits, and apoE4 fragments formed a stronger association than full length apoE4. Also, expressing truncated apoE4 in Neuro-2a cells reduced complex III and IV activity compared to cells expressing full length apoE4. Once again, researchers hypothesize that an AD-associated protein, in this case apoE4 fragments, stimulate neurodegeneration by inhibiting mitochondrial function [114].

The studies outlined above reference mitochondrial dysfunction's role in AD. They largely focus on processes upstream of mitochondria which impact the organelle's function. A reciprocal relationship exists, however. Mitochondrial dysfunction has wide-ranging cellular effects, and disturbed energy production favors AD-like protein alterations. Control fibroblasts

treated with a mitochondrial uncoupler display increased tau phosphorylation at AD-relevant sites. This suggests the uncoupling of oxidative phosphorylation (OXPHOS) observed in the AD brain may contribute to tau abnormalities [115]. Studies with complex I inhibitors also demonstrate a relationship between mitochondrial function and tau alterations. Annonacin and MPP(+), two complex I inhibitors, alter tau splicing in human neurons [116]. Furthermore, chronic rotenone treatment in rat brain stimulates tau hyperphosphorylation and aggregation. Rat brains chronically exposed to rotenone also accumulate alpha-synuclein deposits, although to a lesser extent than tau aggregates [117]. Disruptions in cellular energy production may lie upstream of AD pathology, although more studies need to examine the relationship.

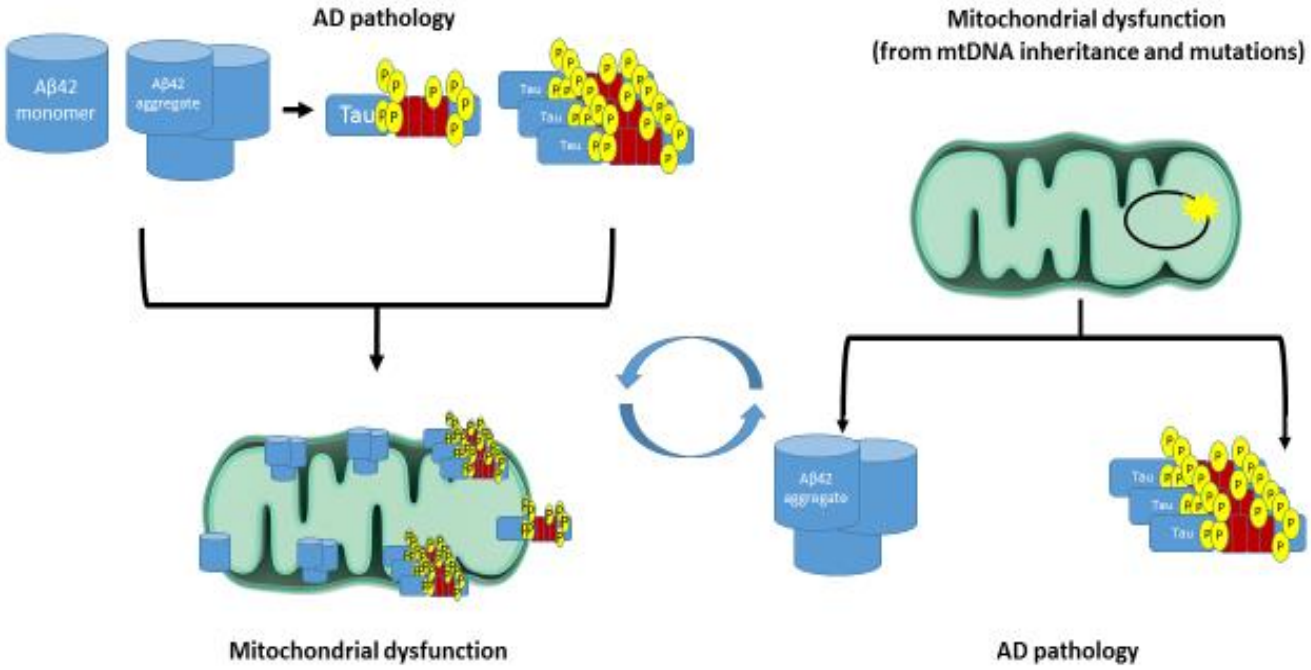
AD pathology
Aβ42 monomer
Aβ42 aggregate
Tau
Mitochondrial dysfunction
(from mtDNA inheritance and mutations)
Aβ42 aggregate
Tau
Mitochondrial dysfunction
AD pathology

Figure 1.2. AD pathology affects mitochondrial function, however, mitochondrial dysfunction may contribute to AD pathology. Classically, AD mitochondrial dysfunction has been thought to occur downstream of amyloid and tau pathology. Alternative hypotheses suggest mitochondrial dysfunction occurs independently of disease pathology and may initiate amyloid plaque and NFT formation.

Mitochondrial Contributions to Cellular Proteostasis

Unfolded protein responses (UPRs) aim to maintain cellular proteostasis and may play an important role in AD, a disease defined by the accumulation of misfolded protein aggregates. Well described mechanisms for responding to unfolded proteins exist in the endoplasmic reticulum (ER) and the cytosol. The UPR in the ER (erUPR) utilizes numerous strategies to maintain cellular proteostasis in the face of diverse cellular stressors. One strategy involves increasing ER chaperone protein expression to restore proper protein folding and prevent aggregation. Simultaneously, ER stress may lead to eukaryotic initiation factor 2α (eIF2α) phosphorylation, inhibiting general protein translation to reduce cellular protein load. The erUPR also stimulates a process known as ER-associated degradation (ERAD). ERAD components degrade misfolded and accumulated protein [118]. Together, these pathways identify and rectify protein misfolding and aggregation in the ER to maintain homeostasis. However, prolonged erUPR activation favors inflammatory responses and apoptosis [119, 120].

The cytosol also senses and responds to misfolded and aggregating proteins. Exposed hydrophobic residues often signal the presence of a misfolded protein. Cytosolic chaperones, including heat shock protein 70 (Hsp70) and heat shock protein 90 (Hsp90) family members, sense misfolding and refold proteins. Meanwhile, the ubiquitin proteasome system (UPS) degrades damaged or unfolded proteins. Members of the E3 ubiquitin ligase family can sense misfolded proteins and mark them for destruction in the proteasome. Additionally, ATP-independent small heat shock proteins (sHsp) help solubilize and prevent protein aggregates through direct binding [121]. Aggresomes represent another cytosolic proteostasis phenomena. Aggresomes form when misfolded proteins accumulate into large inclusion bodies, serving as an important repository for misfolded proteins. Proteasomal components and chaperones move to

aggresomes in an apparent attempt to degrade the structures [122]. Autophagy-lysosomal machinery also works to degrade aggresomes [123]. Aggresome formation typically occurs following proteasomal failure and is thought to help cells manage excess protein aggregation [124]. Researchers have long appreciated the ER and cytosol's contributions to cellular proteostasis but emerging evidence implicates mitochondria in this process as well.

Mitochondria contribute to diverse cellular processes and, recently, growing evidence suggests mitochondria assist in maintaining proteostasis. Mitochondria possess intrinsic chaperones and proteases to handle protein misfolding and aggregation. Unfolded proteins in the mitochondria trigger the mitochondrial unfolded protein response (mtUPR), which upregulates the mitochondria's resident chaperones and proteases [125]. Most evidence for the mtUPR comes from studies in *Caenorhabditis elegans (C. elegans)*. Diverse mitochondrial insults stimulate the mtUPR in *C. elegans*, including decreases in mitochondrial ribosomes, mtDNA depletion and impaired mitochondrial translation. Inhibiting mitochondrial protein complexes and mitochondrial chaperone and protease knockdown also activate the mtUPR in *C. elegans*. The mtUPR occurs independently of cytosolic heat shock and erUPR stress responses [126].

Studies have elegantly described the mechanisms regulating the mtUPR in *C. elegans*. Activating transcription factor associated with stress-1 (ATFS1) mediates the mtUPR based on its subcellular localization. Under non-stressed conditions, mitochondria import ATFS-1 where it undergoes degradation. Mitochondrial stress impairs ATFS-1 import, favoring its translocation to the nucleus. Once in the nucleus, ATFS-1 upregulates the expression of mitochondrial chaperones and proteases [127]. In mammalian cells, activating transcription factor 5 (ATF5) plays a similar role to ATFS-1, mediating the mtUPR under certain conditions. However, the mammalian mtUPR does not respond to diverse mitochondrial stressors in the same way the *C.*

elegans mtUPR does. Treatment with the mitochondrial poison paraquat and overexpressing a mitochondrial-localized misfolded protein both stimulate the mtUPR [128]. Attempts to stimulate the mtUPR in mammalian cells through other mitochondrial interventions have not found success. In one study, researchers inhibited mitochondrial translation, OXPHOS, protein import and dissipated mitochondrial membrane potential. None of these interventions activated the mtUPR.

These various forms of mitochondrial dysfunction failed to trigger the mtUPR, but they activated alternative pathways with implications for cellular proteostasis. Mitochondrial interventions stimulated activating transcription factor 4 (ATF4) stress response pathways. ATF4 lies downstream of eIF2α. While eIF2α phosphorylation represses general cellular translation, certain stress responsive factors, including ATF4, actually experience increased translation rates. This suggests mitochondrial stress inhibits cytosolic translation by increasing eIF2α phosphorylation. Reduced cytosolic translation likely helps maintain cellular proteostasis during mitochondrial energy stress. Furthermore, mitochondrial dysfunction impacted local mitochondrial proteostasis by decreasing mitochondrial ribosomes and translation. ATF4 knockdown inhibited cellular proliferation and slowed cellular recovery following mtDNA depletion via ethidium bromide (EtBr) [129]. Another study found that mitochondrial OXPHOS inhibitors induce an ATF4 dependent stress response [130]. Mitochondrial function can also affect proteostasis by impacting UPS function and mitophagy.

Mitochondrial dysfunction appears to inhibit proteasomal activity. Studies in yeast, *C. elegans*, and mammalian cells reveal a relationship between impaired ETC function and decreased proteasomal activity. Based on recent studies, researchers hypothesize that ROS production favors proteasome disassembly. Antioxidant treatment reverses proteasome

disassembly, further proof that ROS mediates proteasomal defects. Other studies find that decreasing ATP levels also correlate with declining proteasomal function. Therefore, ATP deficits may represent another mechanism linking mitochondrial function to UPS activity [131]. Alternatively, mitochondrial stress can activate proteasomal activity. Defective mitochondrial protein import leads mitochondrial protein precursors to accumulate. The cell senses the accumulating mitochondrial precursors and responds with increased proteasomal activity and decreased protein translation. The response to mitochondrial precursor accumulation has been termed the UPRam [132]. In *C. elegans*, a mitochondrial stress response pathway dependent upon lipid biosynthesis occurs. Knockdown of a mitochondrial chaperone, mtHSP70, triggers cytosolic lipid accumulation which activates certain transcription factors. The transcription factors increase lipid metabolism genes and cytosolic chaperone genes to simultaneously rewire cellular metabolism and decrease proteotoxicity [133]. Further studies need to determine the relevancy of these pathways in mammalian cells.

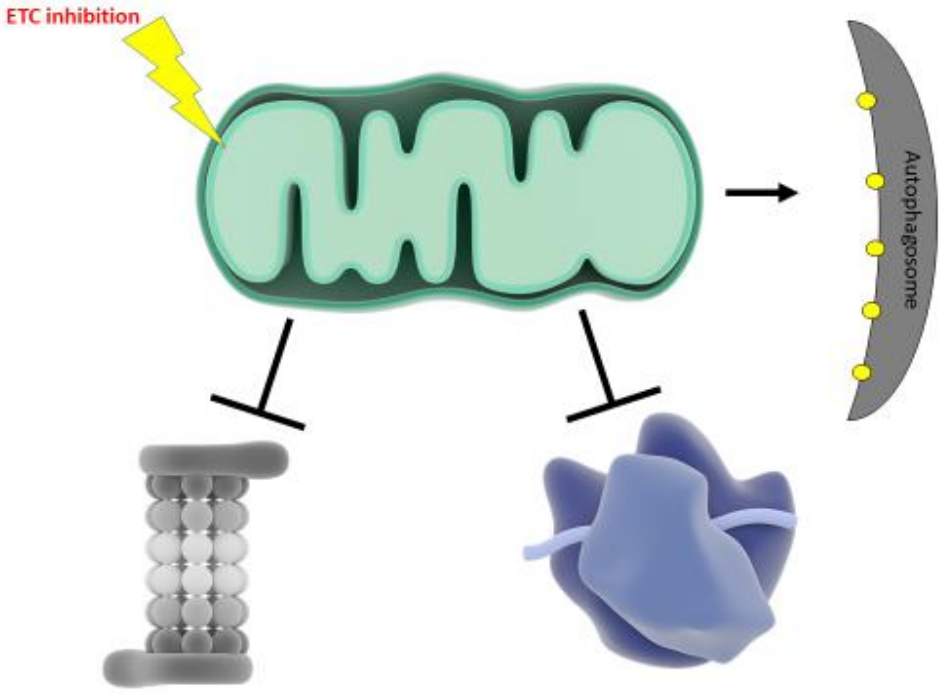
ETC inhibition
Autophagosome

Figure 1.3. Mitochondrial stress impacts cellular proteostasis. ETC inhibition decreases proteasome activity, inhibits protein translation, and increases mitophagy.

Studies in yeast suggest mitochondria degrade aggregation prone proteins to maintain proteostasis. Disrupting mitochondrial import and proteases stabilizes cytosolic protein aggregates. Furthermore, defective cytosolic chaperones caused protein aggregates to accumulate in the mitochondria. For the most part, aggregated proteins only moved to the mitochondria under heat shock stress. A small portion of aggregation prone proteins entered the mitochondria for degradation under basal conditions. The authors also examined whether human cells displayed a similar mechanism. The findings suggest human cells may also degrade aggregation prone proteins in the mitochondria but further studies should attempt to confirm and add to these findings [134]. If mitochondria import and degrade aggregation prone proteins in human neurons, then a breakdown in this system could contribute to AD's hallmark plaque and tangle pathology.

Mitophagy may also contribute to proteostasis. If aggregating proteins localize to the mitochondria, then lysosomal destruction of mitochondria should remove those protein aggregates. Studies in APP transgenic mice (mAPP) suggests mitophagy can reduce amyloid burden. PTEN-induced putative kinase 1 (PINK1) knock down in mAPP mice disturbs mitophagy and hastens amyloid plaque deposition. When mAPP mice overexpress PINK1, however, mitophagy is enhanced and plaque levels decline. PINK1 overexpression also reduced synaptic loss and improved memory in mAPP mice [135]. Another study highlights the important role mitochondrial fission plays in facilitating selective degradation of protein aggregates. Overexpressing a mitochondrial localized aggregation prone protein stimulated Parkin recruitment to specific mitochondrial regions containing protein aggregates. Interestingly, blocking mitochondrial fission did not change the clearance rate of aggregated proteins. Loss of fission instead led to non-specific Parkin recruitment and enhanced mitophagy. The authors

conclude the results suggest fission facilitates selective degradation of mitochondrial protein aggregates, while a loss of fission leads to non-discriminate mitochondrial breakdown. Fission may, therefore, help conserve healthy mitochondrial regions which may be beneficial to cellular energy production [136]. Together, these studies suggest mitophagy plays a role in clearing mitochondrial localized protein aggregates.

Summary

Metabolic defects occur in AD. Reduced brain glucose uptake happens early in disease progression and correlates fairly well with cognitive decline. Systemic mitochondrial dysfunction appears alongside metabolic dysfunction. AD researchers have largely assumed mitochondrial dysfunction stems from upstream disease processes. However, growing evidence suggests mitochondria could play a primary role in AD pathogenesis. The mitochondrial cascade hypothesis suggests mtDNA inheritance and somatic mutations combine to determine an individual's AD risk, and hypothesizes that mitochondrial dysfunction triggers AD's neuropathological hallmarks. Studies suggest mitochondrial dysfunction impacts amyloid and tau homeostasis, potentially favoring their aggregation. Furthermore, growing evidence indicates proper mitochondrial function contributes to proteostasis by affecting protein translation and degradation machinery. Mitochondria themselves appear to degrade aggregating proteins through the combined action of resident proteases and chaperones, while mitochondrial degradation promotes clearance of protein aggregates. Currently, no FDA-approved treatments exist to slow disease progression. Amyloid-centric therapies have experienced numerous failures in clinical trials, suggesting a need for novel therapeutic targets. Based on the evidence presented here, mitochondrial function represents a reasonable therapeutic target in AD. The goal of the

following studies is to learn about the cellular consequences of mitochondrial dysfunction with a particular emphasis on AD pathology.

Chapter 2: Mitochondrial Respiratory Chain Defects Alter Tau and ApoE Homeostasis

Introduction

During the 1980s, researchers found the core of NFTs largely consist of tau protein aggregates [137-139]. Since then, studies have described extensive tau alterations in AD. Following tau's association with NFTs, immunocytochemistry in AD brains quickly revealed changes in tau phosphorylation. An early study on AD tau discovered phosphorylated tau associated with NFTs and in the neuronal cytoplasm of cells free from NFT pathology. The authors suggested that increased tau phosphorylation in the absence of NFTs signals the early stages of degeneration, while NFT formation occurs later. These findings, along with many more, led to one of the prevailing hypotheses on NFT formation in AD, namely, that tau phosphorylation precedes NFTs and contributes to their formation [140]. Around this time, studies began to categorize AD into stages based on tau alterations. Early studies attempted to correlate disease progression with amyloid changes, however, plaque deposition did not follow an AD-specific pattern. Braak staging classified AD brains into six categories based on the extent and localization of tau pathology [141].

Tau hyperphosphorylation occurs at many sites during AD progression. Current theories propose tau hyperphosphorylation inhibits tau microtubule binding, leading to increased cytosolic tau concentration which is thought to favor aggregation. Some findings cast doubt on the relationship between tau phosphorylation and NFT formation. One of these studies found inducing tau phosphorylation actually inhibited tau aggregation, although the methodology employed only achieved phosphorylation at a few sites [142]. Further work in cell-free systems largely agreed with these findings, as inducing tau phosphorylation at multiple AD-relevant sites, i.e. mimicking tau hyperphosphorylation observed in AD tau, slowed tau polymerization. These findings led to a more nuanced view of tau hyperphosphorylation's role in AD toxicity, with

researchers suggesting tau hyperphosphorylation exerts its negative effects while soluble. In this view, NFT formation may protect cells from the toxicity associated with soluble, hyperphosphorylated tau species [143]. Regardless, tau phosphorylation is clearly altered in AD, and many mechanisms could contribute to AD tau hyperphosphorylation. Changes in kinase/phosphatase activity, mutations in the gene encoding tau, covalent modifications, oxidative stress, Aβ-mediated toxicity, inflammation, and mitochondrial dysfunction can all influence tau phosphorylation [144]. Tau phosphorylation may also influence the protein's conformation, which changes during AD.

Changes in tau conformation and increased oligomerization occur in the AD brain, and some propose changes in conformation stimulate oligomerization. The Alz50 antibody was created using crude AD brain homogenates and labels fibrillary tau structures in the AD brain. The Alz50 antibody recognizes a discontinuous tau epitope, which is only available when the protein adopts certain conformations. The tau conformations recognized by Alz-50 appear in AD brains prior to NFT formation [145]. Since this finding, laboratories have developed additional antibodies recognizing AD relevant tau structural changes. The MC-1 antibody binds to similar tau regions as Alz50, with the added benefit of improved tau specificity [146]. More recently, researchers discovered a pathological tau conformation associated with oligomerization. They generated an oligomeric-tau specific antibody using recombinant cross-linked tau dimers, named Tau Oligomeric Complex 1 (TOC1). TOC1 immunoreactivity increases in the AD brain, labeling a conformational epitope which is present in tau dimers and oligomers but absent in monomeric and polymeric tau [147]. The presence of tau conformational alterations in AD brains suggests structural changes to tau may facilitate aggregation.

Traditionally, researchers have viewed tau modifications and aggregation through the lens of the amyloid cascade hypothesis, suggesting amyloid toxicity precipitates NFT formation. Alternative explanations for AD neuropathology have received less attention. Few reports have examined mitochondrial dysfunction's impact on AD-relevant tau alterations. The following studies build upon prior reports suggesting mitochondrial poisons recapitulate AD-like tau alterations, by examining tau alterations in response to chronic and acute mtDNA depletion. Finally, we examine tau alterations in AD cybrids.

To model chronic respiratory deficiency, we utilized ρ0 SH-SY5Y cells. ρ0 cells contain almost undetectable levels of mtDNA due to long term culturing in the presence of EtBr [148]. ρ0 cells maintain mitochondrial structures but possess dysfunctional respiratory chains. Much of our knowledge regarding retrograde responses comes from studies on ρ0 cells [149]. ρ0 cells remain mtDNA-depleted following EtBr removal and maintain viability through continuous culturing. Since they can be cultured in the same media as ρ+ cells, studies in ρ0 cells avoid the off target effects of mitochondrial poisons or other pharmacological treatments.

Acute mtDNA depletion with ethidium bromide allowed us to examine short term responses to mitochondrial respiratory defects. SH-SY5Y cells depleted of mtDNA to varying degrees (50%, 75%, 95%) provide insight into cellular adaptations to acute respiratory chain defects. Cellular responses to acute respiratory defects likely differ from those employed by cells experiencing chronic respiratory deficiencies. These differences may be relevant to different disease states.

Finally, we examined tau alterations in AD cybrids. AD cybrids provide a disease relevant model of mitochondrial dysfunction. Differences between AD and age-matched control cybrids stem exclusively from patient derived mtDNA, as mtDNA is the only material

maintained through the process of cybrid generation. AD cybrids effectively model AD mitochondrial function, or at least changes in AD mitochondrial function resulting from mtDNA. Establishing a link between AD mitochondrial dysfunction and AD-like pathological alterations would provide additional evidence for mitochondrial dysfunction's primary role in AD progression.

Materials and Methods

Generating and culturing SH-SY5Y ρ0 cells

SH-SY5Y ρ0 cells were created earlier through chronic culture with low doses of ethidium bromide as described by Miller et al. 1996 [150]. ρ0 cells were grown in DMEM containing 25mM glucose (gibco #11965). DMEM was supplemented with 10% fetal bovine serum (FBS), 1% penicillin/streptomycin, 100 μg/mL sodium pyruvate and 50μg/mL uridine. ρ0 cells require exogenous pyruvate and uridine to survive. When ρ0 cells were below 50% confluency, media was exchanged every other day. Once flasks surpassed 50% confluency, media was exchanged every day. Control, mtDNA replete cells (ρ+) were grown in the same media used for ρ0 cells.

Acute mtDNA depletion of SH-SY5Y cells via EtBr

During these experiments, control and treated SH-SY5Y cells were grown in 25mM glucose DMEM supplemented with 10% FBS, 1% penicillin/streptomycin, 100 μg/mL sodium pyruvate and 50μg/mL uridine. To deplete mtDNA, EtBr (Cat #) was added to the cell culture media at a concentration of 3 μg/mL. Cells were cultured in the presence of EtBr for either 24 hours, 3 days, or 7 days. Media was exchanged every day during the course of EtBr treatment. EtBr was added to the media just prior to being added to cells and the EtBr containing media was passed through a 0.22μm syringe filter.

Culturing SH-SY5Y control and AD cybrids

Control and AD cybrids were cultured in 5mM glucose DMEM supplemented with 10% FBS and 1% penicillin/streptomycin. D+-glucose was added to glucose free DMEM to make 5mM glucose media. Media was exchanged every day.

Whole cell lysate preparation

For whole cell lysate collection, control and treated SH-SY5Y cells were seeded at similar confluency in 6-well dishes (Corning costar #3516). Next day, the media was aspirated, cells were washed with phosphate buffered saline (PBS), and 150µL RIPA lysis buffer was added to each well. RIPA lysis buffer contained 10mM Tris-Cl (pH 8.0), 1mM EDTA, 0.5mM EGTA, 1% Triton X-100, 0.1% sodium deoxycholate, 0.1% SDS, 140mM NaCl. Thermo Halt Protease and Phosphatase inhibitor cocktail (Thermo #1861284) was added just prior to use. Cells were lysed on ice via scraping and lysates were incubated on ice for 20 minutes. Following incubation, lysates were centrifuged at 3,000xg for 10 minutes. The supernatant was transferred to a fresh tube and stored at -80°C or used immediately for protein quantification. Protein levels were quantified using a BCA assay (Pierce #23225). 5µL whole cell lysate and 25µL albumin protein standards were loaded in duplicate in clear, 96 well plates. Following the addition of 200µL BCA working reagent solution, the plate was incubated at 37°C for at least 30 minutes and absorbance was read on the Tecan at 562nM. Lysates were diluted in water to a concentration of 25µg/30µL and laemmli buffer was added. Samples were then boiled at 95°C for 10 minutes and stored at -20°C or -80°C for future use.

Western blotting

Protein lysates were separated using pre-cast criterion SDS-PAGE gels run at a constant voltage in Tris/glycine/SDS running buffer (BioRad #1610772). For most targets, 4-12% criterion gels were used. When blotting for tau protein, however, 7.5% criterion gels were used to achieve better separation of tau protein bands. 25µg protein was loaded in each well along with 5µL protein ladder. Following SDS-PAGE, protein was transferred to methanol-activated

0.45μM PVDF membrane (GE Amersham Hybond #10600023) in tris/glycine transfer buffer (BioRad #1610771) containing 20% methanol. Protein transfer was achieved using a constant current of 400amps for 1 hour. After transfer, membranes were rinsed with tris buffered saline containing 0.1% tween (TBST) and blocked for 1hr at room temperature in 5% dry milk in TBST or 5% bovine serum albumin (Boston BioProducts P-753) in TBST. Blocked membranes were then incubated overnight at 4°C with shaking in primary antibody diluted with 5% dry milk in TBST or 5% BSA in TBST. The next day, membranes were washed 3 times for 5 minutes each in TBST followed by the addition of appropriate secondary antibody (Invitrogen Superclonal Secondary Antibody, HRP Conjugate #A28177 or #A27036, diluted 1:4000 in 5% dry milk in TBST. Membranes were incubated in secondary antibody for 1 hour at room temperature. Then, membranes were washed in TBST 3 times for 5 minutes each before being incubated in Supersignal West Femto Maximum Sensitivity Substrate (Thermo #34096) and visualized on a BioRad Chemidoc XRS+ imager.

mtDNA and Nuclear DNA Extraction

Control and treated SH-SY5Y cells were plated in 6 well dishes. The next day, the media was aspirated and cells were washed with PBS. 1mL PBS was added to each well, cells were lifted from the dish using a cell scraper and transferred to 1.7mL microcentrifuge tubes. Cells were pelleted at 600xg for 3 minutes and the supernatant was aspirated. The cell pellet was then resuspended in 300uL cold DNA lysis buffer containing 10mM Tris-HCl, 0.1% SDS, 1mM EDTA. 30uL of 20mg/mL proteinase K (Invitrogen #25530-015) was added to each sample and they were then vortexed for 10 seconds to lyse cells. Samples were then incubated in a 55°C water bath overnight to complete the proteinase K treatment. Following proteinase K treatment,

300uL phenol:chloroform:isoamyl alcohol (Sigma #77617) was added, samples were vortexed for 5 seconds, and centrifuged at 8,000xg for 15 minutes. 250µL supernatant was transferred to a new microcentrifuge tube and 250µL chloroform was added. The samples were then mixed by shaking vigorously. The samples were then centrifuged at 8,000xg for 15 minutes and 200µL supernatant were transferred to a new centrifuge tube. To precipitate DNA, 20µL 3M sodium acetate and 220µL isopropanol were added to the sample, and the samples were stored at -20°C overnight. The next day, samples were centrifuged at 8,000xg for 15 minutes to pellet DNA and washed twice in 70% EtOH. The pellet was air dried and resupsended in 250µL nuclease free water. The DNA was then quantified and diluted to a concentration of 5ng/µL.

mtDNA:Nuclear DNA quantification via qPCR

2µL of 5ng/µL DNA was used per qPCR reaction, for a total of 10ng of DNA per reaction. The total reaction volume was 10µL per well, with 2µL sample, 5µL 2x Powerup SYBR Green Master Mix (Applied Biosystems #A25742), 1µL forward primer, 1µL reverse primer, and 1µL nuclease free water. mtDNA levels were measured using primers directed against *MT-ND1* (Forward primer: 5'-CCA CCT CTA GCC TAG CCG TTT-3' ; Reverse primer: 5'-TGT TTG GGC TAC TGC TCG C-3'). Nuclear DNA levels were measured using primers directed against *β2M* (Forward primer: 5'-TGC TGT CTC CAT GTT TGA TGT ATC-3' ; Reverse primer: 5'-TCT CTG CTC CCC ACC TCT AAG T-3'). The qPCR run method was as follows:

1. 50°C for 2 minutes
2. 95°C for 2 minutes
3. 95°C for 3 seconds
4. 60°C for 30 seconds

40 cycles

5. 95°C for 15 seconds
6. 60°C for 1 minute
7. 95°C for 15 seconds

Melt Curve Step and Hold 5 seconds

qPCR were run on an Applied Biosystems Quantstudio 7 Flex (384 well) or Applied Biosystems StepOne Plus Real Time PCR system (96 well), using a 96 well plate (Applied Biosystems #4346906) or 384 plate (Applied Biosystems #4309849). Relative fold change was calculated using the ΔΔCt method with *β2M* serving as the reference gene.

Pseudogene Ratioing

PCR reactions were carried out using the Expand Long Range dNTPack (Roche #4829042001). Primers capable of amplifying both a nuclear, mitochondrial-pseudogene and authentic mtDNA (numt inclusive) had the following sequences: 5′-GAGTCCGAACTAGTCTCAGGCT-3′ and 5′-CTCGAAGTACTCTGAGGCTTGTAGGAGG-3′. Primers specific for authentic mtDNA (numt exclusive) had the following sequences: 5′-TGATTTATCTCTCCACACTAGCAGAGACCAAC-3′ and 5′-GCTACAAAAAATGTTGAGCCGTAGATG-3′. The reactions proceeded as described by Swerdlow et al (2006) [148].

Seahorse extracellular flux analysis

The day before the assay, 80,000 cells were seeded per well in a Seahorse XF24 cell culture plate (#100777-004). Cells were initially seeded in 100µL complete media. 500µL complete media was added to each well 4 hours after initial seeding, bringing the final volume to 600µL per well. The next day, 25 mM glucose, 2 mM glutamine and 1 mM pyruvate were added to mito stress media. Then, the cells were washed twice in assay media, and finally were brought to a final volume of 600µL in assay media. Cells were degassed at 37ºC in a non-CO2 incubator for 45 minutes. Mitochondrial inhibitors were diluted in 3mL assay buffer to the following concentrations (10x): oligomycin (Sigma #75351)= 10 µM, FCCP (Sigma #C2920)= appropriate amount determined through titration experiments, rotenone (Sigma #R8875) and antimycin A (Sigma #A8674) = 5 µM each. The experiment was run on the Seahorse XF24 analyzer using an extracellular flux assay kit (#100850-001) and following the mitochondrial stress test protocol.

Nuclear and cytoplasmic protein enrichment

Nuclear and cytoplasmic enrichment of control and treated SH-SY5Y protein was achieved using Thermo's NE-PER, nuclear and cytoplasmic extraction reagents, kit (Thermo #78833). Cells were grown to confluency in T75 flasks. Media was aspirated, cells were washed with PBS, and a cell scraper was used to lift cells from the flask. Cells were pelleted at 600xg for 3 minutes and the supernatant was aspirated. Cell pellets were resuspended in 200µL cold CER I reagent containing Halt protease and phosphatase inhibitor cocktail (Thermo #1861284). Tubes were vortexed at the highest setting for 15 seconds and the tubes were incubated on ice for 10 minutes. Then, 11µL cold CER II reagent was added. The tubes were then vortexed on the highest setting for 5 minutes followed by another 10 minute incubation on ice. The tubes were then vortexed at the highest setting for 5 seconds and centrifuged at 16,000xg for 10 minutes at

4°C. The supernatant was transferred to a new tube labeled cytoplasmic extract and stored at -80°C. The insoluble pellet from the previous centrifugation step was then resuspended in 75µL cold NER reagent containing Halt protease and phosphatase inhibitor cocktail. To extract nuclear proteins, the pellet was vortexed four times for 15 seconds each, with a ten minute break in between each vortex. Pellets were then left overnight in NER at 4°C. The next day, the pellets were vortexed multiple times and centrifuged at 16,000xg for 10 minutes. The supernatant was then moved to a fresh tube labeled nuclear extract and stored at -80°C. Cytoplasmic and nuclear extract protein levels were then quantified using a BCA assay and diluted to a concentration of 25µg/30µL with water and laemmli buffer. Samples were then boiled for 10 minutes at 95°C and stored at -20°C or -80°C until ready for use.

MAPT siRNA Treatment

SH-SY5Y ρ0 cells were seeded at 25% density in 6 well plates. For each well that was to be treated, MAPT or scramble siRNA were diluted to 25nM in 200µL of serum and antibiotic free media (Dharmacon SMARTPool ON-TARGET PLUS Human MAPT siRNA #L-012488-00-0005). In a separate tube, 5µL DharmaFECT 1 (Dharmacon #T-2001-01) was mixed with 195µL serum and antibiotic free media per sample. The contents of each tube were mixed and incubated at room temperature for 5 minutes. The contents of the tubes were then mixed together and incubated at room temperature for 20 minutes. Following the incubation, each transfection media was diluted to 2mL with antibiotic-free media containing FBS. Growth media was aspirated from the 6 well dishes, and the 2mL transfection reagent mixture was added to each well. The cells were grown in transfection media for 24 hours. Then, the transfection media was removed and replaced with media containing antibiotics and FBS. The cells were incubated for

an additional 48 hours in complete media, and were harvested in RIPA lysis buffer 72 hours post transfection.

RNA Extraction and cDNA generation

Cells were seeded in 6-well dishes and grown to confluency. When cells were ready to be harvested, the media was aspirated and cells were washed with sterile PBS. 500µL Trizol reagent (ambion #15596018) was added and cells were triturated in Trizol until solubilized. The Trizol homogenate was then incubated at room temperature for 10 minutes. Following this incubation, samples were moved to autoclaved 1.7mL microcentrifuge tubes, 200µL chloroform was added to each sample, and tubes were mixed for 15 seconds. Samples were then incubated at room temperature for 10 minutes to allow for phase separation. Following phase separation, samples were centrifuged at 12,000xg for 15 minutes at 4°C. The upper, aqueous layer (~200µL) was then transferred to a fresh, autoclaved microcentrifuge tube. RNA was then precipitated by adding 500µL isopropanol, mixing the tubes, and incubating at room temperature for 10 minutes. After RNA precipitation, the samples were centrifuged at 12,000xg for 10 minutes. The supernatant was removed and RNA pellets were washed with 500µL 75% ethanol. The pellets were centrifuged at 7,500xg for 5 minutes, dried, and resuspended in 100µL nuclease free water. RNA was quantified on the Tecan and 1µg of RNA was loaded for reverse transcription, along with 5x iScript reverse transcription supermix (BioRad #1708840). Reverse transcription was performed according to manufacturer instructions and the resulting cDNA was diluted from 20µL to 100µL.

Taqman-based Quantitative PCR

The quantitative PCR (qPCR) reaction mixture had a final volume of 10µL and consisted of 2µL cDNA, 5µL Taqman Universal Master Mix II, with UNG (Applied Biosystems #4440038), 0.5µL 20x Taqman primer (primers listed in Table 2.2), and 2.5µL water. Negative control reactions, lacking cDNA, were included on each plate. The run method for qPCR reactions utilizing Taqman primers was as follows:

1. 50°C for 2 minutes
2. 95°C for 10 minutes
3. 95°C for 15 seconds
4. 60°C for 1 minute

} 40 cycles

qPCR were run on an Applied Biosystems Quantstudio 7 Flex (384 well) or Applied Biosystems StepOne Plus Real Time PCR system (96 well), using a 96 well plate (Applied Biosystems #4346906) or 384 plate (Applied Biosystems #4309849). Relative fold change was calculated using the ΔΔCt method with *18S* serving as the reference gene.

SYBR-Green Based Quantitative PCR for Tau splice variants

The quantitative PCR (qPCR) reaction mixture had a final volume of 10µL and consisted of 2µL cDNA, 5µL Powerup SYBR Green Master Mix (Applied Biosystems #A25742) 1µL Forward primer (5 µM), 1µL Reverse primer (5 µM) and 1µL water. Negative control reactions, lacking cDNA, were included on each plate. The run method for tau splice variant qPCR reactions was as follows:

1. 95°C for 45 seconds
2. 95°C for 5 seconds
3. 60°C for 30 seconds

} 40 cycles

4. 95°C for 15 seconds
5. 60°C for 1 minute
6. 95°C for 15 seconds

} Melt Curve Step and Hold 5 seconds

qPCR were run on an Applied Biosystems StepOne Plus Real Time PCR system (96 well), using a 96 well plate (Applied Biosystems #4346906). Relative fold change was calculated using the ΔΔCt method with *18S* serving as the reference gene.

Phosphatase treatment of whole cell lysates

Control and treated SH-SY5Y whole cell lysates were harvested with RIPA buffer as described above, however, a few modifications were made to the lysis buffer. Since the lysates were to be treated with a phosphatase to dephosphorylate protein, no phosphatase inhibitors were added to the lysis buffer. Furthermore, EDTA, EGTA, and NaCl were left out of the RIPA buffer and a protease inhibitor cocktail free from EDTA was used, namely, cOmplete, mini, EDTA-free protease inhibitor cocktail (Roche #11836170001). This is due to the strong inhibitory effects of EDTA and weak inhibitory effect of NaCl on lambda phosphatase activity. After protein extraction and quantification, 25µg protein was diluted to 20µL volume with water and then 2.5µL 10x NEBuffer PMP, 2.5µL 10mM MnCl2, and 1.25µL lambda protein phosphatase (400,000units/mL, New England Biolabs #P0753S) were added to make a final reaction volume of ~25µL. The final concentration of lambda protein phosphatase was 20 units/µL. The reaction was incubated at 30°C for 3 hours and stopped by the addition of 6x laemmli buffer and subsequent boiling at 95°C for 10 minutes. Samples were stored at -80°C until being used for SDS-PAGE analysis.

Protein extraction from SH-SY5Y cells for dot blot analysis

Cells were grown to 95% confluency in 6-well dishes. Media was aspirated and cells were washed in PBS. Cells were lysed in NP40 buffer free from SDS, since the TOC1 conformational epitope is destroyed by SDS. The NP40 lysis buffer recipe was: 1% IGEPAL (NP40), 50mM Tris-HCl pH 8.0, 150mM NaCl, Halt protease and phosphatase inhibitor cocktail. 150µL NP40 lysis buffer was added to each well and cells were lysed via scraping. The whole cell lysates were incubated on ice for 20 minutes, then centrifuged at 3,000xg for 10 minutes. The supernatant was moved to a fresh tube and stored at -80^{0}C for future use or immediately quantified via BCA assay. Lysates were diluted to a concentration of 1µg/µL. To maintain TOC1's conformational epitope. no laemmli buffer was added and the samples were not boiled.

Soluble protein extraction from human brain tissue for dot blot analysis

Human control (7) and AD (8) brain tissue samples from the ADC cohort were lysed in a buffer containing: 120mM NaCl, 50mM Tris pH 8.0, and Halt protease and phosphatase inhibitor cocktail. 1mL ice cold buffer was used per ~250mg brain tissue. Samples were processed by 10 strokes in a glass dounce homogenizer. The samples were then centrifuged at 17,000xg for 20 minutes at 4^{o}C and the resulting supernatant containing soluble protein was collected and used for dot blots. Prior to loading on a dot blot, protein was quantified via BCA assay and samples were diluted to a concentration of 1µg/µL.

Dot Blots

Dot blotting was done on 0.45µm nitrocellulose membranes (GE #10600002). 2 µg of protein lysate was loaded per sample. Samples were dotted onto the membrane 0.5 µL at a time, allowing the sample to completely dry in between applications. This helped the sample spread evenly and form a dot rather than a ring-like shape with white space in the middle. After drying

completely, the blot was blocked in 5% dry milk resuspended in TBST for 1 hour at room temperature. Blots were incubated with TOC1 (1:10,000 in 5% milk in TBST) or Tau12 (1:10,000 in 5% milk in TBST) overnight at 4°C. TOC1 is a mouse, immunoglobulin M (IgM) antibody. Therefore, a mouse IgM secondary antibody (1:4000 in 5% milk in TBST, Invitrogen #PA84383) was used with the TOC1 labeled blots and a mouse IgG secondary antibody (1:4000 in 5% milk in TBST, Invitrogen #A28177) was used with the Tau12 labeled blots. Blots were washed three times for 5 minutes each with TBST prior to secondary antibody incubation. Dot blots were incubated in secondary antibody for 1 hour at room temperature and, then, washed three times for 5 minutes each in TBST. Dot blots were visualized using West Pico (Thermo #34580) on a BioRad Chemidoc XRS+ imager.

Protein collection from cell culture media

To collect extracellular protein from ρ+ and ρ0 cells, T75 flasks were grown to ~80% confluency in complete media as described above. Once flasks reached the proper confluency, the complete media was removed, flasks were washed three times with PBS, and 10 mL of serum-free, 25 mM glucose Optimem media (gibco #31985-070) supplemented with 1% pen/strep, 100μg/mL sodium pyruvate, and 50μg/mL uridine. Optimem was used in place of DMEM because ρ0 cells displayed low viability after 24 hours of serum starvation in DMEM. Optimem improved ρ0 viability in serum free conditions. The cells were incubated in serum-free Optimem for 24 hours, at which point the media was collected, spun at 3,000*g* for 10 minutes to clear dead cells and debris, and stored at -80°C. Once samples had thawed on ice, the media was concentrated from 10 mL to ~0.5 mL using Amicon Ultra-15 centrifugal units with a 10 kDa

filter cutoff (Millipore #UFC901024). Protein concentration was measured via BCA assay, and samples were diluted to the desired concentration.

ELISAs

To measure ApoE protein levels in cell culture media, conditioned media was concentrated as described and diluted to a concentration of 1 μg/μL. Then, 50 μL (50 μg) of each sample was loaded in duplicate on a human apolipoprotein E ELISA kit (ab108813). The ELISA was carried out according to the manufacturer's instructions. For total tau ELISAs, conditioned media was diluted to a concentration of 0.3 μg/μL. 50 μL (15μg) of each sample was loaded in duplicate on a tau (total) human ELISA kit (Invitrogen #KHB0041). The ELISA was carried out according to the manufacturer's instructions. ELISA values were obtained (pg/ml) and corrected for total extracellular protein loaded (μg/ml), producing a final unit of pg/μg.

Results

Validation of ρ0 status

Before examining chronic mtDNA depletion's cellular effects, a series of experiments confirmed the successful depletion of mtDNA. We confirmed mtDNA depletion at various levels, including protein, DNA, and mitochondrial oxygen consumption. mtDNA depletion should ablate mtDNA-encoded proteins. As expected, cytochrome c oxidase subunit II (MtCO2), a mtDNA-encoded respiratory chain subunit, protein levels fall below the limit of detection in ρ0 whole cell lysates. Meanwhile, MtCO2 protein is readily labeled via western blotting in ρ+ whole cell lysates. Co-labeling with an antibody against β-actin shows even loading between the groups (Figure 2.1a). Next, we confirmed mtDNA loss via multiple PCR based assays. Quantitative, real-time PCR (qPCR) primers directed against mtDNA, specifically NADH:ubiquinone oxidoreductase core subunit 1 (ND1), and nuclear DNA, specifically β-2-microglobulin (β2M), measured mtDNA levels. qPCR analysis of ρ+ and ρ0 genomic DNA showed greater than 99.9% relative reduction of mtDNA in ρ0 cells (Figure 2.1b).

To further validate these findings, we utilized another pair of primers recognizing a mtDNA-specific region (numt exclusive) and a nuclear mtDNA pseudogene (numt inclusive), respectively. These primers have previously been used to confirm mtDNA depletion in a U251 human glioma cell line. This strategy does not rely on a negative result to confirm mtDNA depletion [148]. The numt inclusive primers amplified a 6kb product from ρ+ and ρ0 genomic DNA. Meanwhile, the numt exclusive primers failed to amplify a product from ρ0 cells, further confirming successful mtDNA depletion (Figure 2.1c). Finally, in order to confirm the loss of mitochondrial function due to mtDNA depletion, we measured cellular oxygen consumption in ρ0 cells using a Seahorse extracellular flux assay. ρ0 cells displayed a basal oxygen consumption

rate similar to, if not lower than, the non-mitochondrial oxygen consumption rate (OCR) observed in ρ+ cells, suggesting a complete lack of mitochondrial oxygen consumption. Furthermore, the ρ0 OCR does not change upon exposure to the mitochondrial poisons oligomycin, FCCP, or rotenone and antimycin A. Changes in OCR following exposure to mitochondrial poisons reflects the presence a functional ETC. Therefore, the failure of ρ0 OCR to respond to mitochondrial poisons suggests ρ0 cells possess a non-functional respiratory chain (Figure 2.1d). In summary, ρ0 cells display MtCO2 protein loss, mtDNA loss, and respiratory chain incompetence. These findings confirm successful mtDNA depletion in our SH-SY5Y ρ0 cell lines.

Antibody Name	Dilution	Source	Catalog #
Tau12	1:10,000 (SY5Y lysates) 1:100,000 (Human brain tissue)	Kind gift of Dr. Christopher Gamblin	N/A
Tau7	1:10,000 (SY5Y lysates)	Kind gift of Dr. Christopher Gamblin	N/A
MtCO2	1:2,000	abcam	ab79393
β-Actin	1:5,000	Cell Signaling	CST3700
HDAC1	1:5,000	abcam	ab19845
GAPDH	1:5,000	Cell Signaling	CST2118
pTau Ser199	1:10,000	abcam	ab81268
TOC1	1:10,000	Kind gift from Dr. Nicholas Kanaan	N/A

Table 2.1. List of antibodies used in experiments

Taqman Primer	Catalog #
MAPT	Hs00902194_m1
ApoE	Hs00171168_m1
18s	Hs03003631_g1
TOMM40	Hs01587378_mH

Table 2.2. List of Taqman primers used in experiments

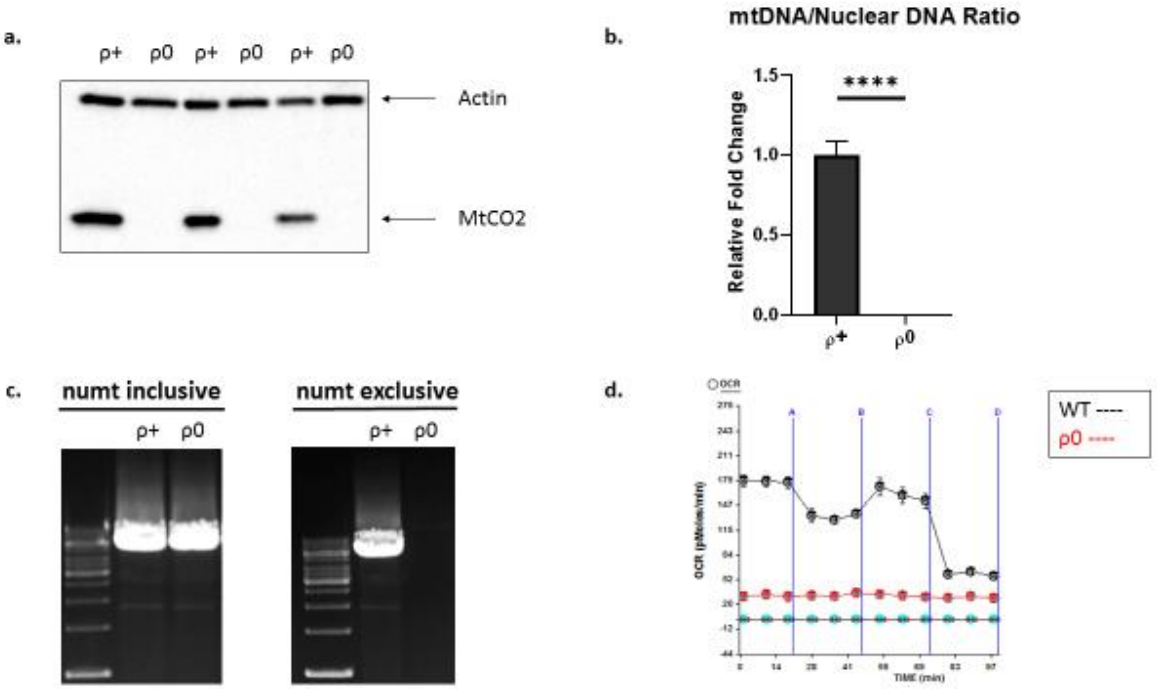
a.
ρ+ ρ0 ρ+ ρ0 ρ+ ρ0
Actin
MtCO2
b.
mtDNA/Nuclear DNA Ratio
****
Relative Fold Change
1.5
1.0
0.5
0.0
ρ+
ρ0
c.
numt inclusive
numt exclusive
ρ+ ρ0
ρ+ ρ0
d.
OCR
WT ----
ρ0 ----

Figure 2.1. Validation of ρ0 status. a) Western blot image of ρ+ and ρ0 whole cell lysates co-labeled with actin and MtCO2 antibodies. b) qPCR analysis of ρ+ and ρ0 DNA with mtDNA specific primers (ND1) and Nuclear DNA specific primers (β2M). n= 12 ρ+, 11 ρ0. c) Long-range PCR analysis of ρ+ and ρ0 DNA with a primer for a mitochondrial pseudogene (numt inclusive) and a primer exclusive for mtDNA (numt exclusive). d) Mitochondrial stress test of ρ+ and ρ0 cells using a Seahorse XF24 analyzer. n= 10 per group. $p<0.05$=*, $p<0.01$=**, $p<0.001$=***, $p<0.0001$=****. Error bars represent SEM.

Chronic mtDNA depletion increases tau protein levels and alters tau electrophoretic mobility

Since studies describe tau alterations following treatment with mitochondrial poisons and because mitochondrial defects occur in AD, we hypothesized respiratory chain incompetence would recapitulate AD-like tau alterations. In order to test this hypothesis, we first examined total tau protein levels in ρ0 whole cell lysates. The Tau12 antibody, whose epitope resides in tau's N-terminal region, revealed a significant, ~2-fold increase of tau protein in ρ0 cells relative to ρ+ cells (Figure 2.2d). Additionally, ρ0 lysates display multiple tau protein bands which are absent in ρ+ lysates. Initial western blots run on 4-15% gradient polyacrylamide gels showed a Tau12-reactive protein smear from ~55-70kDa and SDS-stable, high molecular weight tau (HMW tau) bands at ~110kDa in ρ0 lysates (data not shown). In order to better separate the Tau12 reactive protein smear, we performed subsequent SDS-PAGE analysis with 7.5% polyacrylamide gels. Superior resolution of the tau protein smear showed multiple tau protein bands specific to ρ0 cells along with two SDS-stable HMW tau bands (Figure 2.2b).

The N-terminal tau antibody, Tau12, revealed increased tau protein and HMW tau protein bands in ρ0 lysates. Tau protein is subject to cleavage at numerous sites [109, 151]. For this reason, we also labeled ρ+ and ρ0 lysates with a C-terminal tau antibody, Tau7. C-terminal tau protein labeling showed the same results as N-terminal tau labeling. ρ0 cells have significantly increased C-terminal tau protein levels as well as SDS-stable HMW tau protein bands (Figure 2.2c,d). Since these tau antibodies recognize epitopes in disparate regions of the protein, the similarity between their labeling patterns in ρ0 lysates suggests negligible differences in tau cleavage between the groups. Furthermore, the consistent labeling patterns observed between Tau12 and Tau7 antibodies suggests the extra bands in ρ0 lysates represent tau species rather than non-specific labeling.

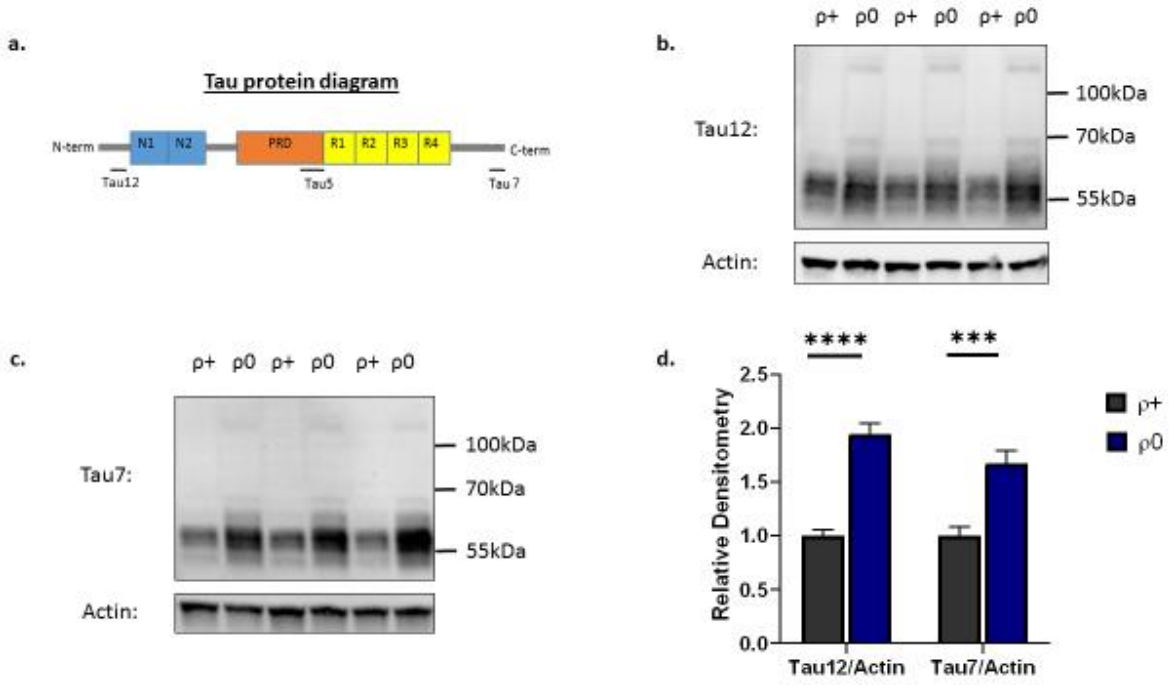
a.
Tau protein diagram
N-term
N1
N2
PRD
R1
R2
R3
R4
C-term
Tau12
Tau5
Tau 7
b.
ρ+ ρ0 ρ+ ρ0 ρ+ ρ0
Tau12:
100kDa
70kDa
55kDa
Actin:
c.
ρ+ ρ0 ρ+ ρ0 ρ+ ρ0
Tau7:
100kDa
70kDa
55kDa
Actin:
d.
****
***
Relative Densitometry
2.5
2.0
1.5
1.0
0.5
0.0
Tau12/Actin
Tau7/Actin
ρ+
ρ0

Figure 2.2. Chronic mtDNA depletion increases tau protein levels. a) Diagram of tau's protein domains, including the epitope locations of total tau antibodies. b) Western blot image of tau protein levels in ρ+ and ρ0 whole cell lysates using the Tau12 antibody. Tau12 antibody recognizes several additional tau protein bands in ρ0 lysates, including a HMW tau band. Actin serves as a loading control. c) Western blot image of tau protein levels in ρ+ and ρ0 whole cell lysates using the Tau7 antibody. Tau7 antibody also recognizes additional tau protein bands in ρ0 lysates, including a HMW tau band. Actin serves as a loading control. d) Densitometry analysis reveals significant increases in N-terminal and C-terminal tau relative to actin in ρ0 cells. n= 12 per group. $p<0.05$=*, $p<0.01$=**, $p<0.001$=***, $p<0.0001$=****. Error bars represent SEM.

Although tau's role in cytosolic microtubule stability has received much attention, tau also localizes to the nucleus. Tau's role in the nucleus remains unclear, but nuclear tau may protect genomic stability during times of stress. Tau also interacts with DNA and nuclear proteins [152]. We prepared cytosolic and nuclear enriched fractions to examine tau's subcellular localization in ρ+ and ρ0 cells. We found a consistent tau labeling pattern in the cytosolic and nuclear enriched fractions, with more tau localized in the cytosol. ρ0 cells displayed extra tau protein bands, including HMW tau bands, in both fractions. We labeled the fractions with Tau12 antibody, along with another N-terminal antibody, Tau13. Tau13 showed the same banding pattern as the other two tau antibodies, further substantiating the idea that the extra ρ0 protein bands represent bona fide tau species (Figure 2.3). The data does not suggest a change in tau's subcellular trafficking between the groups, but the results do reinforce the idea that additional tau protein species of higher molecular weight accumulate in ρ0 SH-SY5Y cells, and reveal that additional tau protein species localize to both the cytosol and nucleus.

Next, we used small interfering RNA (siRNA) directed against microtubule associated protein tau (MAPT) mRNA to confirm tau antibody specificity. Based on our prior experiments showing that three different tau antibodies (Tau12, Tau7, and Tau13) recognize additional HMW protein bands in ρ0 lysates, we predicted that MAPT siRNA treatment would reduce the levels of these protein species. Indeed, treating ρ0 cells with MAPT siRNA decreased the levels of all protein species recognized by the Tau12 and Tau7 antibodies (Figure 2.4). This provides additional evidence that the tau antibodies used in these experiments specifically label tau protein. After confirming tau antibody specificity, we feel comfortable claiming that ρ0 cells possess increased tau protein and additional tau protein bands of an unknown nature.

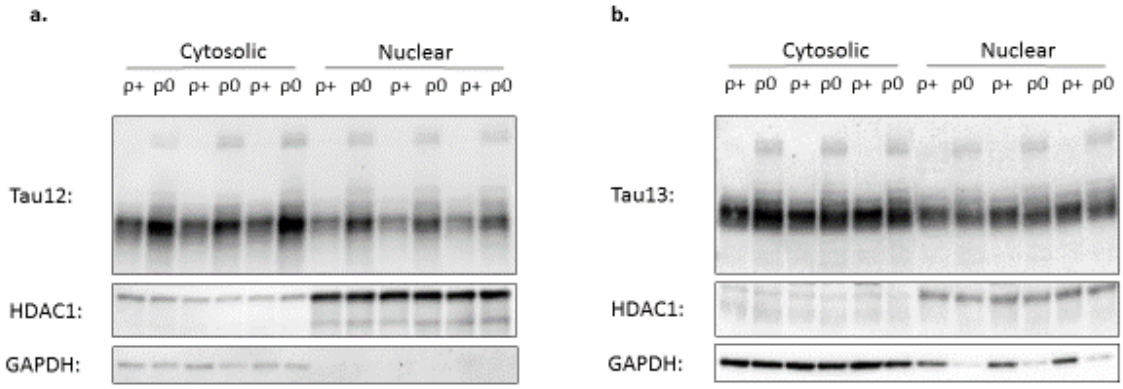
a.
Cytosolic
Nuclear
ρ+ ρ0 ρ+ ρ0 ρ+ ρ0 ρ+ ρ0 ρ+ ρ0 ρ+ ρ0
Tau12:
HDAC1:
GAPDH:
b.
Cytosolic
Nuclear
ρ+ ρ0 ρ+ ρ0 ρ+ ρ0 ρ+ ρ0 ρ+ ρ0 ρ+ ρ0
Tau13:
HDAC1:
GAPDH:

Figure 2.3. Cytosolic and nuclear enriched ρ0 protein fractions mirror the tau alterations observed in whole cell lysates. a) Western blot image of cytosolic and nuclear enriched protein fractions from ρ+ and ρ0 cells labeled with Tau12 antibody. HDAC1 serves as a marker of nuclear enrichment while GAPDH serves as a marker of cytosolic enrichment. b) Western blot image of cytosolic and nuclear enriched protein fractions from ρ+ and ρ0 cells labeled with Tau13 antibody. HDAC1 serves as a marker of nuclear enrichment while GAPDH serves as a marker of cytosolic enrichment.

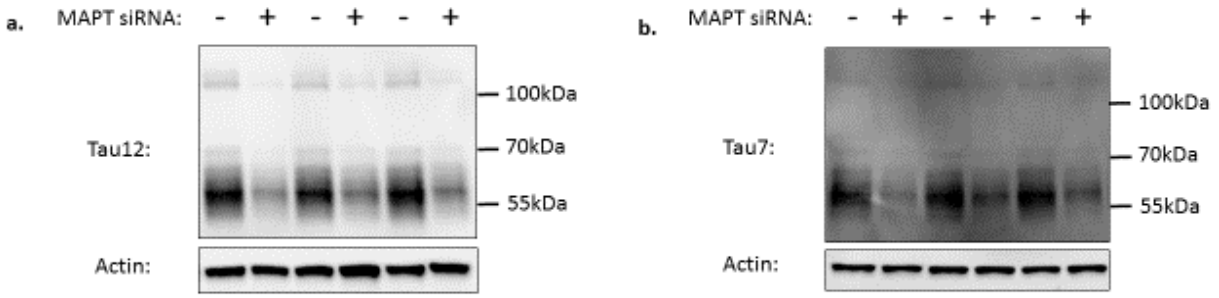
a.
MAPT siRNA: - + - + - +
Tau12:
Actin:
100kDa
70kDa
55kDa
b.
MAPT siRNA: - + - + - +
Tau7:
Actin:
100kDa
70kDa
55kDa

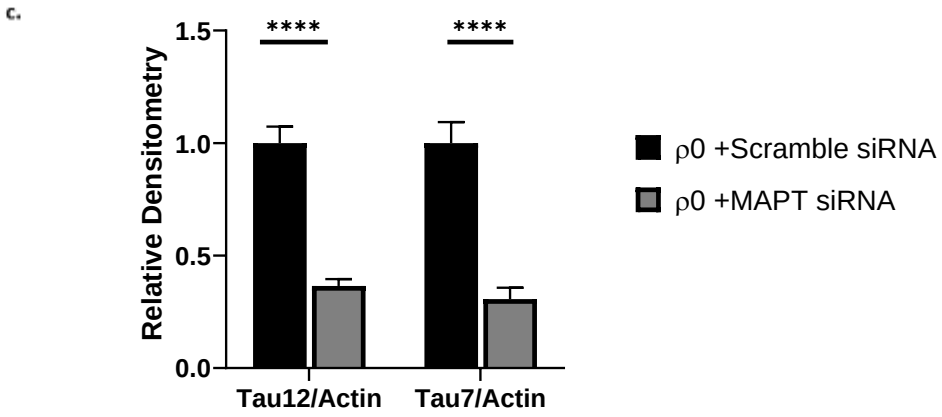
c.
Relative Densitometry
1.5
1.0
0.5
0.0
****
****
Tau12/Actin
Tau7/Actin
ρ0 +Scramble siRNA
ρ0 +MAPT siRNA

Figure 2.4. MAPT siRNA confirms tau antibody specificity. a) Western blot image of ρ0 whole cell lysates treated with scramble siRNA (-) or MAPT siRNA (+) labeled with Tau12 antibody. Actin served as a loading control. b) Western blot image of ρ0 whole cell lysates treated with scramble siRNA (-) or MAPT siRNA (+) labeled with Tau7 antibody. Actin served as a loading control. c) Densitometry analysis reveals a significant decrease in Tau12 and Tau7 labeling upon MAPT siRNA treatment relative to scramble siRNA treatment. n=12 per group. $p<0.05$=*, $p<0.01$=**, $p<0.001$=***, $p<0.0001$=****. Error bars represent SEM.

Chronic mtDNA depletion alters tau splicing, without affecting total tau mRNA levels

We next examined MAPT mRNA levels in ρ+ and ρ0 cells via qPCR. We chose MAPT primers designed to detect all MAPT mRNA isoforms, as the MAPT transcript undergoes alternative splicing [153]. Since tau protein levels increase in ρ0 cells, we predicted a concomitant increase in MAPT mRNA relative to ρ+ cells. However, the qPCR results showed no significant difference between ρ+ and ρ0 MAPT mRNA levels, suggesting increases in ρ0 tau protein do not occur due to increased tau transcript levels (Figure 2.5).

Although we found no change in total MAPT mRNA levels in mtDNA depleted cells, tau western blot results suggested changes in MAPT splicing may occur in ρ0 cells. SH-SY5Y ρ+ cells predominantly express the fetal tau isoform referred to as 0N3R [154]. The tau protein banding pattern observed in ρ0 cells resembles that of cells expressing multiple tau protein isoforms. With this in mind, we examined mRNA levels of various MAPT splice variants using qPCR. We designed multiple qPCR primers specific for MAPT's exon 2, which is subject to splicing, and primers specific for transcripts lacking exon 2. ρ0 cells show no change in MAPT transcripts lacking exon 2 (Figure 2.6b). However, ρ0 cells possess increased transcripts containing exon 2, suggesting the additional protein bands might stem from altered mRNA splicing (Figure 2.6c,d). We attempted to assess the level of other MAPT exons, however, these transcripts were below the limit of detection (data not shown).

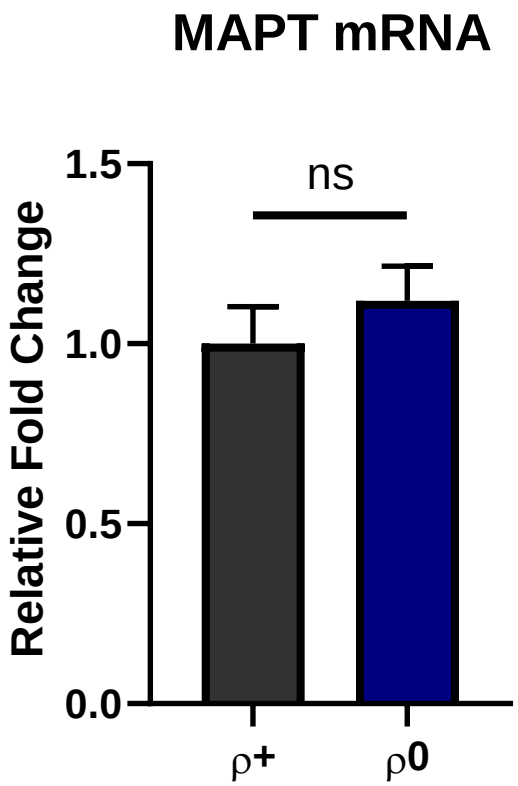
MAPT mRNA
ns
1.5
1.0
0.5
0.0
Relative Fold Change
ρ+
ρ0

Figure 2.5. Chronic mtDNA depletion does not alter MAPT mRNA levels. qPCR analysis of ρ+ and ρ0 MAPT mRNA levels reveals no significant difference between treatment groups. n= 12 per group. ns= No significant difference. Error bars represent SEM.

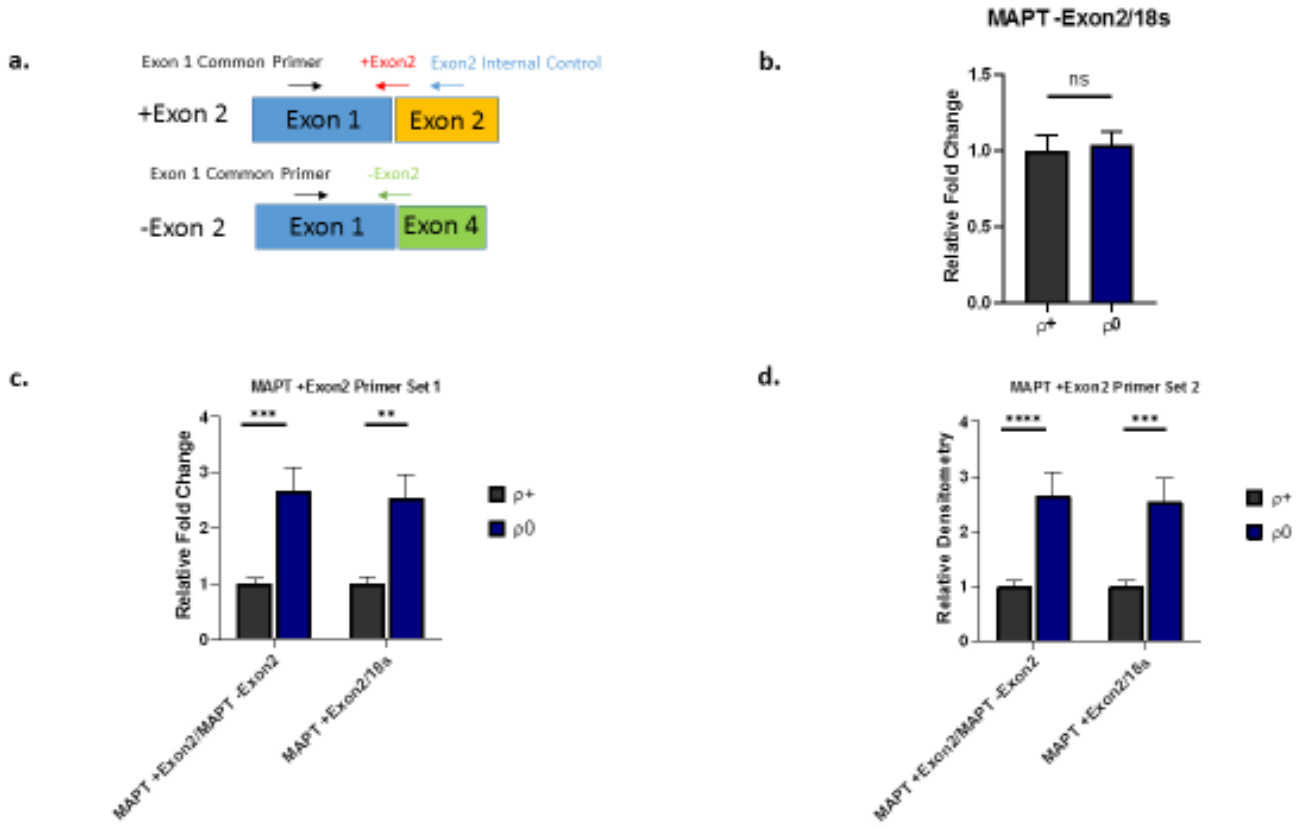
a.
Exon 1 Common Primer
+Exon2
Exon2 Internal Control
+Exon 2
Exon 1
Exon 2
Exon 1 Common Primer
-Exon2
-Exon 2
Exon 1
Exon 4
b.
MAPT -Exon2/18s
ns
Relative Fold Change
1.5
1.0
0.5
0.0
ρ+
ρ0
c.
MAPT +Exon2 Primer Set 1
***
**
Relative Fold Change
4
3
2
1
0
ρ+
ρ0
MAPT +Exon2/MAPT -Exon2
MAPT +Exon2/18s
d.
MAPT +Exon2 Primer Set 2
****
***
Relative Densitometry
4
3
2
1
0
ρ+
ρ0
MAPT +Exon2/MAPT -Exon2
MAPT +Exon2/18s

Figure 2.6. Chronic mtDNA depletion increases MAPT Exon2 mRNA levels. a) Diagram of MAPT primers designed to recognize mRNA species with exon 2 and without exon 2. b) qPCR analysis of MAPT mRNA lacking exon 2 reveals no significant difference between treatment groups. c) qPCR analysis with MAPT primers recognizing exon 2 reveals a significant increase in MAPT exon 2 levels in ρ0 cells. d) A second set of primers confirms the increase in MAPT exon 2 levels in ρ0 cells. ns= no significant difference. n= 12 per group. $p<0.05$=*, $p<0.01$=**, $p<0.001$=***, $p<0.0001$=****. Error bars represent SEM.

Next, we examined whether the additional ρ0 tau protein bands arise due to hyperphosphorylation. Tau electrophoretic mobility shifts based on phosphorylation status. We treated ρ+ and ρ0 lysates with lambda protein phosphatase to remove phosphate groups. Following lambda phosphatase treatment, the tau protein in ρ+ lysates shifted downwards into one sharp protein band. Lambda phosphatase treatment in ρ0 lysates also shifted the tau protein bands downward, although the additional tau protein bands persisted, suggesting hyperphosphorylation does not explain ρ0 tau's aberrant electrophoretic mobility (Figure 2.7a). Tau's electrophoretic mobility shifted following the lambda phosphatase treatment, suggesting the process effectively dephosphorylated tau protein. Tau dephosphorylation allowed for easier comparison of the major tau band present in ρ+ cells. This band likely represents the smallest tau isoform, 0N3R tau. 0N3R tau levels increase in ρ0 cells relative to ρ+ cells, as does total tau protein level (Figure 2.7b).

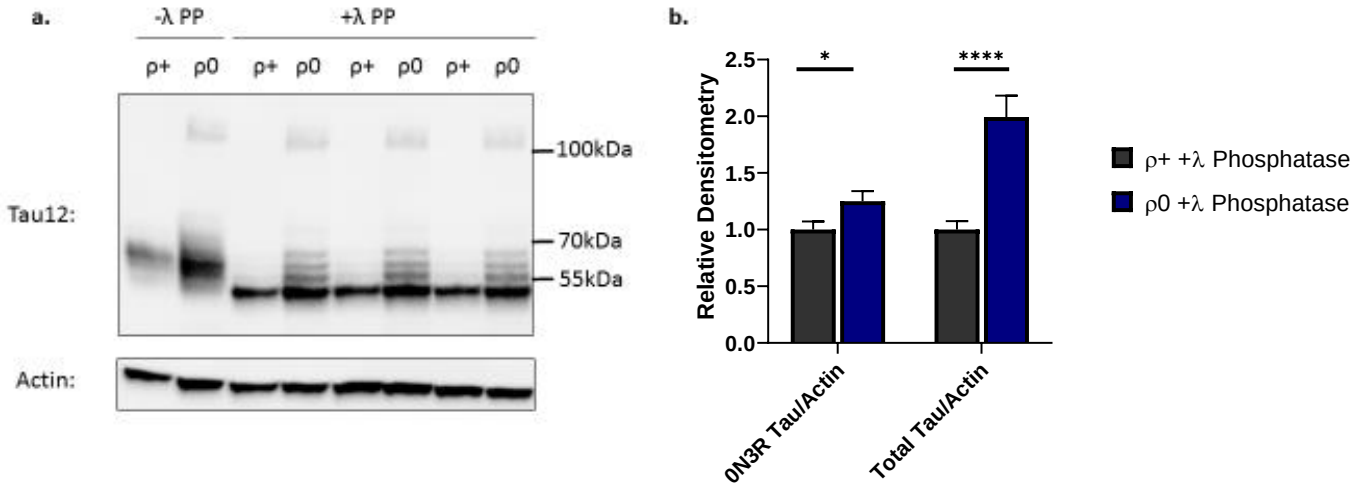
a.
-λ PP
+λ PP
ρ+ ρ0 ρ+ ρ0 ρ+ ρ0 ρ+ ρ0
Tau12:
Actin:
100kDa
70kDa
55kDa
b.
Relative Densitometry
2.5
2.0
1.5
1.0
0.5
0.0
*
****
0N3R Tau/Actin
Total Tau/Actin
ρ+ +λ Phosphatase
ρ0 +λ Phosphatase

Figure 2.7. Phosphatase treatment fails to remove extra ρ0 tau protein bands. a) Western blot image of ρ+ and ρ0 whole cell lysates treated with lambda phosphatase (λ PP) labeled with Tau12 antibody. Tau protein bands experience an electrophoretic mobility shift, while extra ρ0 tau protein bands and HMW tau persist following λ PP treatment. b) Densitometry analysis reveals increased levels of the smallest tau isoform (0N3R) and increased total tau levels in ρ0 cells following λ PP treatment. n= 12 per group. $p<0.05$=*, $p<0.01$=**, $p<0.001$=***, $p<0.0001$=****. Error bars represent SEM.

Chronic respiratory chain deficiency causes AD-relevant tau species to accumulate

Although our data suggests tau hyperphosphorylation does not cause tau protein's electrophoretic mobility shift in mtDNA-depleted lysates, we examined AD-relevant phospho-tau sites in ρ0 lysates. Tau hyperphosphorylation occurs in AD brains and a recent study found phosphorylation increases heavily at Ser199 in late Braak stages [155]. We found that chronic respiratory chain incompetence increases pTau Ser199 levels relative to β-actin. However, the ρ0 cells do not display a change in the pTau Ser199/total tau ratio, suggesting this increase may stem from general tau protein accumulation rather than altered kinase/phosphatase activities (Figure 2.8). It is interesting to note that the pTau Ser199 antibody labels a HMW band (above 100kDa) in both ρ+ and ρ0 lysates. This is in contrast to the HMW tau band labeled by total tau antibodies, which only appears in ρ0 lysates.

Based on the molecular weight of the ρ0 HMW tau protein bands (~110kDa), we hypothesize that they may represent SDS-stable tau dimers/oligomers. SDS-stable tau oligomers increase in AD brains, and *in vitro* experiments suggest they are a transition state between monomeric tau and higher order polymeric species which constitute insoluble NFTs [156]. To assess oligomeric tau levels in ρ+ and ρ0 cells, we used an antibody named tau oligomeric complex 1 (TOC1). TOC1 specifically recognizes tau dimers and slightly larger oligomers, with minimal reactivity towards monomeric and polymeric tau species. TOC1 recognizes a conformational tau epitope associated with dimerization [147]. Denaturing conditions destroy the TOC1 epitope, thus we examined TOC1 levels using dot blots, a non-denaturing assay. Dot blot analysis of ρ+ and ρ0 lysates reveal significantly increased TOC1 reactivity in ρ0 lysates, suggesting increased tau dimers/oligomers. Similar to tau phosphorylation at Ser199, ρ0 oligomeric tau levels increase relative to total protein but no change occurs in the oligomeric tau

to total tau ratio (Figure 2.9). The results suggest ρ0 cells accumulate tau protein without changing the rate of tau oligomerization.

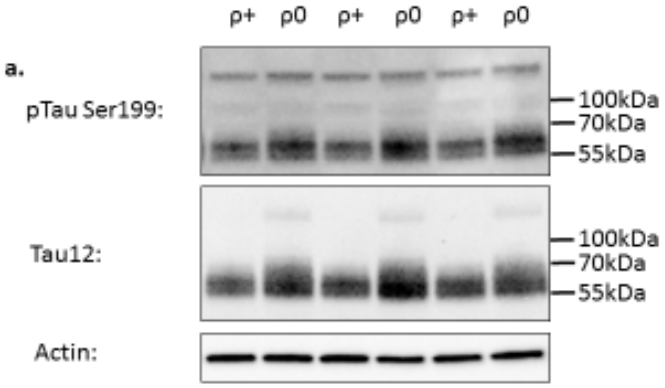
a.
ρ+ ρ0 ρ+ ρ0 ρ+ ρ0
pTau Ser199:
100kDa
70kDa
55kDa
Tau12:
100kDa
70kDa
55kDa
Actin:

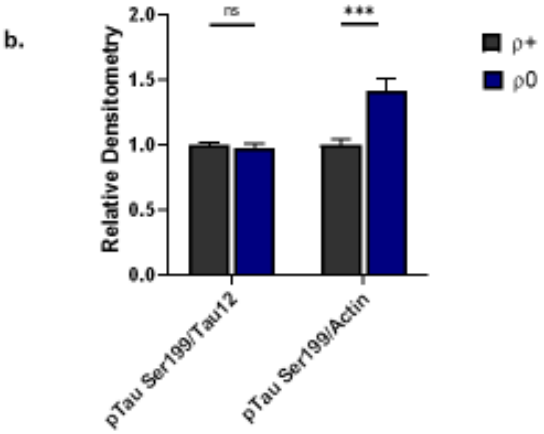
b.
Relative Densitometry
2.0
1.5
1.0
0.5
0.0
ns
***
ρ+
ρ0
pTau Ser199/Tau12
pTau Ser199/Actin

Figure 2.8. Chronic mtDNA depletion leads to accumulation of tau phosphorylated at serine 199. a) Western blot image of ρ+ and ρ0 whole cell lysates labeled with pTau Ser199 antibody. b) Densitometry analysis reveals no significant change in the pTau Ser199/Tau12 ratio but a significant increase in the pTau Ser199/Actin ratio. n= 12 per group. ns= no significant difference. p<0.05=*, p<0.01=**, p<0.001=***, p<0.0001=****. Error bars

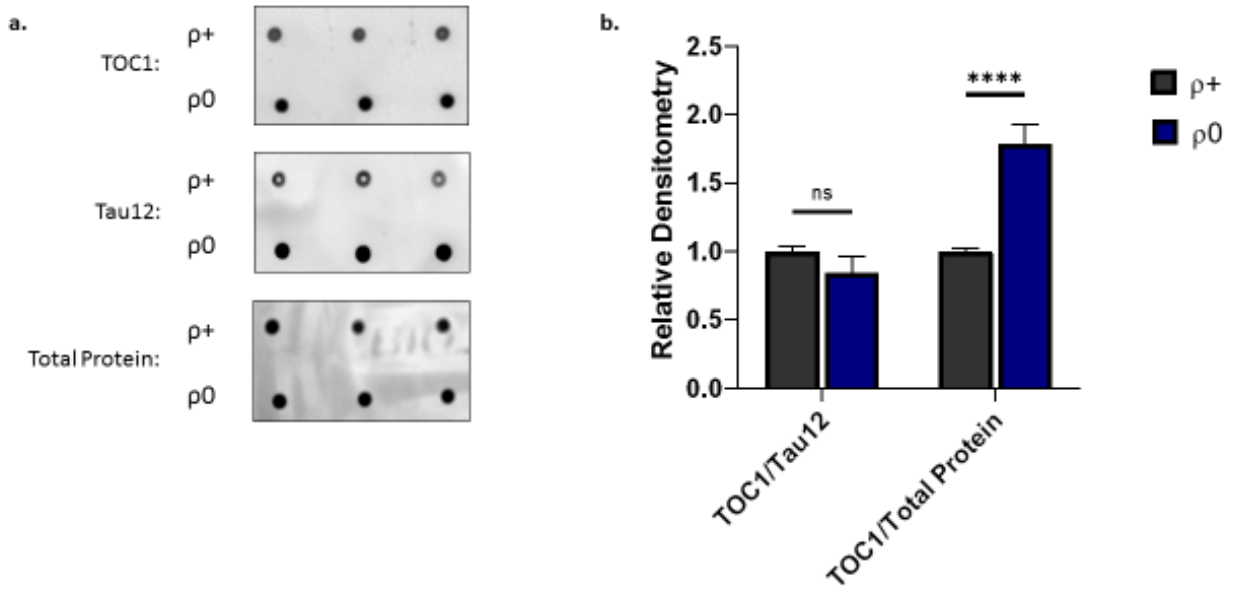
a.
TOC1:
ρ+
ρ0
Tau12:
ρ+
ρ0
Total Protein:
ρ+
ρ0
b.
Relative Densitometry
2.5
2.0
1.5
1.0
0.5
0.0
ns
****
ρ+
ρ0
TOC1/Tau12
TOC1/Total Protein

Figure 2.9. Chronic mtDNA depletion leads to oligomeric tau accumulation. Dot blot images of ρ+ and ρ0 whole cell lysates labeled with TOC1 and Tau12 antibody. Amido black staining labels total protein as a loading control. b) Densitometry analysis reveals no significant difference in the TOC1/Tau12 ratio between treatment groups, while ρ0 cells have a significantly elevated TOC1/Total Protein ratio. n= 12 per group. ns= no significant difference. $p<0.05$=*, $p<0.01$=**, $p<0.001$=***, $p<0.0001$=****. Error bars represent SEM.

Acute mtDNA depletion increases tau oligomerization

ρ0 cells experience chronic respiratory deficiency and display alterations in tau homeostasis. We also examined tau alterations following acute respiratory deficiency. mtDNA depletion via EtBr treatment caused acute respiratory defects. We treated SH-SY5Y cells with EtBr for 24hrs, 3days and 7days. These time points corresponded to ~50%, ~75%, and ~95% mtDNA depletion, respectively (Figure 2.10). First, we measured tau mRNA levels following EtBr treatment, and found no change in mRNA levels (Figure 2.11). We examined tau oligomerization at each of these time points. 24hr EtBr treatment had no effect on tau oligomer levels when normalized to total tau protein levels or total cellular protein levels. 3 day and 7 day EtBr treatment significantly increased the levels of tau oligomers relative to untreated SH-SY5Y cells (Figure 2.12). TOC1 immunoreactivity increased regardless of whether the values were normalized to total tau or total protein, suggesting a shift in tau oligomerization rate occurs upon mtDNA depletion.

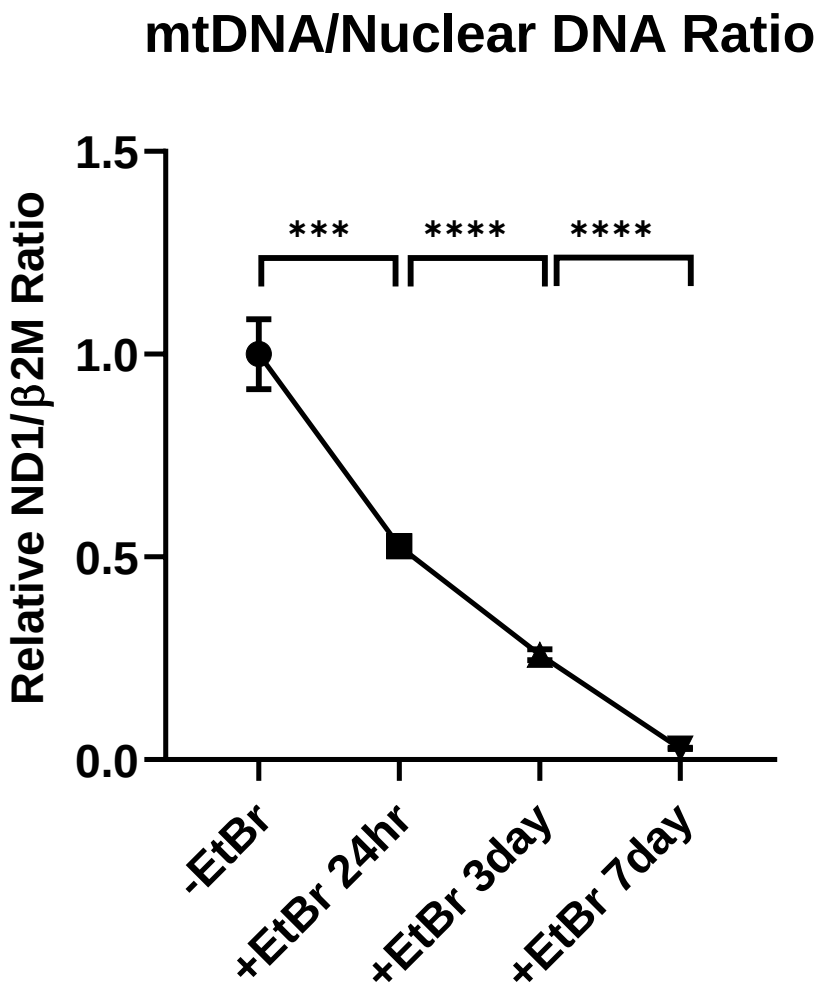
mtDNA/Nuclear DNA Ratio
Relative ND1/β2M Ratio
1.5
1.0
0.5
0.0
***
****
****
-EtBr
+EtBr 24hr
+EtBr 3day
+EtBr 7day

Figure 2.10. EtBr treatment reduces mtDNA levels. qPCR analysis utilizing primers specific for mtDNA (ND1) and nuclear DNA (β2M) reveals significant, time course dependent decreases in the mtDNA/Nuclear DNA ratio in SH-SY5Y cells treated with EtBr. n= 12 per group. $p<0.05$=*, $p<0.01$=**, $p<0.001$=***, $p<0.0001$=****. Error bars represent SEM.

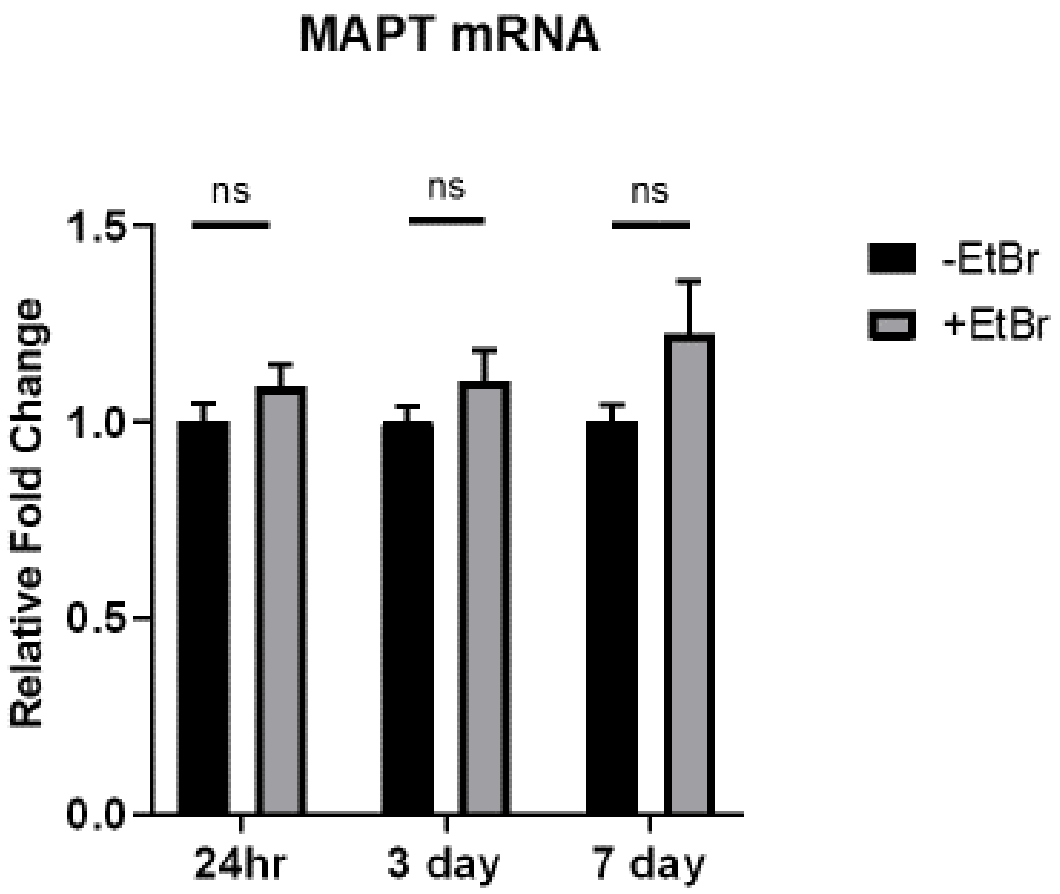
MAPT mRNA
ns
ns
ns
1.5
1.0
0.5
0.0
Relative Fold Change
24hr
3 day
7 day
-EtBr
+EtBr

Figure 2.11. EtBr treatment does not affect MAPT mRNA levels. qPCR analysis utilizing MAPT primers reveals no significant changes in MAPT mRNA levels in SH-SY5Y cells treated with EtBr. n= 12 per group. ns= no significant difference. Error bars represent SEM.

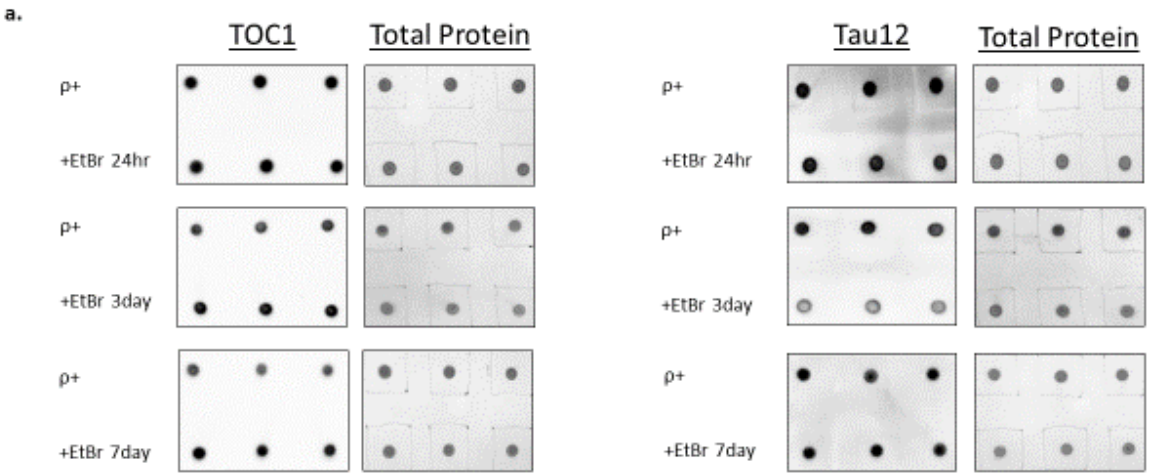
a.
TOC1
Total Protein
Tau12
Total Protein
ρ+
+EtBr 24hr
ρ+
+EtBr 3day
ρ+
+EtBr 7day
ρ+
+EtBr 24hr
ρ+
+EtBr 3day
ρ+
+EtBr 7day

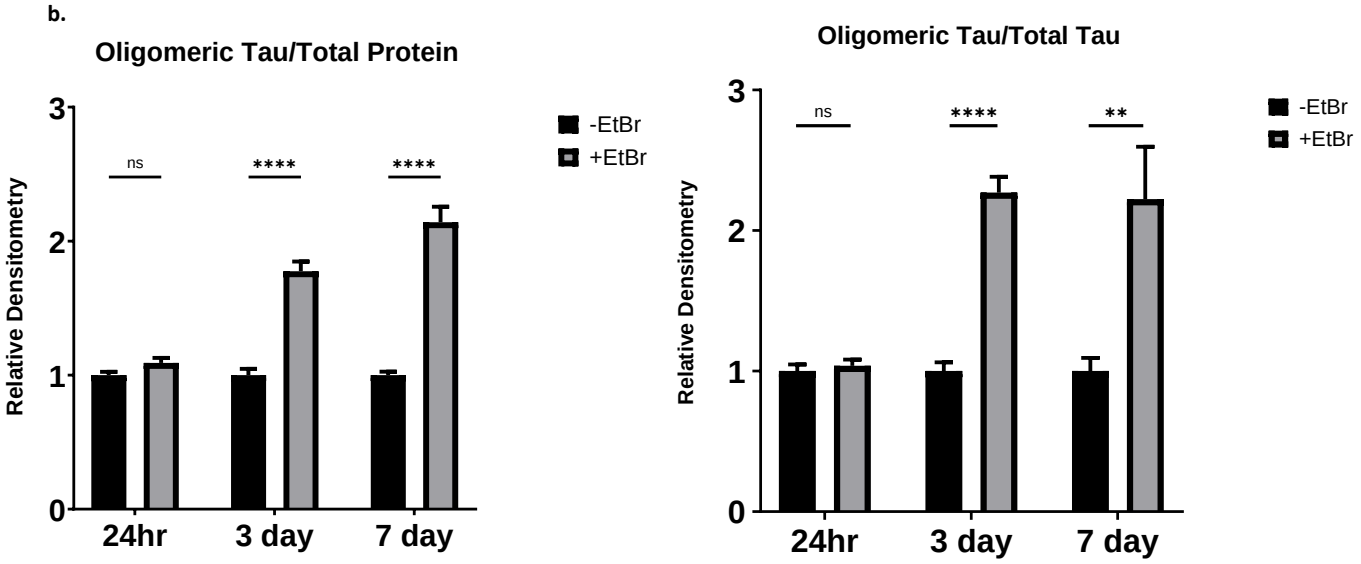
b.
Oligomeric Tau/Total Protein
Relative Densitometry
3
2
1
0
ns
****
****
24hr
3 day
7 day
-EtBr
+EtBr
Oligomeric Tau/Total Tau
Relative Densitometry
3
2
1
0
ns
****
**
24hr
3 day
7 day
-EtBr
+EtBr

Figure 2.12. Acute mtDNA depletion increases tau oligomerization. a) Dot blot images of EtBr treated SH-SY5Y cells labeled with TOC1 and Tau12. Amido black staining labels total protein as a loading control. b) Densitometry analysis reveals significant increases in the TOC1/Tau12 and TOC1/Total protein ratios following 3 days and 7 days EtBr treatment. n= 12 per group. $p<0.05$=*, $p<0.01$=**, $p<0.001$=***, $p<0.0001$=****. Error bars represent SEM.

AD brain tissue and AD cybrids both increase tau oligomerization

Prior reports have shown increased TOC1 immunoreactivity in AD brain tissue relative to controls, suggesting AD brains possess increased tau oligomers [156]. Here, as a positive control, we examined TOC1 levels via dot blot in AD and age-matched, non-demented control (ND) brain tissue. The AD brains displayed an increased TOC1 to total tau ratio and TOC1 to total protein ratio relative to ND brain tissue, confirming results from earlier studies (Figure 2.13). Next, we examined tau oligomerization in ND and AD cybrids. We found increased TOC1 immunoreactivity in AD cybrids relative to ND cybrids. The TOC1 to total tau ratio and TOC1 to total protein ratio both significantly increased in AD cybrids, suggesting not only an increase in TOC1 levels but also a shift in the tau oligomerization rate (Figure 2.14).

Since we observed that acute mtDNA depletion increases tau oligomerization, we examined mtDNA levels in the ND and AD cybrids. The AD cybrids displayed a modest, but significant, 9% decrease in mtDNA levels relative to ND cybrids (Figure 2.15a). We also examined the level of mtDNA D-loop relative to ND1 DNA as a measure of mtDNA synthesis rate. No change in the mtDNA synthesis rate exists between the ND and AD cybrids, according to this assay (Figure 2.15b). We also measured total tau protein levels and tau phosphorylated at Ser199 in AD cybrids. AD cybrids display no change in total tau protein levels or the level of tau phosphorylation at Ser199 (Figure 2.16).

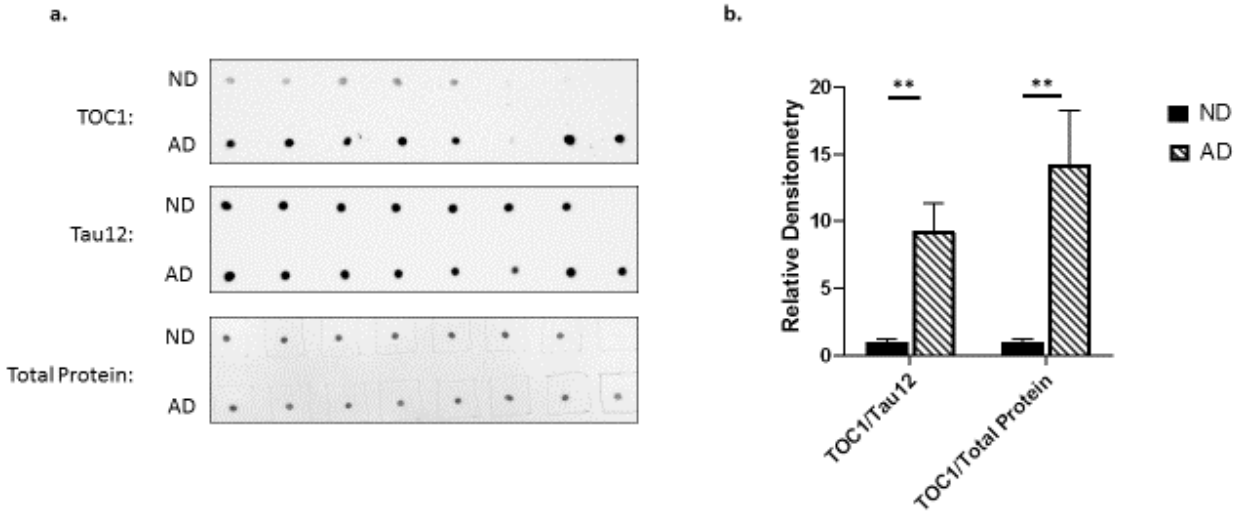
a.
TOC1:
ND
AD
Tau12:
ND
AD
Total Protein:
ND
AD
b.
Relative Densitometry
20
15
10
5
0
**
**
ND
AD
TOC1/Tau12
TOC1/Total Protein

Figure 2.13. AD brains possess increased tau oligomers. a) Dot blot images of non-demented, age-matched control (ND) brain tissue and AD brain tissue labeled with TOC1 and Tau12 antibodies. Amido black labels total protein as a loading control. b) Densitometry analysis reveals a significant increase in the TOC1/Tau12 and TOC1/Total protein ratios in AD brain tissue. n= 7 ND, 8 AD. $p<0.05$=*, $p<0.01$=**, $p<0.001$=***, $p<0.0001$=****. Error bars represent SEM.

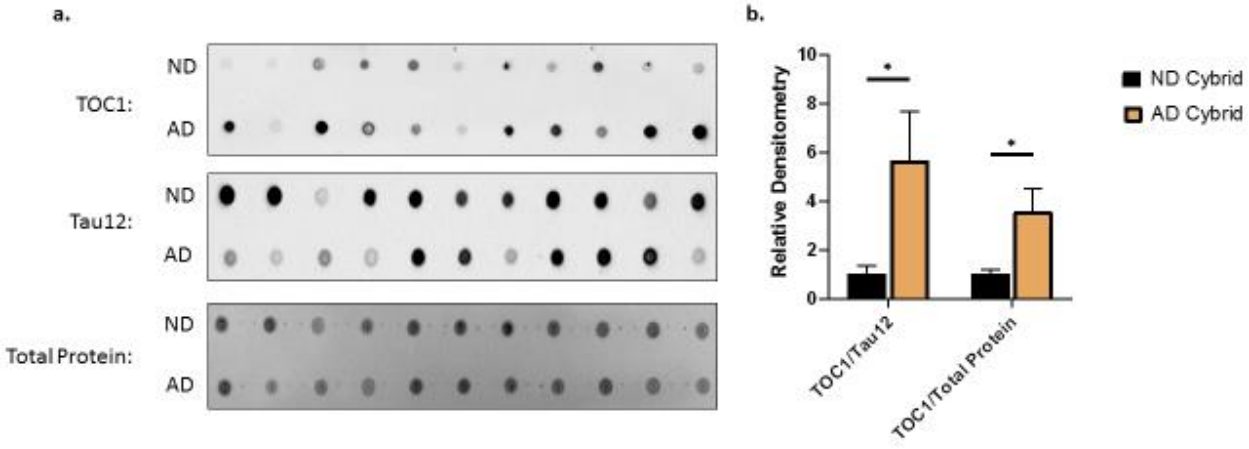
a.
TOC1:
ND
AD
Tau12:
ND
AD
Total Protein:
ND
AD
b.
Relative Densitometry
10
8
6
4
2
0
*
*
TOC1/Tau12
TOC1/Total Protein
ND Cybrid
AD Cybrid

Figure 2.14. AD cybrids display increased oligomeric tau levels. a) Dot blot image of non-demented, age matched control cybrids and AD cybrids labeled with TOC1 and Tau12 antibodies. b) Densitometry analysis reveals significant increases in the TOC1/Tau12 ratio and TOC1/Total protein ratio among AD cybrids relative to ND cybrids. n= 11 per group. $p<0.05$=*, $p<0.01$=**, $p<0.001$=***, $p<0.0001$=****. Error bars represent SEM.

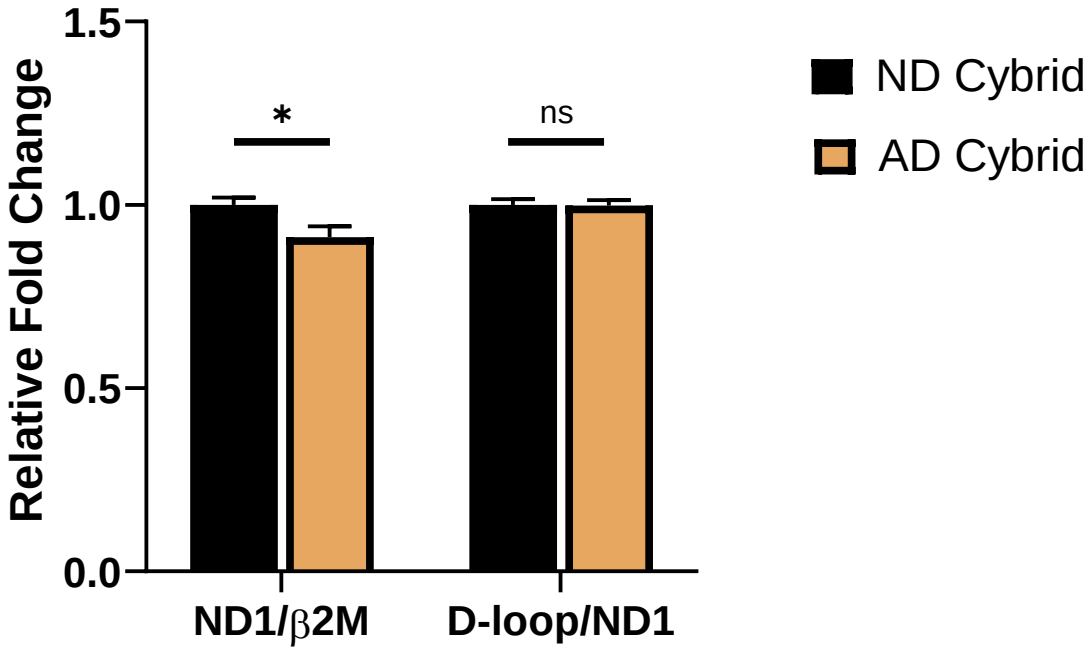
1.5
1.0
0.5
0.0
Relative Fold Change
*
ns
ND1/β2M
D-loop/ND1
ND Cybrid
AD Cybrid

Figure 2.15. mtDNA levels decrease in AD cybrids. qPCR analysis utilizing primers specific for mtDNA (ND1) and nuclear DNA (β2M) reveals a significant decrease in the mtDNA/Nuclear DNA ratio in AD cybrids relative to control cybrids. D-loop/ND1 ratios do not change in the AD cybrids. n= 11 per group. $p<0.05$=*, $p<0.01$=**, $p<0.001$=***, $p<0.0001$=****. Error bars represent SEM.

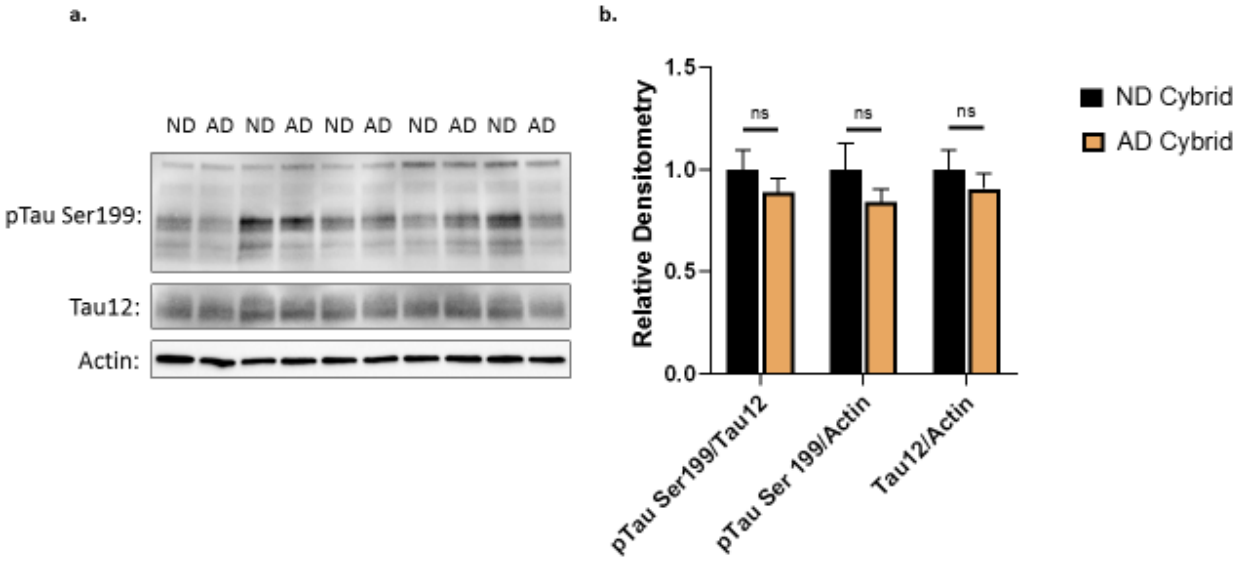
a.
ND AD ND AD ND AD ND AD ND AD
pTau Ser199:
Tau12:
Actin:
b.
Relative Densitometry
1.5
1.0
0.5
0.0
ns
ns
ns
pTau Ser199/Tau12
pTau Ser 199/Actin
Tau12/Actin
ND Cybrid
AD Cybrid

Figure 2.16. AD cybrids display no change in pTau Ser199 or total tau protein levels. a) Western blot images of non-demented, age-matched controls (ND) and Alzheimer's disease (AD) cybrid whole cell lysates labeled with phospho-Tau Ser199, Tau12 (total tau), and actin antibodies. b) Densitometry analysis reveals no significant difference in pTau Ser199/Tau12, pTau Ser199/Actin, and Tau12/Actin protein levels between ND and AD cybrids. ns= No significant difference. Error bars represent SEM.

Chronic respiratory chain incompetence increases ApoE mRNA and protein levels

Next, we examined mitochondrial dysfunction's effects on ApoE and translocase of the outer mitochondrial membrane 40 (TOMM40). Studies have established ApoE as the strongest genetic risk factor for sporadic AD. Certain ApoE variants appear to impact mitochondrial function but, here, we asked whether mitochondrial dysfunction impacts ApoE [157]. We found that ρ0 cells possess ~50-fold more ApoE mRNA relative to ρ+ cells. We also measured TOMM40 mRNA in ρ+ and ρ0 cells because the TOMM40 gene exists in linkage disequilibrium with the ApoE gene and groups have suggested TOMM40 variants may contribute to the AD risk associated with the ApoE gene region [158]. ρ0 cells display decreased TOMM40 mRNA levels relative to ρ+ cells (Figure 2.17). Since ApoE is secreted from the cell, we measured ApoE protein levels in ρ+ and ρ0 cell culture media. ApoE ELISAs revealed significantly increased ApoE levels in the ρ0 media relative to ρ+ media (Figure 2.18).

a.

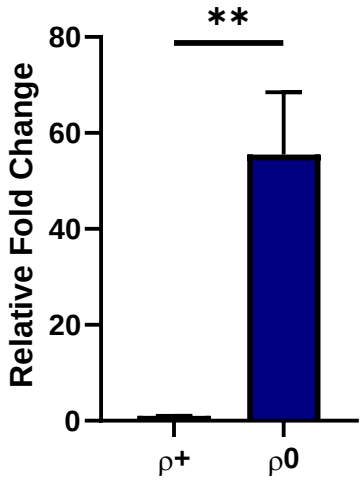
ApoE mRNA
**
Relative Fold Change
80
60
40
20
0
ρ+
ρ0

b.

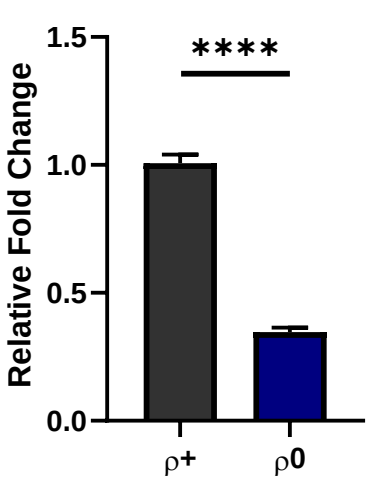
TOMM40 mRNA
****
Relative Fold Change
1.5
1.0
0.5
0.0
ρ+
ρ0

Figure 2.17. Chronic mtDNA depletion increases ApoE mRNA while decreasing TOMM40 mRNA. a) qPCR analysis reveals a significant increase in ApoE mRNA in ρ0 cells relative to control. b) qPCR analysis reveals a significant decrease in TOMM40 mRNA in ρ0 cells relative to control. n= 12 per group. $p<0.05$=*, $p<0.01$=**, $p<0.001$=***, $p<0.0001$=****. Error bars represent SEM.

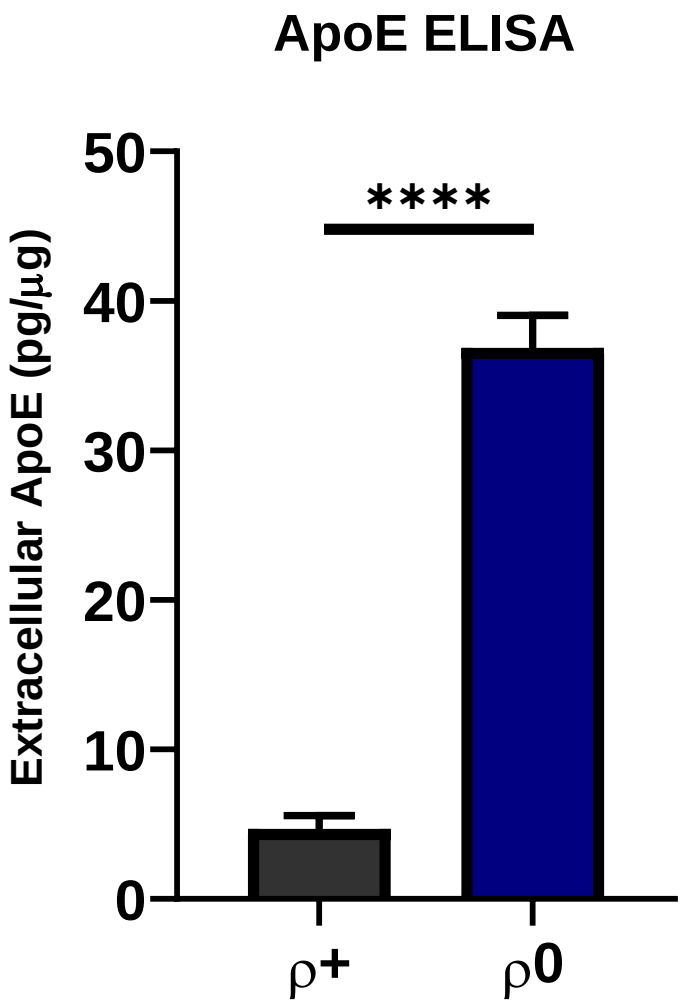
ApoE ELISA
Extracellular ApoE (pg/µg)
50
40
30
20
10
0
****
ρ+
ρ0

Figure 2.18. Chronic mtDNA depletion increases extracellular ApoE protein levels. The ELISA reveals a significant increase in ApoE in the cell culture media of ρ0 cells relative to control. n= 12 per group. $p<0.05$=*, $p<0.01$=**, $p<0.001$=***, $p<0.0001$=****. Error bars represent SEM.

Discussion

Here, we studied the relationship between mitochondrial dysfunction and AD-pathology. We examined tau alterations following chronic (ρ0) and acute mtDNA depletion, and in AD cybrids. By manipulating the cell's mtDNA, we were able to alter mitochondrial function and learn how mtDNA impacts aggregation-prone proteins. Respiratory chain deficiency triggered numerous AD-like tau alterations, suggesting bioenergetic failure could contribute to AD pathology.

We observed tau protein accumulation in ρ0 cells. Three tau antibodies, all recognizing different epitopes, revealed similar increases in ρ0 tau protein levels. Two of the tau antibodies (Tau12 and Tau13) recognize N-terminal epitopes, while one antibody (Tau7) recognizes a C-terminal epitope. It was important to label N-terminal and C-terminal tau, as caspases and calpains can cleave tau and tau cleavage is associated with aggregation [159, 160]. The fact that N-terminal and C-terminal tau antibodies showed similar changes in ρ0 tau suggests that high rates of tau cleavage do not occur in ρ0 cells. Despite increased tau protein levels in ρ0 cells, we found no corresponding change in *MAPT* mRNA levels between ρ+ and ρ0 cells. This suggests tau accumulates in ρ0 cells due to post-transcriptional mechanisms, such as an altered translation or clearance rate.

In addition to showing increased total tau levels, western blot analysis of ρ0 tau protein revealed changes in tau's electrophoretic mobility. Initially, we electrophoretically separated ρ0 protein using 4-12% polyacrylamide gels. Under these conditions, ρ0 tau protein appeared as a smear between 55 and 70 kDa, with an additional, high molecular weight band above 100 kDa. To better resolve the protein smear from 55 kDa to 70 kDa, we began using 7.5% polyacrylamide gels. 7.5% gels provide superior protein separation around these molecular

weights and revealed a number of discrete tau protein bands exist in ρ0 cells, which are absent in ρ+ lysates. Tau hyperphosphorylation can cause electrophoretic mobility shifts similar to those observed in AD brain lysates [161, 162]. To determine whether tau hyperphosphorylation causes the ρ0 tau electrophoretic mobility shift, we treated ρ+ and ρ0 lysates with lambda phosphatase to dephosphorylate tau. Consistent with the literature, SH-SY5Y ρ+ lysates displayed one major tau protein band following lambda phosphatase treatment. This band likely represents the fetal tau isoform, 0N3R, the major tau isoform expressed in undifferentiated SY5Y cells [163, 164]. The extra tau protein bands in ρ0 lysates persisted following lambda phosphatase treatment, suggesting that hyperphosphorylation does not explain the observed electrophoretic mobility shift.

Six tau isoforms exist in the human adult brain, due to alternative splicing. Their molecular weights range between 45 and 65 kDa on SDS-PAGE [165]. Altered tau splicing is implicated in numerous tauopathies, and may favor tau aggregation [166, 167]. Prior studies establish a relationship between mitochondrial dysfunction and tau splicing. Complex I inhibition increases 4-repeat tau [116]. The additional tau protein bands from 55 kDa to 75 kDa in ρ0 lysates likely represent tau isoforms which ρ+ cells do not express at an appreciable level. In support of this idea, we found changes in ρ0 tau mRNA splicing. ρ0 cells increase *MAPT* exon 2 inclusion as evidenced by qPCR analysis with exon 2 specific primers. Future analysis of ρ0 tau splicing with splice variant specific antibodies could answer questions that were left unaddressed in these studies.

Although splice variants seem a likely explanation for the extra ρ0 tau protein bands from 55-75 kDa, the tau protein bands above 100 kDa (HMW tau) could represent another tau splice variant or tau dimers/oligomers. Cells of the peripheral nervous system express a tau splice

variant referred to as “big tau” or “high molecular weight tau”, which migrates around 110-130 kDa on SDS-PAGE [168]. HMW tau species of a similar molecular weight have been observed at low levels in AD brains and as a component of PHFs, although the precise nature of these HMW tau species remains unclear [169, 170]. A publication observing HMW tau species in AD brains hypothesized that the high molecular weight bands represented tau dimers/oligomers [156]. We cannot definitively say whether the HMW tau band in ρ0 cells represents a tau splice variant or dimer/oligomer. However, we can say with confidence that this protein species represents some form of tau, rather than a non-specific protein band. *MAPT* siRNA confirmed the specificity of the Tau12 and Tau7 antibodies, as tau mRNA knockdown led to decreases in all ρ0 protein bands recognized by these antibodies.

Knowing that ρ0 HMW tau runs at a molecular weight consistent with tau dimers/oligomers, we next assayed ρ+ and ρ0 lysates with the TOC1 antibody, which is specific for tau oligomers and displays minimal reactivity with tau monomers or polymers. Tau dimerization favors tau aggregation into larger insoluble aggregates, suggesting tau dimers occur early in the disease process [156]. While numerous lines of evidence suggest NFTs do not impart severe toxicity, studies suggest tau oligomers contribute to neurodegeneration [171]. Since the TOC1 antibody recognizes a conformational epitope, we used dot blots, a non-denaturing assay, to measure oligomeric tau levels. We found increased oligomeric tau levels in ρ0 cells relative to ρ+ cells, however, there was no change in the ratio of oligomeric tau to total tau. Similarly we saw increased tau phosphorylated at Ser199 in ρ0 cells, but no shift in the ratio of pTau Ser199 to total tau. Based on these results, it appears chronic respiratory chain incompetence causes multiple tau species to accumulate, rather than shifting the ratio of tau species.

Altered tau secretion could contribute to ρ0 intracellular tau accumulation. Previous studies show that SY5Y cells secrete endogenous tau in a manner sensitive to calcium homeostasis. The classical secretory pathway does not appear to mediate tau export, nor does tau appear to be released in large quantities via exosomes. Other studies suggest tau exits neurons via the type I unconventional protein secretion pathway. In this paradigm, tau associates with heparin sulfate proteoglycans in the plasma membrane which facilitates its exit from the cell [172, 173]. Since tau's release depends on calcium homeostasis, and previous reports show SY5Y ρ0 calcium homeostasis is disturbed, it seems possible that chronic mtDNA depletion could affect tau secretion by altering calcium signaling [174].

We found that acute mtDNA depletion triggered tau alterations, although the effects differed from those observed under chronic mtDNA depletion. Similar to chronic mtDNA depletion, acute mtDNA depletion did not change *MAPT* mRNA levels. Although acute mtDNA depletion did not increase intracellular tau, it did stimulate tau oligomerization. We observed significantly increased oligomeric tau following acute mtDNA depletion. In contrast to chronic mtDNA depletion, acute mtDNA depletion changed the oligomeric tau to total tau ratio. Oligomeric tau levels increased following 3 days and 7 days EtBr treatment, and total tau levels did not increase under these conditions. These findings suggest acute mtDNA depletion shifts the intracellular tau pool towards a more aggregated state. Although we only measured soluble tau oligomers, it would be interesting to know whether NP40-insoluble tau levels increase following acute mtDNA depletion.

mtDNA depletion stimulates tau oligomerization, although how decreased mtDNA favors tau oligomerization remains unclear. The current leading hypotheses suggest tau hyperphosphorylation favors tau release from microtubules, ultimately leading tau monomers to

bind, forming oligomers [171]. Indeed, one study found tau hyperphosphorylation can favor oligomer formation, but has no effect on tau fibril formation. Tau hyperphosphorylation alone was not sufficient to induce tau oligomerization, however. Hyperphosphorylated tau formed oligomeric tau species only when tau levels became concentrated [175]. Additional reports show cleavage by a matrix mettaloprotease can favor oligomeric tau formation, while tau hyperphosphorylation in the presence of metal ions enhances tau oligomerization [176, 177]. Here, we observe increased tau oligomers absent increased tau phosphorylation, suggesting acute mtDNA depletion does not increase oligomers by inducing tau hyperphosphorylation. Furthermore, we do not observe increased tau protein levels upon acute mtDNA depletion. Increased tau concentration can favor oligomerization, but increased tau concentration is not observed under these conditions.

In order to tie these findings more closely to AD, we examined oligomeric tau levels in AD brain tissue and AD cybrids. Previous studies found increased soluble tau oligomers in AD brains relative to age-matched controls [156]. Here, we confirmed these results in the ADC's AD cohort. We observed a drastic increase in soluble oligomeric tau in our AD cohort, with no concomitant change in soluble total tau levels.

To our knowledge, no one has measured oligomeric tau levels in AD cybrids. AD cybrids model AD mitochondrial function on a stable nuclear background. During the cybrid generation process, patient-derived mtDNA persists while all other patient-derived materials become diluted out over time. We found that AD cybrids display no changes in total or pTau Ser199 protein levels. However, tau oligomerization increases in AD cybrids relative to age-matched control cybrids, suggesting mtDNA variants associated with AD are sufficient to cause increased tau oligomerization.

Since mtDNA depletion increases tau oligomerization, we examined mtDNA levels in AD and control cybrids. We found a ~10% decrease in mtDNA levels in AD cybrids relative to control cybrids. Although mtDNA levels only decrease slightly in AD cybrids, a chronic 10% decrease in mtDNA levels may contribute to COX defects in AD cybrids [73]. Decreased COX activity could contribute to the increased tau oligomerization in AD cybrids. Other reports have shown AD-like tau alterations following COX inhibition, although a potential link between COX inhibition and tau oligomerization has not been examined. Chronic COX inhibition in rats leads to neuronal AT8-positive tau granules [178]. Alternatively, certain mtDNA SNPs could impair AD cybrid mitochondrial function and result in increased tau oligomerization. Regardless of the mechanism, results from the AD cybrids suggest mtDNA alterations associated with AD are sufficient to increase tau oligomerization.

Finally, we observed that chronic mtDNA depletion increases apoE mRNA levels and apoE protein levels in the cell culture media. While apoE variants affect AD risk, the mechanisms by which apoE exerts its effects on disease risk are not completely understood. Studies show that the apoe4 allelle, which increases an individual's AD risk, preferentially forms neurotoxic fragments that inhibit mitochondrial function. ApoE4 production also disrupts cytoskeletal stability and potentially induces tau phosphorylation. Most apoE is made in astrocytes, however, neurons can produce apoE during times of neuronal injury or stress [179]. Our findings suggest severe mitochondrial dysfunction upregulates apoE production, perhaps in an attempt to bring cholesterol or other lipids to cells experiencing energy stress. ApoE4 production under these circumstances could enhance cellular toxicity, or fail to protect cells in the same way that apoE3 or apoE2 production would. Under this paradigm, individuals with an apoE4 allele may be more susceptible to the deleterious consequences of neuronal energy stress.

Chapter 3: Chronic Respiratory Chain Incompetence Alters Cellular Proteostasis

Introduction

Numerous proteostasis pathways become impaired in the AD brain. In fact, the mere presence of NFTs and amyloid plaques suggests a severe disruption in brain proteostasis. Researchers hypothesize that modulating proteostasis pathways may serve as a viable therapy for AD [180]. Three of the major cellular proteostasis processes include the ubiquitin proteasome system, the lysosomal degradation system, and general protein translation rate. In addition to these pathways, most subcellular compartments appear to possess their own proteostasis pathways largely comprised of chaperones and proteases. Compartment-specific protein maintenance mechanisms include the erUPR and ERAD, the mtUPR, and the cytosolic heat shock response. These pathways become dysfunctional in the AD brain, although the reasons for their decline remain unclear.

The ubiquitin proteasome system (UPS) marks and destroys diverse protein targets. Ubiquitin ligases polyubiquitinate target proteins, sending them to the 26S proteasome for destruction. 26S proteasomes accept and unfold ubiquitinated proteins in an ATP-dependent manner, while also removing ubiquitin. Protein unfolding and ubiquitin removal occur in the lid complex, also referred to as the 19S cap. Following 19S cap processing, loosely folded proteins lacking ubiquitin can be degraded by the 20S proteasome and associated peptidases. UPS function contributes to cell cycle regulation, cell survival, protein folding, and ERAD [181].

In neurodegenerative diseases characterized by protein misfolding and aggregation, such as AD, researchers propose disrupted UPS function contributes to protein aggregation. Supporting this hypothesis, ubiquitin often associates with plaques and tangles [182-184]. Naturally, these findings led researchers to suggest that proteasomal defects contribute to plaque and tangle formation. Furthermore, ubiquitin carboxy-terminal hydrolase L1 (UCH-L1), which

removes ubiquitin from polyubiquitinated proteins, becomes oxidized and inactivated in AD brains. UCH-L1 inactivation reduces proteasome activity by decreasing the free monomeric ubiquitin pool and stalling polyubiquitinated proteins in the proteasome. Genetic studies implicate UCH-L1 point mutations in rare forms of familial Parkinson's disease, and a deletion in the gene encoding UCH-L1 causes axonal degeneration in a mouse model used to study gracile axonal dystrophy [185]. Studies also suggest proteasomal activity decreases in AD brains. Decreased proteasome activity occurs in brain regions typically affected by AD including the hippocampus and inferior parietal lobule, while the cerebellum shows no change in proteasome activity. Proteasomal protein levels do not change in AD brains, suggesting reduced proteasome function stems from post-translational modifications [186, 187].

While the accumulation of ubiquitinated protein aggregates in AD may stem from decreased proteasome activity, alterations in lysosomal function could also contribute. Ubiquitination can affect autophagy flux by regulating transcription factor EB (TFEB), a major regulator of autophagy and lysosome biogenesis, or by marking autophagy factors for degradation through the UPS [188, 189]. Ubiquitination also serves as a signal for selective autophagy. While selective autophagy can occur in a ubiquitin-dependent or ubiquitin-independent fashion, ubiquitin drives nearly half of the known selective autophagy processes [189]. Aggrephagy, the selective lysosomal degradation of protein aggregates, generally relies upon Lys-63 polyubiquitin chains to recruit autophagy receptors. Autophagy receptors, such as p62, bind to ubiquitin and bring protein aggregates to autophagosomes for degradation [190, 191].

Evidence suggests autophagy defects occur in the AD brain. Beclin-1, an important autophagy regulator, declines in AD brains early in disease progression. Beclin-1 is necessary for

proper autophagy function, as heterozygous deletion of beclin 1 in mice impaired neuronal autophagy and lysosomal function [192]. Along with decreases in beclin 1, lysosomes, lysosomal hydrolases, and autophagic vacuoles accumulate in the AD brain. The build-up of immature autophagic vacuoles suggests AD hinders autophagosome maturation to lysosomes [193]. As referenced earlier, AD brains also display defective mitophagy [83]. Taken together, the evidence suggests a clear disruption in AD brain auto-lysosomal function.

Beyond the UPS and lysosomal systems, cellular compartments maintain proteostasis through resident unfolded protein responses. Studies have examined these pathways in AD brain tissue, finding some evidence for the activation of the erUPR and mtUPR [194-196]. Specifically, studies find increased hippocampal eIF2α phosphorylation in the AD brain [194]. eIF2α phosphorylation contributes to proteostasis by reducing general protein translation. Indeed, AD brains possess altered translation machinery and a reduced rate and capacity for protein synthesis [197, 198].

Few studies directly address mitochondrial influences on proteostasis, however, some evidence suggests a link between mitochondrial dysfunction and reduced proteasomal activity. For example, Liu et al. show mutant PINK1 or loss of PINK1 function causes mitochondrial dysfunction, proteasomal defects, and α-synuclein accumulation. The authors could not determine how mitochondrial dysfunction, proteasome impairment, and α-synuclein accumulation were functionally related. However, they postulate that since PINK1 mainly resides in the mitochondria, mitochondrial dysfunction likely represents the primary defect [199]. Another study in cell culture shows increased ubiquitinylated proteins in ρ0 cells and cells treated with the complex I inhibitor, MPP+. The study also demonstrates reduced 20S

proteasome activity in ρ0 cells and cells treated with MPP+ for 24hrs [200]. Mitochondrial dysfunction also triggers eIF2 phosphorylation, inhibiting protein translation [129].

Here, we examine mtDNA depletion's effects on cellular proteostasis pathways, including the UPS, autophagy/mitophagy, and the erUPR and mtUPR. We hypothesize mitochondrial dysfunction triggers pathogenic protein accumulation by inhibiting these key proteostatic pathways. We begin by examining proteostasis pathways in cells experiencing chronic respiratory chain incompetence, SH-SY5Y ρ0 cells, and proceed to measure these same markers in cells experiencing acute respiratory chain dysfunction through EtBr treatment.

Materials and Methods

Methodology relevant to multiple chapters is not repeated in each chapter. Please refer to the materials and methods section of Chapter 2 for techniques common across all chapters (*e.g.* cell culture methods, whole cell lysate preparation, RNA extraction, western blotting, qPCR, etc.)

Bafilomycin A1 treatment

SH-SY5Y ρ+ and ρ0 cells were grown to 95% confluency in 6 well plates. The media was aspirated and Bafilomycin A1 (Sigma #B1793), reconstituted in DMSO, was added at a 100nM concentration for 6 hours. Vehicle treated cells received media containing the equivalent concentration of DMSO for 6 hours. Following treatment, whole cell protein was harvested using RIPA lysis buffer.

Integrated Stress Response Inhibitor B (ISRIB) Treatment

SH-SY5Y ρ0 cells were grown to 95% confluency in T75 flasks. Prior to treatment, the media was aspirated and fresh media containing 200nM ISRIB (Sigma #SML0843), reconstituted in DMSO. For vehicle treated flasks, media was aspirated and cells were received media containing DMSO at an equivalent concentration to the treatment group. Cells were treated for 3 hours and then harvested using the NE-PER, nuclear and cytosolic extraction, kit (Thermo #78833).

Thapsigargin Treatment

SH-SY5Y ρ+ cells were grown to 95% confluency in 6 well plates or T75 flasks. Prior to treatment, media was aspirated and fresh media containing Thapsigargin (Calbiochem #586005). Thapsigargin was reconstituted in ethanol. Treatment concentrations and time were altered based on the downstream application. For whole cell lysate preparation (to examine eIF2α phosphorylation) and RNA preparation (to examine XBP1 splicing and HSPA5 mRNA), cells

were treated with a range of thapsigargin doses: 0.5 μM, 1 μM, 1.5 μM, 2 μM, and 5 μM, for 1 hour. For nuclear and cytosolic-enrichment (to examine nuclear ATF4 and CHOP protein levels), cells were treated with 1 μM thapsigargin for 3 hours. For all treatments, control cells were treated with media containing the vehicle, ethanol, for the same time period.

Propidium iodide cell cycle analysis

SH-SY5Y ρ+ and ρ0 cells were grown to 95% confluency in 10cm dishes. Upon reaching desired confluency, the media was aspirated and cells were washed in PBS. Then, the cells were gently scraped off the dish in 6mL PBS and counted. 2 million cells per dish were then pelleted at 600xg for 3 minutes, the supernatant was aspirated, and the pellet was resuspended in 1 mL of 0.9% NaCl in water. Cold, 90% ethanol was then added to the cell suspension in a slow, dropwise manner, with constant, gentle vortexing to avoid cell clumping. The cell suspension was then incubated 30 minutes at room temperature to allow for fixation. Following this step, cells were moved to 4°C for long term storage, or immediately processed. For staining, a 500 μg/mL propidium iodide stock (Sigma #P4864) was made in water. To prepare the working propidium iodide solution, the 500 μg/mL stock was diluted 1:10 in PBS. The cells were then pelleted, washed in PBS, and the pellet was resuspended in 1 mL of the propidium iodide working solution. Next, 100 μL of 1 mg/mL RNase A (DNase-free) (Thermo #EN0531) and incubated at 37°C for 30 minutes. Samples were then taken to the flow cytometry core for analysis.

Proteasome Activity Assay

Proteasome activity was measured using abcam's proteasome activity kit (ab107921). The assay was performed according to manufacturer's instructions.

Results

Chronic respiratory chain incompetence increases basal autophagy flux and autophagy adaptor proteins

Since altered tau homeostasis occurs in ρ0 cells, we examined the major proteostatis pathways, starting with autophagy. First, we examined basal autophagy flux using bafilomycin A1 to block lysosomal acidification. Bafilomycin A1 causes autophagosome accumulation, as evidenced by buildup of LC3BII, the autophagosome marker. Comparing LC3BII levels prior to and following bafilomycin treatment gives insight into the flux through the lysosomal system. ρ0 cells displayed greater LC3BII accumulation during bafilomycin treatment, suggesting ρ0 cells increase autophagy flux relative to ρ+ cells (Figure 3.1a,b). Since increases in LC3BII suggested increased autophagy flux, we looked to verify this finding by examining the flux of p62, an autophagy adaptor protein. p62 associates with NFTs in AD brains and evidence suggests p62 contributes to tau degradation [201]. p62 also contributes to mitophagy, and, since multiple reports suggest mitophagy clears aggregation prone proteins [134, 135], we became interested in mitophagy and relevant markers. We found elevated basal p62 protein levels in ρ0 cells. Following bafilomycin treatment, p62 levels increased in both ρ+ and ρ0 cells. p62 levels accumulated to a greater extent upon autophagy inhibition in ρ0 cells relative to ρ+ cells (Figure 3.1c).

Next, we examined the MAP1LC3B (LC3B) and SQSTM1 (p62) mRNA levels since we observed increased LC3B and p62 protein flux in ρ0 cells. p62 mRNA levels increase in ρ0 cells relative to ρ+ cells, consistent with the increase in basal p62 protein levels and increased p62 flux (Figure 3.1e). However, LC3B mRNA levels do not change in ρ0 cells relative to ρ+ cells,

suggesting the observed increases in LC3B protein do not occur due to increased mRNA expression (Figure 3.1d).

Antibody Name	Dilution	Source	Catalog #
LC3B	1:1,000	Cell Signaling	CST3868
p62	1:1,000	Cell Signaling	CST5114
NDP52	1:2,000	Cell Signaling	CST60732
Optineurin	1:1,000	Cell Signaling	CST58981
BNIP3	1:1,000	Cell Signaling	CST44060
BNIP3L/Nix	1:1,000	Cell Signaling	CST60732
Parkin	1:1,000	Cell Signaling	CST4211
PARIS/ZNF746	1:1,000	NeuroMab Facility	Clone N196/16
ATF5	1:5,000	abcam	ab184923
Hsp60	1:5,000	Cell Signaling	CST4870
ClpP	1:2,000	abcam	ab124822
p-eIF2α	1:1,000	Abcam	ab32157
eIF2α	1:1,000	Cell Signaling	CST9722
ATF4	1:1,000	Cell Signaling	CST11815
CHOP	1:500	Invitrogen	MA1-250
p-AKT Thr308	1:1,000	Cell Signaling	CST2965
p-AKT Ser473	1:1,000	LifeTech	700392
AKT	1:2,000	Cell Signaling	CST4685
SirT3	1:1,000	Cell Signaling	CST5490
HDAC1	1:5,000	abcam	ab19845
β-Tubulin	1:5,000	Cell Signaling	CST2128
β-Actin	1:5,000	Cell Signaling	CST3700

Table 3.1. List of antibodies used in experiments.

Taqman Primer	Catalog #
ATF4	Hs00909569_m1
BNIP3L/NIX	Hs00188949_m1
CLPP	Hs00971639_m1
DDIT3	Hs00358796_g1
HSPA5	Hs00607129_gH
HSPD1	Hs01036753_g1
HIF1α	Hs00153153_m1
MAP1LC3B	Hs00917682_m1
PARIS/ZNF746	Hs00978838_m1
PPARGC1	Hs01016719_m1
SQSTM1/p62	Hs01061917_g1
XBP1 (unspliced)	Hs02856596_m1
XBP1 (spliced)	Hs03929085_g1
18s	Hs03003631_g1

Table 3.2. List of Taqman primers used in experiments.

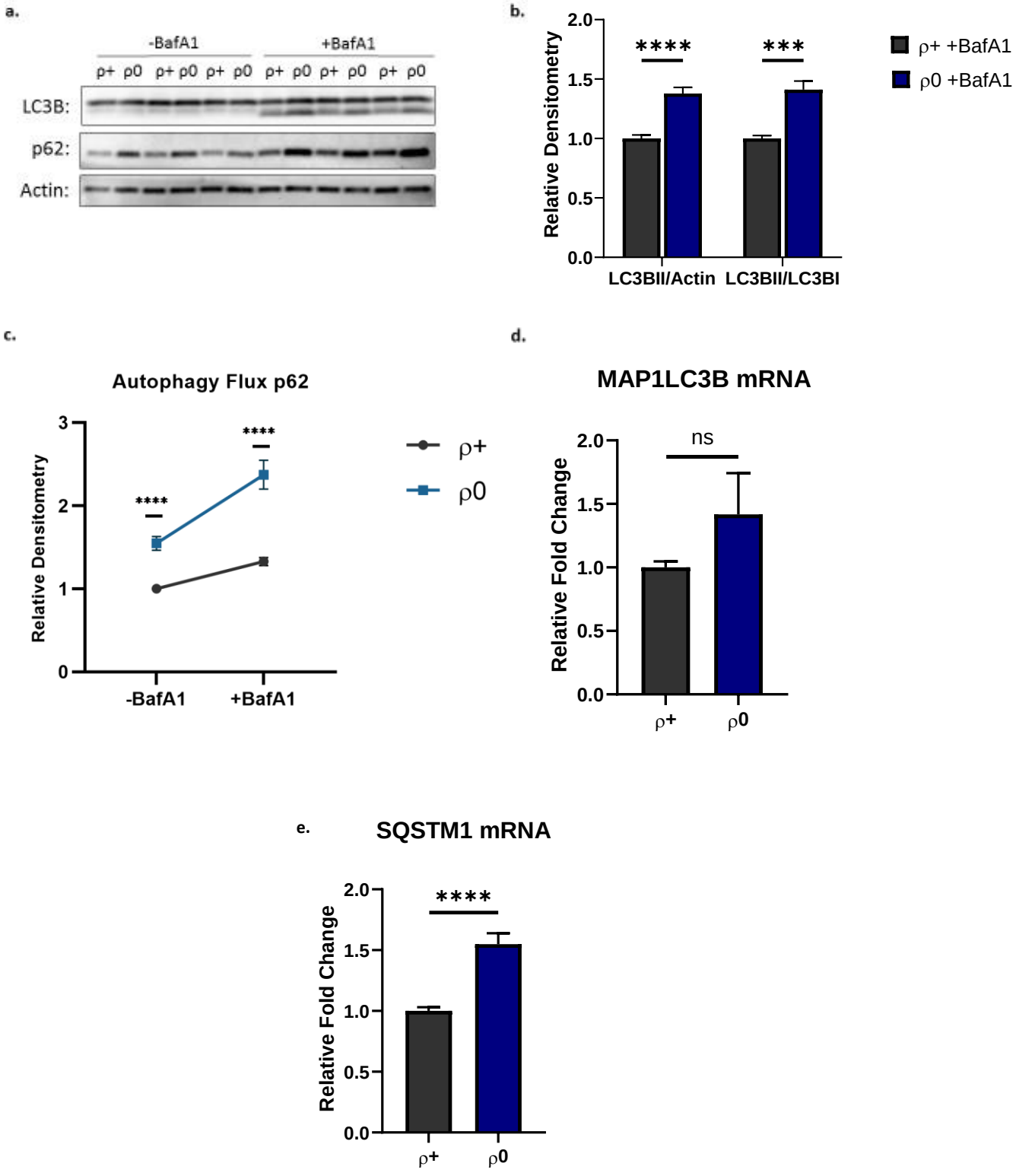
a.
-BafA1
+BafA1
ρ+ ρ0 ρ+ ρ0 ρ+ ρ0 ρ+ ρ0 ρ+ ρ0 ρ+ ρ0
LC3B:
p62:
Actin:
b.
Relative Densitometry
2.0
1.5
1.0
0.5
0.0
****
***
LC3BII/Actin
LC3BII/LC3BI
ρ+ +BafA1
ρ0 +BafA1
c.
Autophagy Flux p62
Relative Densitometry
3
2
1
0
****
****
-BafA1
+BafA1
ρ+
ρ0
d.
MAP1LC3B mRNA
Relative Fold Change
2.0
1.5
1.0
0.5
0.0
ns
ρ+
ρ0
e.
SQSTM1 mRNA
Relative Fold Change
2.0
1.5
1.0
0.5
0.0
****
ρ+
ρ0

Figure 3.1. Chronic mtDNA depletion increases basal autophagy flux and p62 protein levels. a) Western blot images of LC3B and p62 protein in ρ+ and ρ0 whole cell lysates treated with vehicle (-BafA1) or bafilomycin A1 at 100nM for 6 hours (+BafA1). Actin serves as a loading control. b) Densitometry analysis reveals a significant increase in the ratio of LC3BII/Actin and LC3BII/LC3BI. Baseline LC3BII levels (-BafA1) were too low to be quantified. c) Densitometry analysis reveals significant increases in p62 protein levels in BafA1 untreated and treated ρ0 lysates relative to ρ+ lysates. d) qPCR analysis reveals no significant difference in MAP1LC3B mRNA levels between ρ+ and ρ0 cells. e) qPCR analysis reveals a significant increase in SQSTM1 mRNA levels ρ0 cells relative to ρ+ cells. n= 12 per group. $p<0.05$=*, $p<0.01$=**, $p<0.001$=***, $p<0.0001$=****. Error bars represent SEM.

We examined additional autophagy receptors associated with mitophagy, including NDP52 and optineurin. Like p62, NDP52 and optineurin bind to ubiquitinated proteins through ubiquitin binding domains and possess a LC3-interacting region which recruits the receptor to autophagosomes [202]. Recent studies suggest NDP52 and optineurin serve as the major cytosolic mitophagy receptors by promoting Unc-51 like autophagy activating kinase 1 (ULK1) recruitment to begin autophagosome formation around the mitochondria [203]. ρ0 cells increase basal NDP52 and optineurin protein levels. NDP52 levels increase in both ρ+ and ρ0 cells with bafilomycin treatment, while optineurin levels do not increase upon autophagy inhibition (Figure 3.2). While ρ0 cells increase NDP52 protein levels, no difference in NDP52 flux occurs between ρ+ and ρ0 cells (Data not shown).

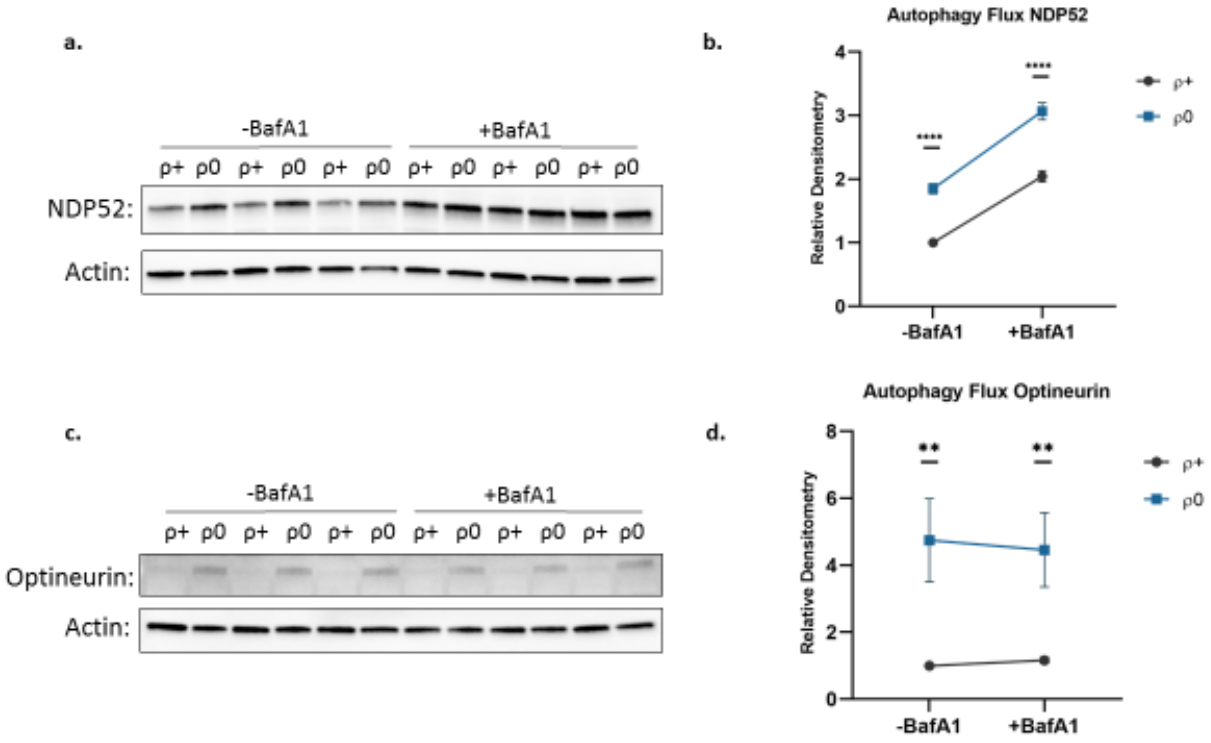
a.
-BafA1
+BafA1
ρ+ ρ0 ρ+ ρ0 ρ+ ρ0 ρ+ ρ0 ρ+ ρ0 ρ+ ρ0
NDP52:
Actin:
b.
Autophagy Flux NDP52
Relative Densitometry
****
****
ρ+
ρ0
-BafA1
+BafA1
c.
-BafA1
+BafA1
ρ+ ρ0 ρ+ ρ0 ρ+ ρ0 ρ+ ρ0 ρ+ ρ0 ρ+ ρ0
Optineurin:
Actin:
d.
Autophagy Flux Optineurin
Relative Densitometry
**
**
ρ+
ρ0
-BafA1
+BafA1

Figure 3.2. Chronic mtDNA depletion increases autophagy adaptor proteins. a) Western blot image of ρ+ and ρ0 whole cell lysates treated with vehicle (-BafA1) or Bafilomycin A1 (+BafA1) labeled with NDP52. Actin serves as a loading control. b) Densitometry analysis reveals a significant increase in NDP52 protein levels in ρ0 lysates relative to control. c) Western blot images of ρ+ and ρ0 whole cell lysates treated with vehicle (-BafA1) or Bafilomycin A1 (+BafA1) labeled with optineurin. Actin serves as a loading control. d) Densitometry analysis reveals a significant increase in optineurin protein levels in ρ0 lysates relative to control. n= 12 per group. $p<0.05$=*, $p<0.01$=**, $p<0.001$=***, $p<0.0001$=****. Error bars represent SEM.

Chronic respiratory chain incompetence reduces numerous mitophagy related proteins

Numerous mitophagy pathways exist. Classically, parkin and PTEN-induced kinase (PINK1)-mediated mitophagy has received the most attention due to the genetic association with Parkinson's disease [204]. PINK1-parkin mediated mitophagy canonically occurs when mitochondrial membrane potential decreases, an indicator of mitochondrial dysfunction. In this way, the cell can selectively degrade poorly functioning mitochondria [205]. However, other cellular changes can trigger mitophagy. Amino acid starvation and hypoxia can both stimulate mitochondrial clearance. BCL2/adenovirus E1B 19 kDa protein-interacting protein 3 (BNIP3) localizes to the outer mitochondrial membrane and hypoxia induces BNIP3 expression. BNIP3 expression is required for mitophagy induction following hypoxia. Another outer mitochondrial membrane protein, Nix, is highly homologous to BNIP3 and also contributes to mitophagy [206].

Due to BNIP3's involvement in mitophagy, we examined BNIP3 levels in ρ0 cells. BNIP3 accumulated in ρ+ cells upon bafilomycin treatment, showing that BNIP3 undergoes lysosomal degradation. ρ0 cells drastically reduce basal BNIP3 protein levels. Bafilomycin treatment does not increase BNIP3 levels in ρ0 cells, suggesting that the BNIP3 loss does not result from increased lysosomal degradation (Figure 3.3a,b). Next, we measured Nix protein levels before and after bafilomycin treatment in mtDNA-depleted cells. Nix accumulated upon autophagy inhibition in ρ+ cells, although to a lesser extent than BNIP3. Similar to BNIP3, ρ0 cells drastically reduce Nix protein levels, and bafilomycin treatment fails to rescue Nix protein levels (Figure 3.3a,c). We also measured hypoxia-inducible factor 1α (HIF1α) mRNA levels and Nix mRNA levels in ρ+ and ρ0 cells. We observed a significant decrease in HIF1α and Nix mRNA levels (Figure 3.3e). Finally, we examined parkin protein levels in ρ0 cells. Parkin

protein did not significantly accumulate following bafilomycin treatment. ρ0 cells display decreased parkin protein levels relative to ρ+ cells (Figure 3.5).

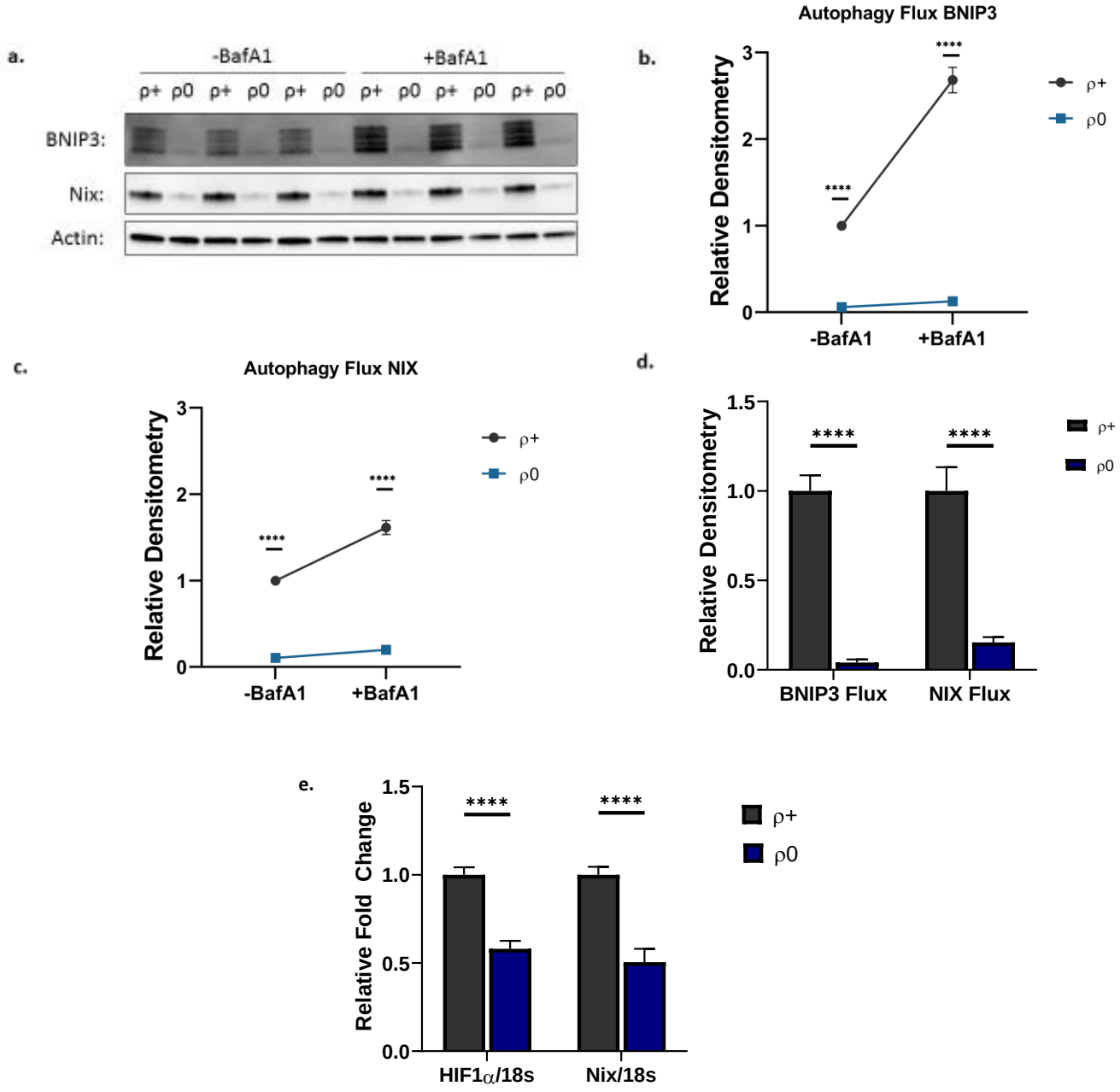
a.
-BafA1
+BafA1
ρ+ ρ0 ρ+ ρ0 ρ+ ρ0 ρ+ ρ0 ρ+ ρ0 ρ+ ρ0
BNIP3:
Nix:
Actin:
b.
Autophagy Flux BNIP3
Relative Densitometry
****
****
ρ+
ρ0
-BafA1
+BafA1
c.
Autophagy Flux NIX
Relative Densitometry
****
****
ρ+
ρ0
-BafA1
+BafA1
d.
Relative Densitometry
****
****
ρ+
ρ0
BNIP3 Flux
NIX Flux
e.
Relative Fold Change
****
****
ρ+
ρ0
HIF1α/18s
Nix/18s

Figure 3.3. Chronic mtDNA depletion reduces mitochondrial localized autophagy adaptors. a) Western blot images of ρ+ and ρ0 whole cell lysates treated with vehicle (-BafA1) or Bafilomycin A1 (+BafA1) labeled with BNIP3 and Nix. b) Densitometry analysis reveals significant decreases in BNIP3 protein levels in ρ0 cells relative to ρ+. c) Densitometry analysis reveals significant decreases in BNIP3 protein levels in ρ0 cells relative to ρ+. d) Graphical representation of protein flux (difference between protein levels before and after BafA1 treatment). ρ0 cells accumulate significantly less BNIP3 and Nix upon autophagy inhibition. e) qPCR analysis of ρ+ and ρ0 cDNA reveals decreased HIF1α and NIX mRNA levels. 18s served as the reference gene. n= 12 per group. $p<0.05$=*, $p<0.01$=**, $p<0.001$=***, $p<0.0001$=****. Error bars represent SEM.

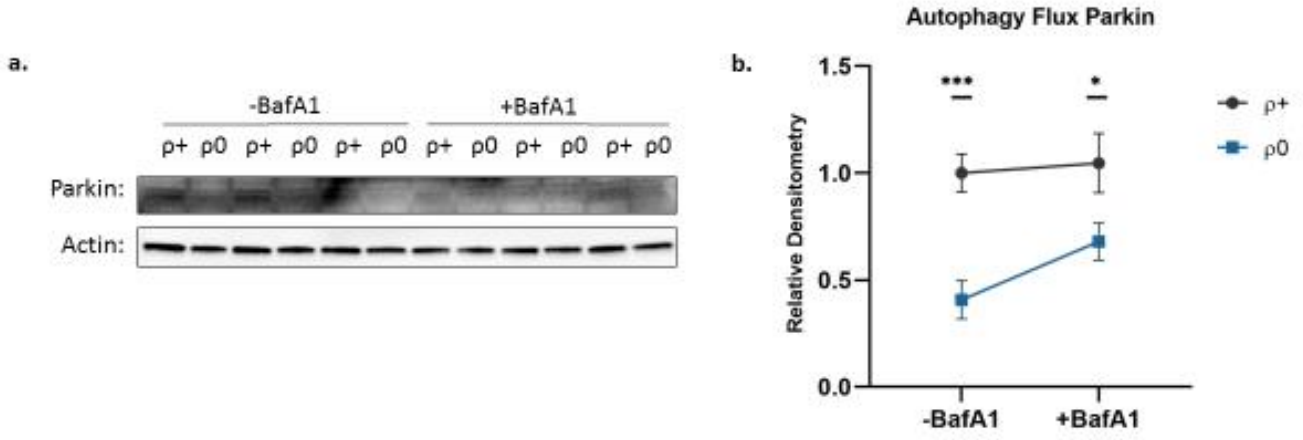
a.
-BafA1
+BafA1
ρ+ ρ0 ρ+ ρ0 ρ+ ρ0 ρ+ ρ0 ρ+ ρ0 ρ+ ρ0
Parkin:
Actin:
b.
Autophagy Flux Parkin
Relative Densitometry
1.5
1.0
0.5
0.0
***
*
-BafA1
+BafA1
ρ+
ρ0

Figure 3.4. Chronic mtDNA depletion decreases Parkin protein levels. a) Western blot images of ρ+ and ρ0 whole cell lysates treated with vehicle (-BafA1) or Bafilomycin A1 (+BafA1) labeled with parkin. Parkin protein levels barely surpassed the limit of detection. Actin served as the loading control. b) Densitometry analysis reveals a significant decrease in parkin protein levels in ρ0 cells relative to ρ+ cells. n= 12 per group. $p<0.05$=*, $p<0.01$=**, $p<0.001$=***, $p<0.0001$=****. Error bars represent SEM.

Autophagy inhibition does not affect total tau protein levels

Initially, we hypothesized the increased tau protein levels in ρ0 cells stemmed from decreased autophagy/mitophagy. For this reason, we examined tau protein levels following autophagy inhibition. Bafilomycin treatment failed to increase tau protein levels in either ρ+ or ρ0 cells (Figure 3.5).

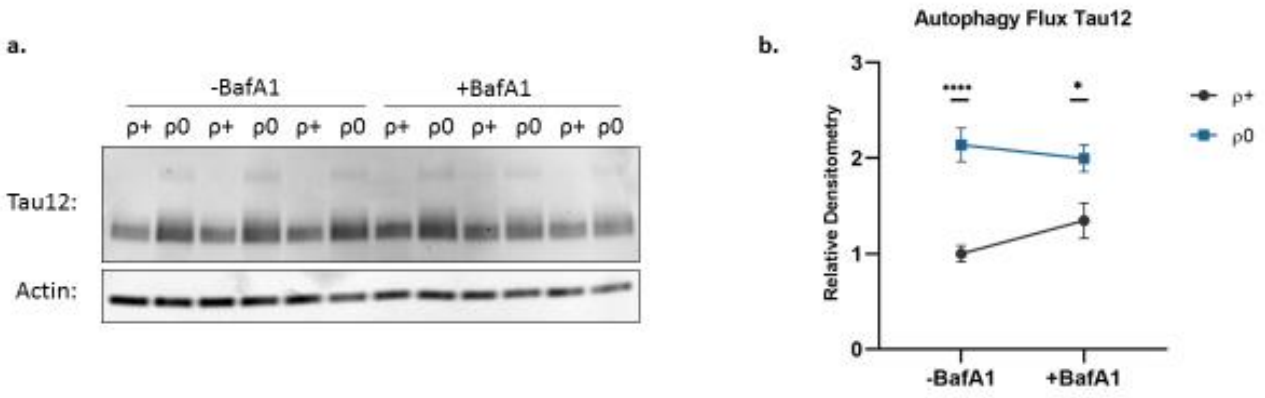
a.
-BafA1
+BafA1
ρ+ ρ0 ρ+ ρ0 ρ+ ρ0 ρ+ ρ0 ρ+ ρ0 ρ+ ρ0
Tau12:
Actin:
b.
Autophagy Flux Tau12
Relative Densitometry
3
2
1
0
****
*
ρ+
ρ0
-BafA1
+BafA1

Figure 3.5. Autophagy inhibition does not increase tau levels. a) Western blot images of ρ+ and ρ0 whole cell lysates treated with vehicle (-BafA1) or Bafilomycin A1 (+BafA1) labeled with Tau12. Actin served as the loading control. b) Densitometry analysis reveals significant increases in Tau12 protein levels in ρ0 cells relative to ρ+ cells. Tau does not accumulate with BafA1 treatment. n= 9 per group. $p<0.05$=*, $p<0.01$=**, $p<0.001$=***, $p<0.0001$=****. Error bars represent SEM.

Chronic respiratory chain incompetence reduces proteasome activity, increases PARIS protein, and decreases PGC1α mRNA

The proteasome plays an important role in cellular proteostasis, and mitochondrial dysfunction tends to associate with reduced proteasome activity. Here, we performed fluorescence-based measurements of ρ+ and ρ0 proteasome activity. We found reduced proteasome activity in ρ0 cells relative to ρ+ cells (Figure 3.6). Since we observed decreased parkin protein levels and decreased proteasome activity in ρ0 cells, we next examined the levels of a parkin substrate, Parkin Interacting Substrate (PARIS/ZNF746). Parkin regulates PARIS levels via ubiquitination. PARIS accumulates following parkin inactivation and in Parkinson's disease brains. PARIS accumulation decreases peroxisome proliferator-activated receptor gamma co-activator 1alpha (PGC1α) transcription, as PARIS binds to insulin response elements in the promoter region and acts as a transcriptional repressor. Furthermore, PARIS knockdown reduces the cellular toxicity associated with parkin inactivation [207]. We observed an approximate 3-fold increase in PARIS protein levels in ρ0 cells (Figure 3.7a,b). We measured PARIS mRNA levels to determine whether the increase in ρ0 PARIS protein stems from increased mRNA levels. We observed a 34% increase in ρ0 PARIS mRNA levels, suggesting that additional mechanisms beyond increased mRNA levels contribute to PARIS protein's 3-fold increase in ρ0 cells. As PARIS negatively regulates PGC1α transcription, we measured PGC1α mRNA levels in ρ0 cells. ρ0 cells drastically decrease PGC1α mRNA levels, suggesting a decrease in PGC1α transcription (Figure 3.7c).

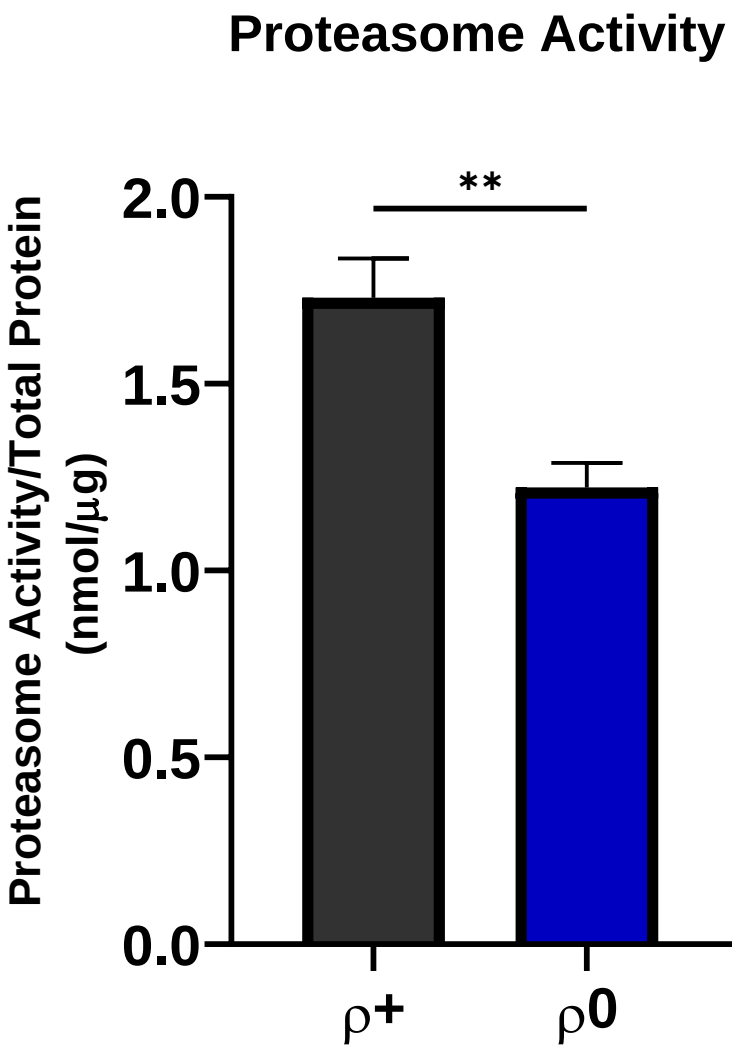
Proteasome Activity
Proteasome Activity/Total Protein
(nmol/μg)
2.0
1.5
1.0
0.5
0.0
**
ρ+
ρ0

Figure 3.6. Chronic mtDNA depletion reduces 20S proteasome activty. Relative proteasome activity based on the production of fluorescent AMC (Ex/Em 350/440 nm). Proteasome activity is normalized to total protein. n=6 per group. $p<0.05$=*, $p<0.01$=**, $p<0.001$=***, $p<0.0001$=****. Error bars represent SEM.

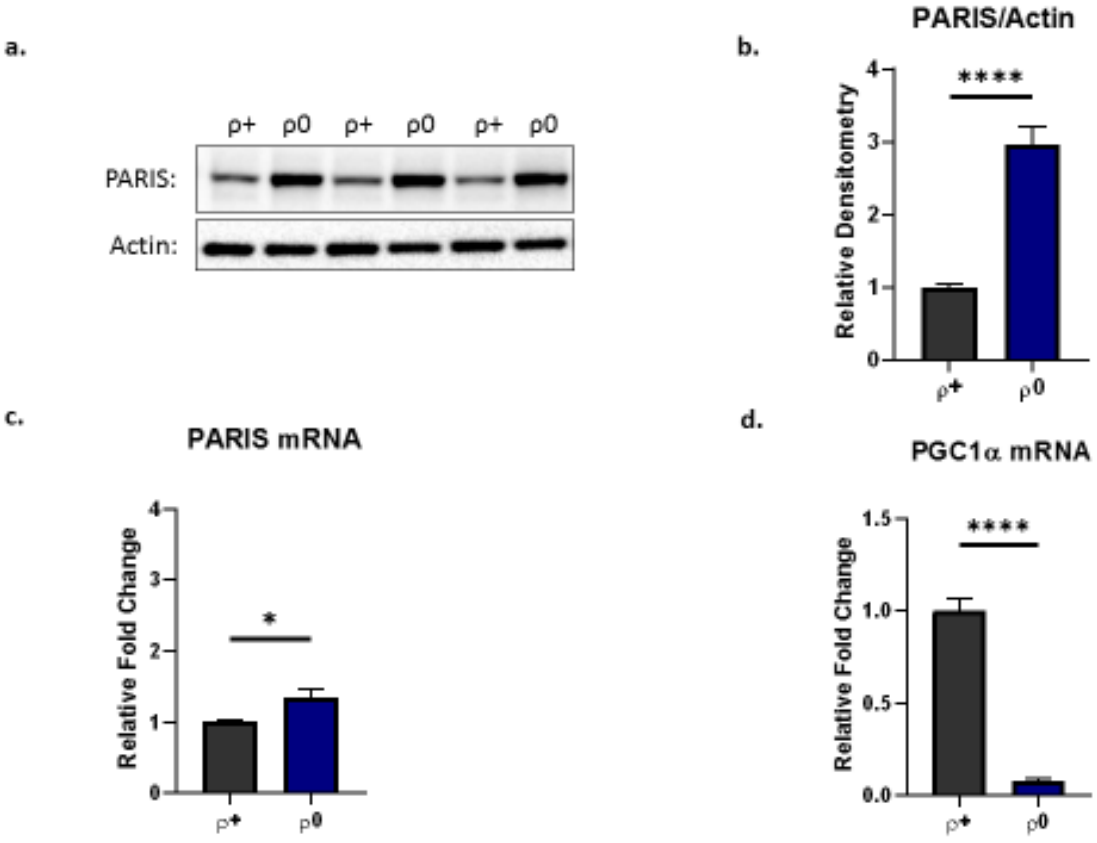
a.
ρ+ ρ0 ρ+ ρ0 ρ+ ρ0
PARIS:
Actin:
b.
PARIS/Actin
****
Relative Densitometry
0
1
2
3
4
ρ+
ρ0
c.
PARIS mRNA
*
Relative Fold Change
0
1
2
3
4
ρ+
ρ0
d.
PGC1α mRNA
****
Relative Fold Change
0.0
0.5
1.0
1.5
ρ+
ρ0

Figure 3.7. Chronic mtDNA depletion increases PARIS protein levels, a PGC1α transcriptional repressor, while decreasing PGC1α mRNA levels. a) Western blot image of ρ+ and ρ0 whole cell lysates labeled with PARIS. Actin serves as a loading control. b) Densitometry analysis reveals significantly increased PARIS protein levels in ρ0 cells relative to ρ+ cells. c) qPCR analysis reveals significantly increased PARIS mRNA levels in ρ0 cells relative to ρ+ cells. d) qPCR analysis reveals significantly decreased PGC1α mRNA levels in ρ0 cells relative to ρ+. n= 12 per group. $p<0.05$=*, $p<0.01$=**, $p<0.001$=***, $p<0.0001$=****. Error bars represent SEM.

Chronic respiratory chain incompetence reduces mtUPR components, while acute mtDNA depletion fails to activate mtUPR signaling

Next, we examined the mtUPR in ρ+ and ρ0 cells. The mtUPR increases mitochondrial chaperone and protease levels to maintain mitochondrial proteostasis. ATF5 mediates the mtUPR in response to certain mitochondrial stressors by inducing mitochondrial protease and chaperone transcription [128]. To determine whether mtDNA depletion activates mtUPR signaling, we extracted enriched cytosolic and nuclear protein fractions from ρ+ and ρ0 cells. In both ρ+ and ρ0 cells, most ATF5 protein localized to the cytosol. We found decreased ATF5 protein levels in the ρ0 cytosolic and nuclear fractions relative to the ρ+ fractions (Figure 3.8a,b).

After observing decreased ATF5 protein levels in ρ0 cells, we measured mRNA levels of two ATF5 target genes, HSPD1 (Heat shock protein 60, Hsp60) and ATP-dependent Clp protease proteolytic subunit (ClpP). Studies show certain mitochondrial stressors cause nuclear translocation of ATF5, leading to increased Hsp60 and ClpP transcription. Consistent with decreasing ATF5 levels, ρ0 cells decrease Hsp60 and ClpP mRNA levels relative to ρ+ cells (Figure 3.8c). Next, we examined Hsp60 and ClpP protein levels. We discovered decreased Hsp60 and ClpP protein levels in ρ0 cells, suggesting a decrease in mtUPR activity (Figure 3.8d,e).

To see whether acute mtDNA depletion activates the mtUPR, we measured Hsp60 and ClpP mRNA levels in EtBr-treated cells. We observed no change in Hsp60 or ClpP mRNA levels following acute mtDNA depletion (Figure 3.9). This suggests acute mtDNA depletion does not activate the mtUPR in SY5Y cells.

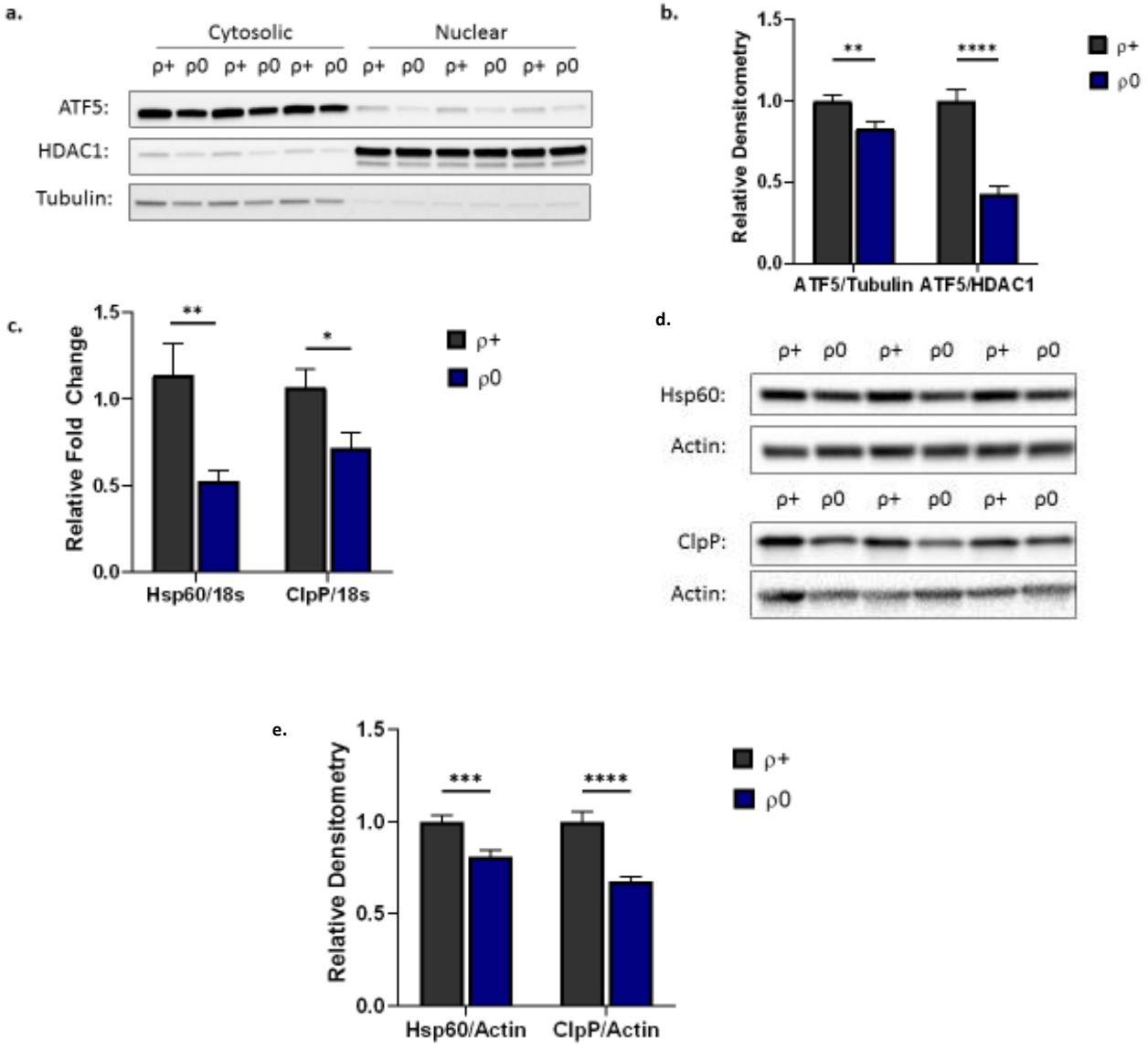
a.
Cytosolic
Nuclear
ρ+ ρ0 ρ+ ρ0 ρ+ ρ0 ρ+ ρ0 ρ+ ρ0 ρ+ ρ0
ATF5:
HDAC1:
Tubulin:
b.
Relative Densitometry
1.5
1.0
0.5
0.0
**
****
ρ+
ρ0
ATF5/Tubulin
ATF5/HDAC1
c.
Relative Fold Change
1.5
1.0
0.5
0.0
**
*
ρ+
ρ0
Hsp60/18s
ClpP/18s
d.
ρ+ ρ0 ρ+ ρ0 ρ+ ρ0
Hsp60:
Actin:
ρ+ ρ0 ρ+ ρ0 ρ+ ρ0
ClpP:
Actin:
e.
Relative Densitometry
1.5
1.0
0.5
0.0
***
****
ρ+
ρ0
Hsp60/Actin
ClpP/Actin

Figure 3.8. Chronic mtDNA depletion reduces mtUPR signaling. a) Western blot image of ρ+ and ρ0 cytosolic and nuclear enriched fractions labeled with ATF5. HDAC1 serves as a marker of nuclear enrichment and tubulin serves as a marker of cytosolic enrichment. b) Densitometry analysis reveals decreased cytosolic and nuclear ATF5 protein levels in ρ0 cells relative to ρ+. c) qPCR analysis reveals decreased HSP60 (HSPD1) and ClpP mRNA levels in ρ0 cells relative to ρ+. d) Western blot images of ρ+ and ρ0 whole cell lysates labeled with Hsp60 and ClpP. Actin serves as a loading control. e) Densitometry analysis reveals decreased Hsp60 and ClpP protein levels in ρ0 lysates relative to ρ+ lysates. n= 12 per group. $p<0.05$=*, $p<0.01$=**, $p<0.001$=***, $p<0.0001$=****. Error bars represent SEM.

a.

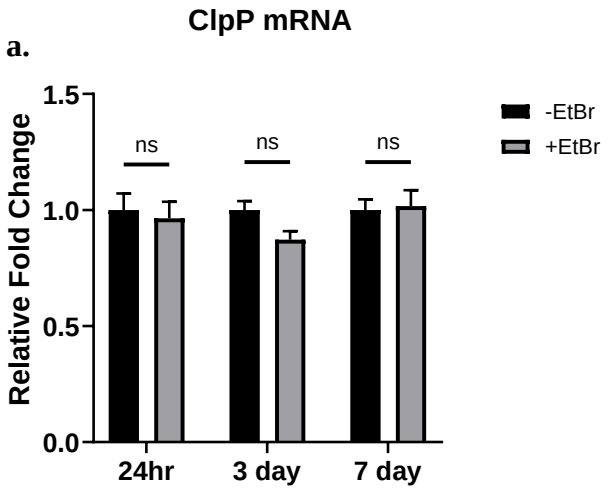
ClpP mRNA
Relative Fold Change
1.5
1.0
0.5
0.0
ns
ns
ns
24hr
3 day
7 day
-EtBr
+EtBr

b.

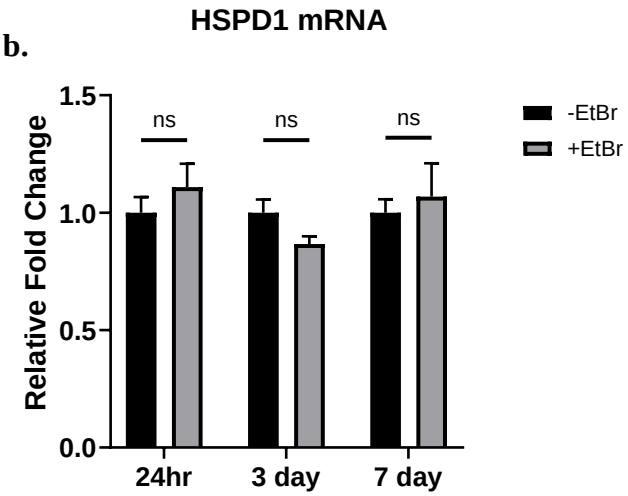
HSPD1 mRNA
Relative Fold Change
1.5
1.0
0.5
0.0
ns
ns
ns
24hr
3 day
7 day
-EtBr
+EtBr

Figure 3.9. Acute mtDNA depletion fails to activate mtUPR components. a) qPCR analysis reveals no change in ClpP mRNA levels in ρ0 cells relative to ρ+ b) qPCR analysis reveals no change in HSP60 (HSPD1) mRNA levels in ρ0 cells relative to ρ+. n= 12 per group. ns= no significant difference. Error bars represent SEM.

Chronic respiratory chain incompetence activates the ISR

Numerous cellular compartments can respond to unfolded proteins, including the cytosol, mitochondria, and the ER. As we already examined mtUPR components, we next measured factors associated with the erUPR. One pathway associated with the erUPR, among other cellular stressors, begins with eIF2α phosphorylation. eIF2α phosphorylation at serine 51 impedes general protein translation to help cells maintain homeostasis during stress [208]. ρ0 cells increase eIF2α Ser51 phosphorylation relative to ρ+ cells (Figure 3.10a,b). As mentioned previously, eIF2α phosphorylation slows general protein translation; however, eIF2α phosphorylation also increases translation of specific stress response proteins. One such protein is ATF4, whose protein levels increase following eIF2α phosphorylation. ATF4 acts as a transcription factor, rewiring cellular metabolism and stress response pathways [129].

Since ATF4 functions as a nuclear transcription factor, we measured ATF4 levels in ρ+ and ρ0 nuclear-enriched fractions. Consistent with increased eIF2α phosphorylation, we observed increased nuclear ATF4 protein levels in ρ0 cells (Figure 3.10c,d). We measured ATF4 mRNA levels to determine whether the increase in ρ0 ATF4 protein stemmed from increased mRNA levels. We found a 53% increase in ρ0 ATF4 mRNA levels, suggesting other mechanisms contribute to the bulk of the approximate 4-fold increase in ρ0 ATF4 protein levels (Figure 3.10e).

Nuclear ATF4 induces C/EBP homologous protein (CHOP), a transcription factor associated with cell cycle arrest and apoptosis. With this knowledge, we next examined CHOP, also known as DNA damage inducible transcript 3 (DDIT3), mRNA levels. ρ0 cells display an approximate 6-fold increase in CHOP mRNA levels relative to ρ+ cells (Figure 3.11a). We followed up by examining CHOP protein levels in ρ+ and ρ0 nuclear enriched fractions. CHOP

protein levels exist below the western blot limit of detection in ρ+ cytosolic and nuclear-enriched fractions. In ρ0 cells, cytosolic CHOP levels also exist below the limit of detection, however, CHOP protein appears in ρ0 nuclear-enriched lysates (Figure 3.11b,c). We also measured CHOP mRNA (DDIT3) levels in EtBr-treated SY5Y cells. 24 hour and 3 day EtBr did not affect CHOP mRNA levels; however, 7 day EtBr treatment increased CHOP mRNA levels (Figure 3.11d). The concomitant activation of eIF2α phosphorylation, ATF4, and CHOP suggests ISR activation in ρ0 cells.

To validate ISR activation in ρ0 cells, we treated with integrated stress response inhibitor B (ISRIB). ISRIB blocks the ISR by negating the effects of eIF2α phosphorylation. eIF2α phosphorylation blocks translation by hindering the formation of the ternary complex which facilitates translation. ISRIB appears to act as sort of "molecular staple", bringing the ternary complex together regardless of eIF2α's phosphorylation status. Therefore, ISRIB blocks the ISR by allowing translation to occur, rather than by modulating eIF2α phosphorylation. ISRIB treatment in ρ0 cells reduced ATF4 and CHOP protein levels, suggesting eIF2α phosphorylation mediates the increased ATF4 and CHOP protein levels (Figure 3.12).

Finally, we used thapsigargin as a positive control to validate the observed ISR activation. Thapsigargin inhibits the ER calcium ATPase, leading to ER-stress. Thapsigargin treatment in SY5Y cells causes heavy eIF2α phosphorylation (Figure 3.13a). Then, we examined cytosolic and nuclear enriched fractions from cells treated with thapsigargin. Thapsigargin treatment increased nuclear ATF4 and CHOP (Figure 3.13b,c).

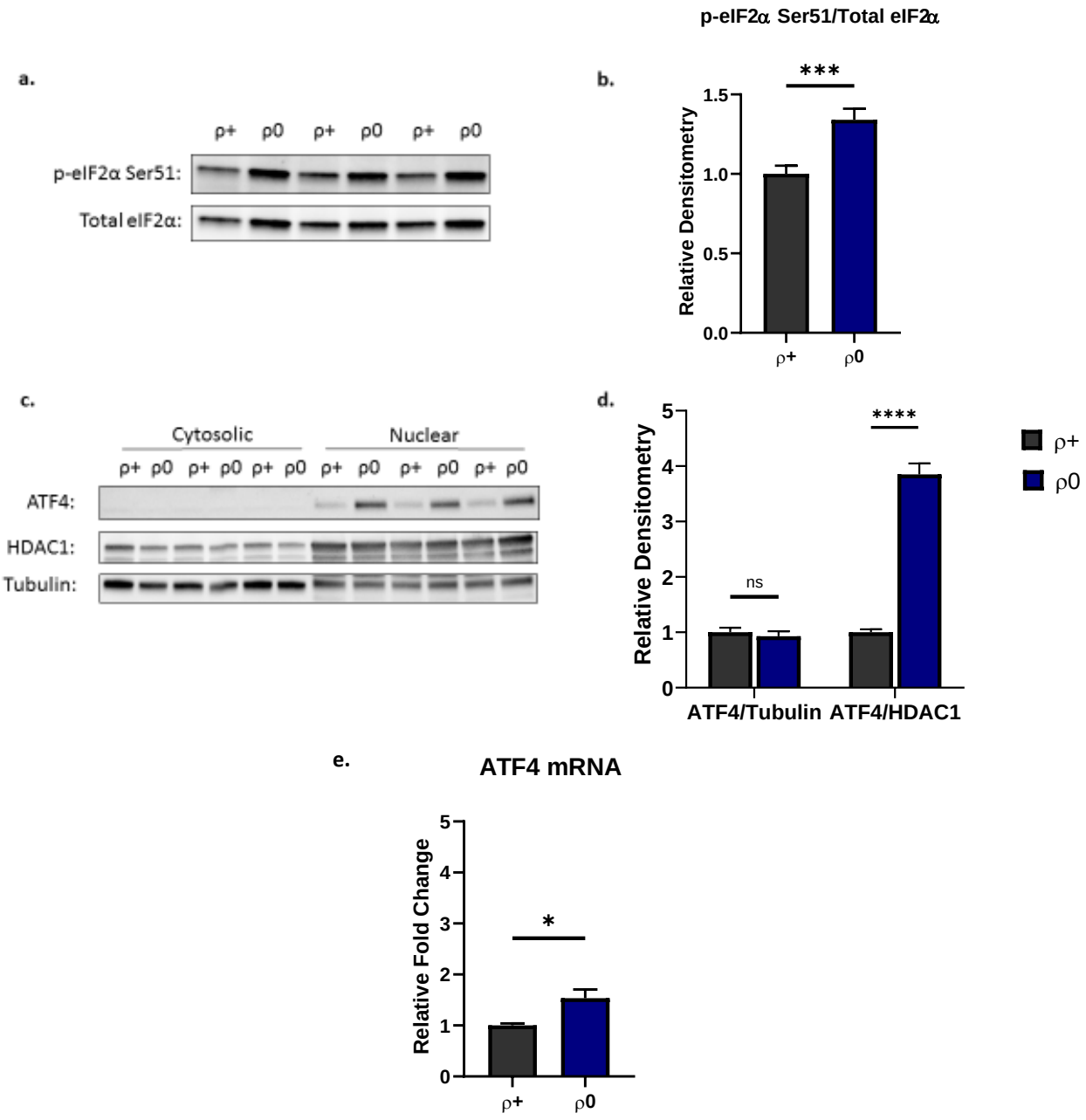
a.
ρ+ ρ0 ρ+ ρ0 ρ+ ρ0
p-eIF2α Ser51:
Total eIF2α:
b.
p-eIF2α Ser51/Total eIF2α
***
Relative Densitometry
1.5
1.0
0.5
0.0
ρ+
ρ0
c.
Cytosolic
Nuclear
ρ+ ρ0 ρ+ ρ0 ρ+ ρ0 ρ+ ρ0 ρ+ ρ0 ρ+ ρ0
ATF4:
HDAC1:
Tubulin:
d.
****
ns
Relative Densitometry
5
4
3
2
1
0
ATF4/Tubulin
ATF4/HDAC1
ρ+
ρ0
e.
ATF4 mRNA
Relative Fold Change
*
5
4
3
2
1
0
ρ+
ρ0

Figure 3.10. Chronic mtDNA depletion activates the ISR, increasing eIF2α phosphorylation and nuclear ATF4 protein levels. a) Western blot image of ρ+ and ρ0 whole cell lysates labeled with p-eIF2α Ser51 and total eIF2α. b) Densitometry analysis reveals a significant increase in the p-eIF2α/Total eIF2α ratio in ρ0 lysates relative to ρ+. c) Western blot image of ρ+ and ρ0 cytosolic and nuclear enriched extracts labeled with ATF4. HDAC1 serves as a marker of nuclear enrichment and tubulin serves as a marker of cytosolic enrichment. d) Densitometry analysis significantly increased nuclear ATF4 protein levels in ρ0 fractions relative to ρ+. e) qPCR analysis reveals significantly increased ATF4 mRNA levels in ρ0 cells relative to ρ+ cells. n= 12 per group. ns= no significant difference. $p<0.05$=*, $p<0.01$=**, $p<0.001$=***, $p<0.0001$=****. Error bars represent SEM.

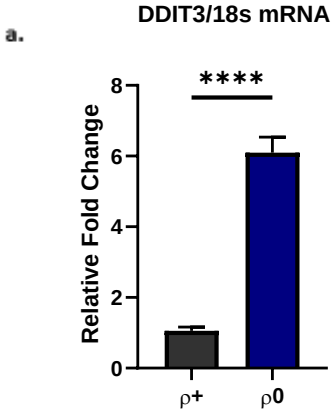
a.
DDIT3/18s mRNA
****
Relative Fold Change
8
6
4
2
0
ρ+
ρ0

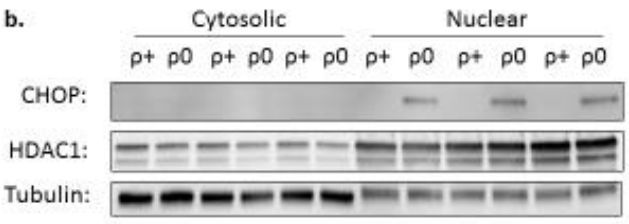
b.
Cytosolic
Nuclear
ρ+ ρ0 ρ+ ρ0 ρ+ ρ0 ρ+ ρ0 ρ+ ρ0 ρ+ ρ0
CHOP:
HDAC1:
Tubulin:

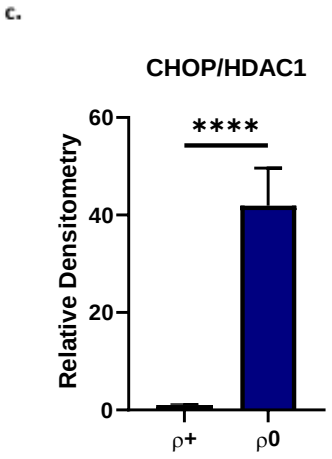
c.
CHOP/HDAC1
****
Relative Densitometry
60
40
20
0
ρ+
ρ0

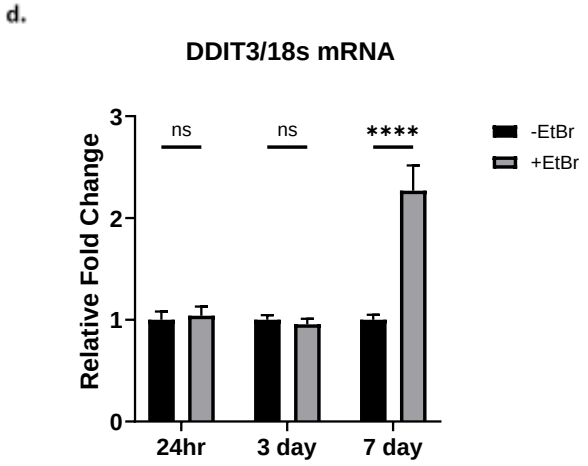
d.
DDIT3/18s mRNA
ns
ns
****
-EtBr
+EtBr
Relative Fold Change
3
2
1
0
24hr
3 day
7 day

Figure 3.11. Chronic and acute mtDNA depletion stimulates CHOP (DDIT3) expression. a) qPCR analysis reveals significantly increased CHOP (DDIT3) mRNA levels in ρ0 cells relative to ρ+ cells. b) Western blot image of ρ+ and ρ0 cytosolic and nuclear enriched fractions labeled with CHOP. HDAC1 serves as a marker of nuclear enrichment and tubulin serves a marker of cytosolic enrichment. c) Densitometry analysis reveals significantly increased nuclear CHOP protein levels in ρ0 fractions relative to ρ+ fractions. d) qPCR analysis reveals significantly increased CHOP (DDIT3) mRNA levels in SY5Y cells treated with EtBr for 7 days. n= 12 per group. ns= no significant difference. $p<0.05$=*, $p<0.01$=**, $p<0.001$=***, $p<0.0001$=****. Error bars represent SEM.

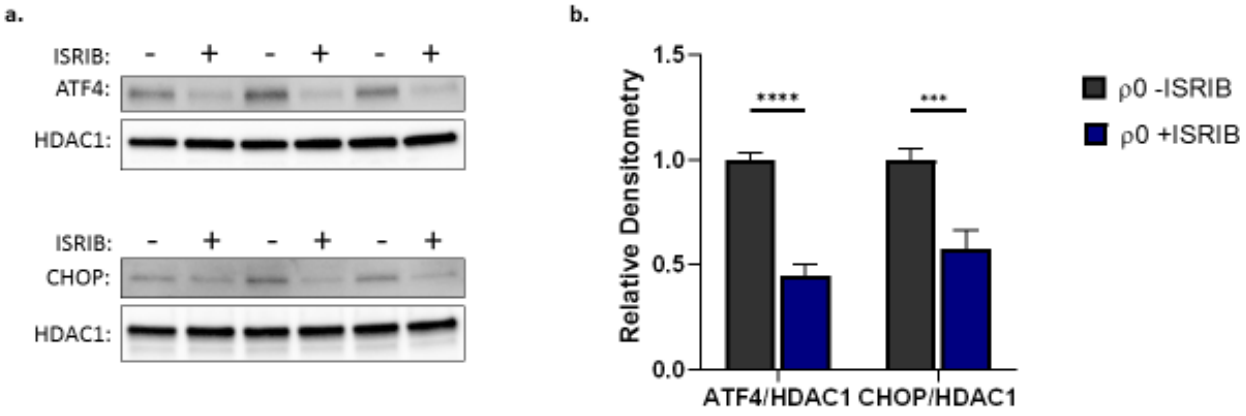
a.
ISRIB: - + - + - +
ATF4:
HDAC1:
ISRIB: - + - + - +
CHOP:
HDAC1:
b.
Relative Densitometry
1.5
1.0
0.5
0.0
****
***
ATF4/HDAC1
CHOP/HDAC1
ρ0 -ISRIB
ρ0 +ISRIB

Figure 3.12. Integrated stress response inhibitor B (ISRIB) treatment reduces ρ0 ISR activation. a) Western blot images of ρ0 nuclear enriched extracts treated with ISRIB at 200nM for 3hr and labeled with ATF4 and CHOP. b) Densitometry analysis reveals significantly decreased nuclear ATF4 and CHOP protein levels following ISRIB treatment. n= 12 per group. $p<0.05$=*, $p<0.01$=**, $p<0.001$=***, $p<0.0001$=****. Error bars represent SEM.

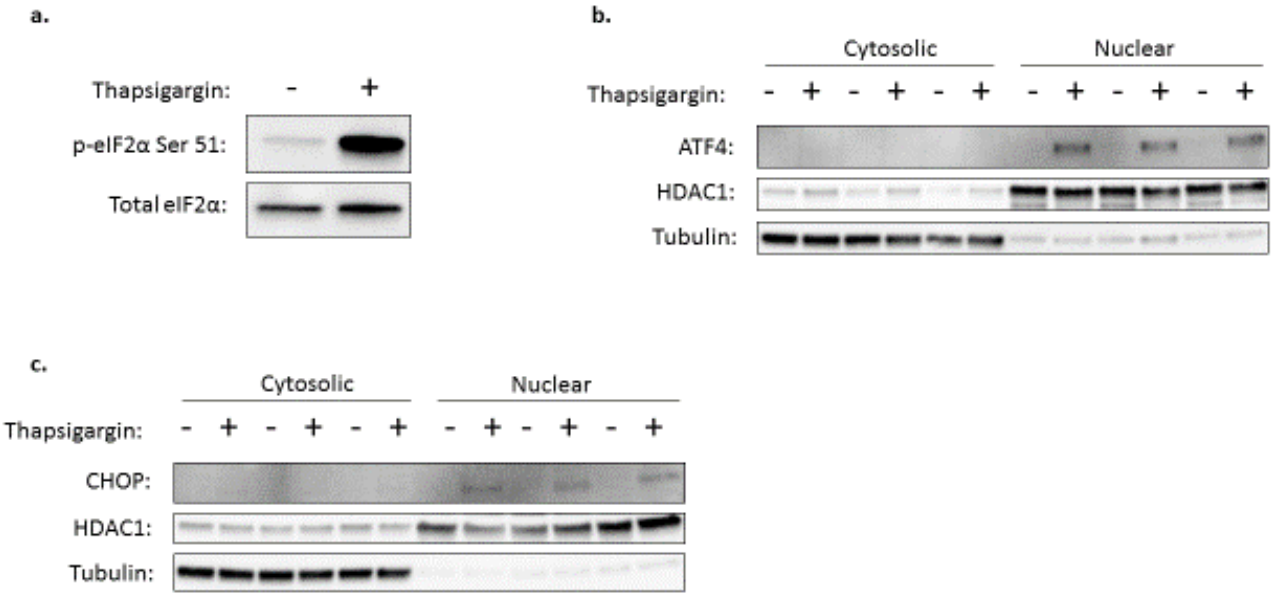
a.
Thapsigargin: - +
p-eIF2α Ser 51:
Total eIF2α:
b.
Cytosolic
Nuclear
Thapsigargin: - + - + - + - + - + - +
ATF4:
HDAC1:
Tubulin:
c.
Cytosolic
Nuclear
Thapsigargin: - + - + - + - + - + - +
CHOP:
HDAC1:
Tubulin:

Figure 3.13. Thapsigargin treatment stimulates ISR activation in ρ+ cells. a) Thapsigargin treatment at 1uM for 1hr stimulates eIF2α phosphorylation. b) Western blot image of SH-SY5Y cytosolic and nuclear extracts treated with 1uM thapsigargin for 3hr and labeled with ATF4. c) Western blot image of SH-SY5Y cytosolic and nuclear extracts from cells treated with 1uM thapsigargin for 3hr and labeled with CHOP.

Chronic mtDNA depletion does not activate erUPR pathways outside the ISR

ρ0 cells display clear ISR activation. ER-stress and unfolded protein accumulation activate the ISR as part of the erUPR, although various stressors cause ISR activation. To determine whether ρ0 cells activate erUPR pathways outside the ISR, we examined classic erUPR markers. The erUPR consists of three major arms, including the ISR. One arm begins with inositol requiring enzyme 1α (IRE1α) activation, leading to X-box binding protein 1 (XBP1) splicing. Therefore, XBP1 splicing serves as a marker of IRE1α activation and ER-stress [209].

We examined the levels of spliced and unspliced XBP1 mRNA using primers specific to each form. ρ0 cells display decreased XBP1 splicing, suggesting the IRE1α arm of the ER-stress response is not activated by chronic mtDNA depletion (Figure 3.14a). ER-stress also causes transcription of ER chaperones, including HSPA5, the gene encoding binding immunoglobulin protein (BiP) [210]. We measured HSPA5 mRNA levels in ρ+ and ρ0 cells, finding no difference between the groups (Figure 3.14b). Finally, we treated SY5Y cells with thapsigargin as a positive control for ER-stress, and measured XBP1 splicing and HSPA5 mRNA levels. We observed a strong induction of XBP1 splicing and HSPA5 mRNA levels following thapsigargin treatment (Figure 3.14c,d).

a.

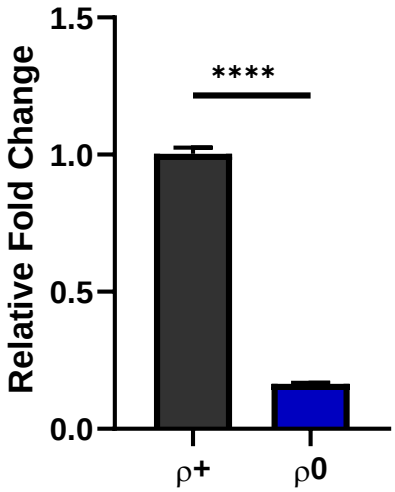
XBP1s/XBP1u
Relative Fold Change
1.5
1.0
0.5
0.0
****
ρ+
ρ0

b.

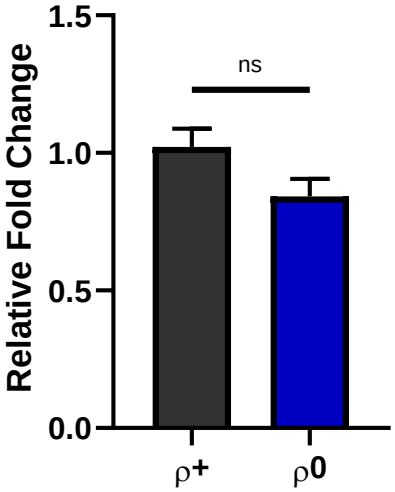
HSPA5 mRNA
Relative Fold Change
1.5
1.0
0.5
0.0
ns
ρ+
ρ0

c.

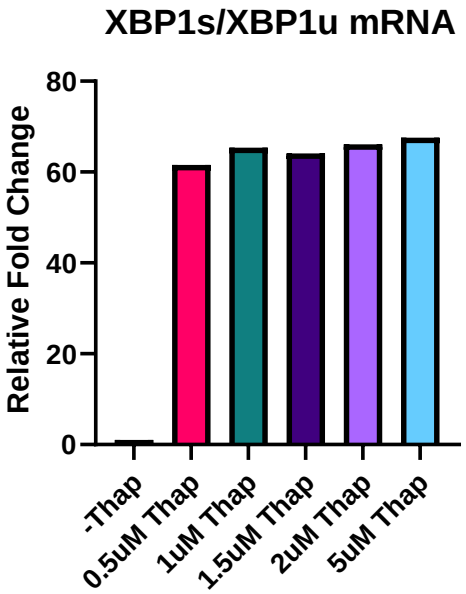
XBP1s/XBP1u mRNA
Relative Fold Change
80
60
40
20
0
-Thap
0.5uM Thap
1uM Thap
1.5uM Thap
2uM Thap
5uM Thap

d.

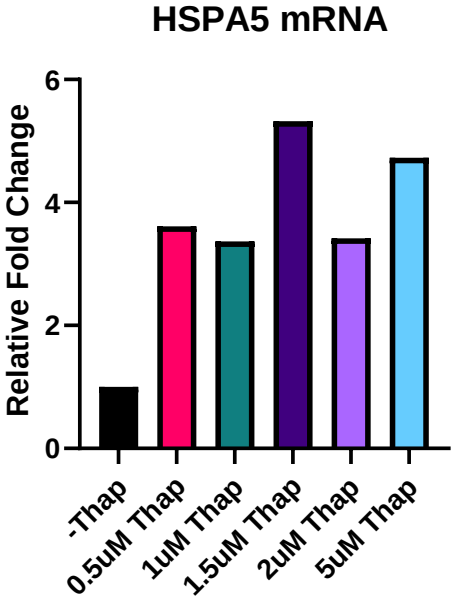
HSPA5 mRNA
Relative Fold Change
6
4
2
0
-Thap
0.5uM Thap
1uM Thap
1.5uM Thap
2uM Thap
5uM Thap

Figure 3.14. Chronic mtDNA depletion does not stimulate classical ER stress markers outside of the ISR. a) qPCR analysis reveals a significant decrease in the ratio of spliced XBP1 (XBP1s) to unspliced XBP1 (XBP1u) mRNA in ρ0 cells relative to ρ+ cells. b) qPCR reveals no significant difference in HSPA5 mRNA levels between ρ+ and ρ0 cells. n= 12 per group. c) 1hr treatment with thapsigargin causes increased XBP1 splicing. d) 1hr treatment with thapsigargin increases HSPA5 mRNA levels. n=1 per group. ns= no significant difference. $p<0.05$=*, $p<0.01$=**, $p<0.001$=***, $p<0.0001$=****. Error bars represent SEM.

Chronic mtDNA depletion activates additional MSR pathways

Reports describe numerous mitochondrial stress responses (MSRs). To learn whether mtDNA depletion activates MSRs beyond the ISR, we examined protein kinase B/AKT phosphorylation and SirT3 protein levels in ρ0 cells. AKT phosphorylation plays important roles in cell survival, growth and differentiation. Dual phosphorylation at Thr308 and Ser473 results in full AKT activation [211]. Three AKT isoforms exist, AKT1, AKT2, and AKT3. AKT signaling mediates insulin-stimulated glucose uptake and increases glycolytic flux, although this function is mostly associated with the AKT2 isoform, whose expression is largely restricted to insulin-responsive tissues. AKT1 expresses widely throughout the body, and AKT3 mainly expresses in the testes and brain [212]. Experiments in AKT1 knockout mice and AKT1 null cells suggest this isoform contributes to cell survival, while AKT3 is necessary for brain development [213]. SY5Y cells express all three AKT isoforms [214]. SY5Y ρ0 cells increased AKT phosphorylation at both Thr308 and Ser473, suggesting full AKT activation (Figure 3.15).

Sirtuin 3 (SirT3) is a stress-responsive deacetylase with mitochondrial localization. Several disease states have been associated with altered SirT3 activity. SirT3 controls mitochondrial activity and energy utilization during starvation and exercise, likely by modulating protein acetylation. SirT3 knockout mice display features indicative of pre-mature aging, including cancer, heart disease, and metabolic syndrome [215]. In ρ0 cells, SirT3 protein levels increased relative to ρ+ cells (Figure 3.15).

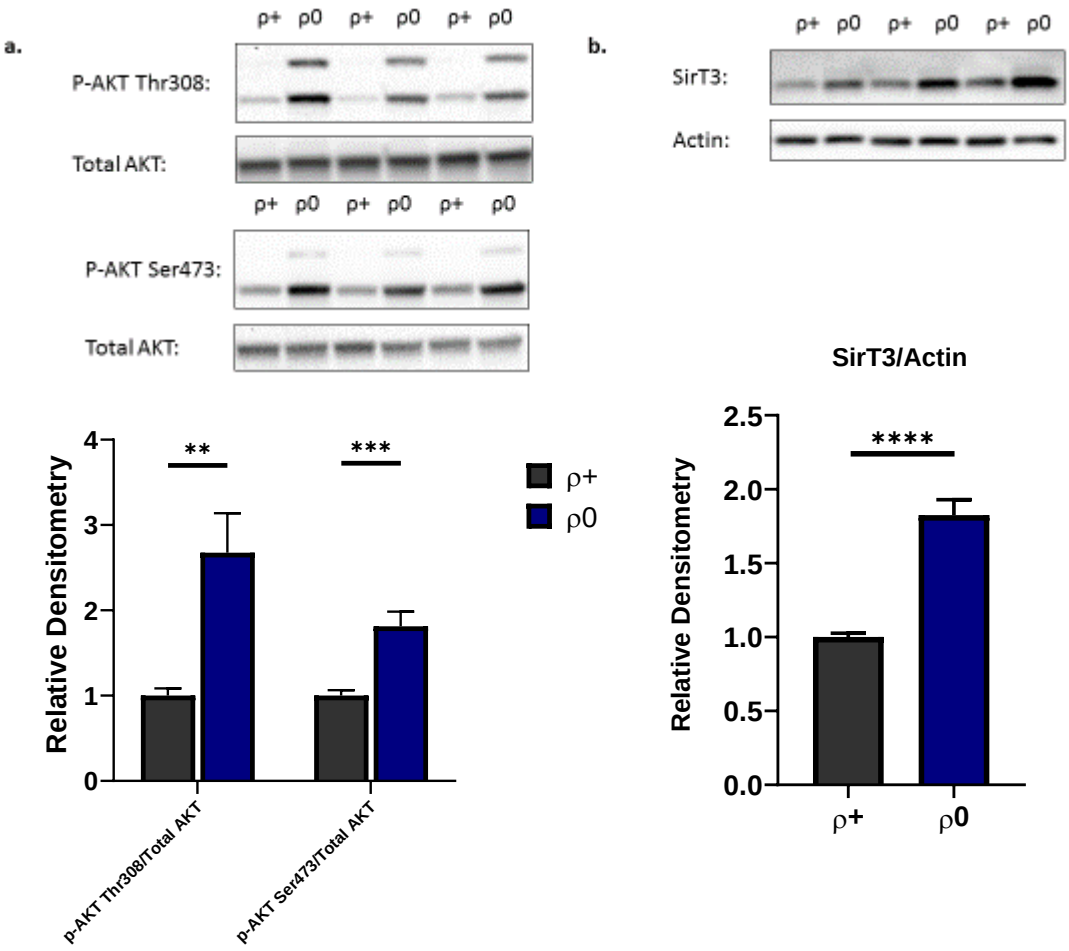
a.
ρ+ ρ0 ρ+ ρ0 ρ+ ρ0
P-AKT Thr308:
Total AKT:
ρ+ ρ0 ρ+ ρ0 ρ+ ρ0
P-AKT Ser473:
Total AKT:
b.
ρ+ ρ0 ρ+ ρ0 ρ+ ρ0
SirT3:
Actin:
SirT3/Actin
Relative Densitometry
2.5
2.0
1.5
1.0
0.5
0.0
****
ρ+
ρ0
Relative Densitometry
4
3
2
1
0
**
***
ρ+
ρ0
p-AKT Thr308/Total AKT
p-AKT Ser473/Total AKT

Figure 3.15. Chronic mtDNA depletion activates additional MSR pathways, increasing AKT phosphorylation and SirT3 protein levels. a) Western blot image of ρ+ and ρ0 whole cell lysates labeled with p-AKT Thr308, p-AKT Ser473, and total AKT. Densitometry analysis reveals a significant increase in the p-AKT/Total AKT at Thr308 and Ser473 in ρ0 lysates relative to ρ+. n= 10 per group b) Western blot image of ρ+ and ρ0 whole cell lysates labeled with SirT3. Actin serves as a loading control. Densitometry analysis significantly increased SirT3 protein levels in ρ0 cells relative to ρ+. n= 12 per group. $p<0.05$=*, $p<0.01$=**, $p<0.001$=***, $p<0.0001$=****. Error bars represent SEM.

Chronic respiratory chain incompetence slows cell cycle progression

Prior studies show that mtDNA loss in *Saccharomyces cerevisiae* causes G1 cell cycle arrest and slowed cellular proliferation [216]. Human cells depleted of mtDNA also down-regulate cell cycle control proteins and reduce cellular replication [217]. Here, we used propidium iodide staining coupled with flow cytometry to analyze cellular proliferation in SY5Y ρ+ and ρ0 cells. We found the ρ0 population has a significantly increased percentage of cells in G1 phase relative to ρ+ cells, as well as significant decreases in the percentage of ρ0 cells in S and G2 phase (Figure 3.16). These findings suggest that ρ0 cells experience G1 cell cycle arrest.

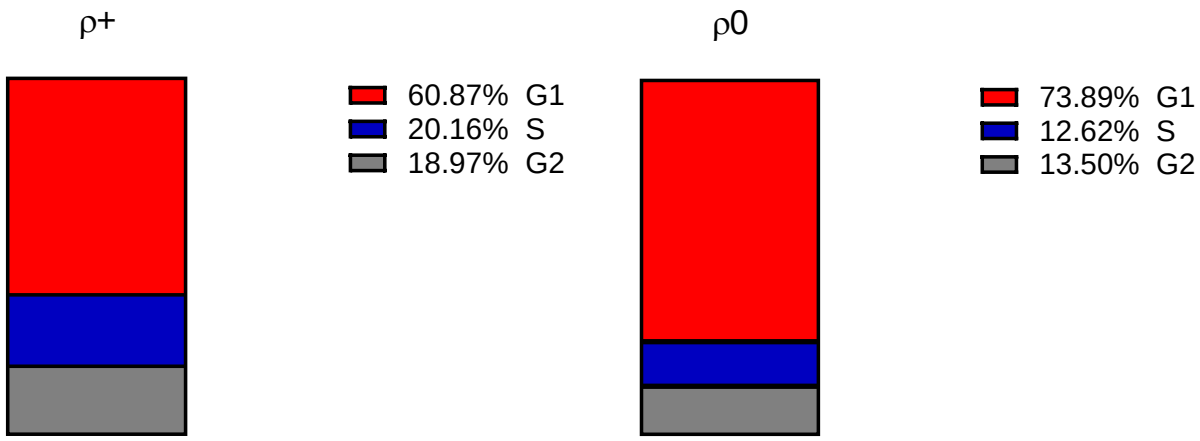
ρ+
60.87% G1
20.16% S
18.97% G2
ρ0
73.89% G1
12.62% S
13.50% G2

Figure 3.16. Chronic mtDNA depletion slows cell cycle progression. Graphical representation of the percentage of ρ+ and ρ0 cells in each stage of the cell cycle. Cell cycle analysis was performed using propidium iodide staining together with flow cytometry analysis. ρ0 cells display a significant decrease in the percentage of cells in S and G2 phase and a significantly increased percentage of cells in G1 phase.

Discussion

We observed numerous changes in cellular proteostasis pathways following chronic respiratory chain incompetence. We examined four major pathways, the autophagy-lysosomal system, the UPS, UPRs, and the ISR. Consistent with prior reports, we found that mitochondrial dysfunction reduced proteasome activity and activated the ISR [129, 200, 218]. mtDNA depletion also decreased mtUPR and erUPR activation. Finally, we found mtDNA depletion increased basal autophagy flux, while altering numerous proteins important to mitophagy.

Chronic mtDNA depletion led to increased basal autophagy flux, as evidenced by increased LC3BII accumulation following lysosomal de-acidification. ρ0 cells also displayed increases in numerous cytosolic autophagy adaptor proteins, including p62, NDP52, and optineurin. Together these results suggest that chronic mtDNA depletion increases degradation of cellular materials through the lysosomal system, likely in an attempt to recycle nutrients for the energy stressed cells. Lysosomal de-acidification with bafilomycin did not affect intracellular tau levels, suggesting autophagy is not a major regulator of basal tau protein levels in SY5Y cells. ρ0 cells also displayed decreases in numerous mitophagy related proteins.

Chronic mtDNA depletion drastically decreased parkin, BNIP3, and Nix protein levels. We also observed decreased HIF1α mRNA levels and reductions in mRNA levels of the HIF1α target gene, Nix. HIF1α, along with BNIP3 and Nix, can stimulate mitophagy. Typically, HIF1α mediated mitophagy occurs in response to hypoxia. Hypoxia stabilizes HIF1α, leading to increased BNIP3 and NIX levels [219]. In ρ0 cells, we observe decreased HIF1α mRNA levels, which may explain the decreased Nix mRNA and protein levels. Based on these results alone, we cannot claim whether ρ0 cells experience increased or decreased mitophagy rates. However, we hypothesize that mitophagy decreases in ρ0 cells due to the decrease in these key mitophagy

proteins. Alternatively, NDP52 and optineurin contribute to mitophagy, so the increase in these markers could argue for increased mitophagy in ρ0 cells. Future experiments using electron microscopy or pH-sensitive mitophagy markers could resolve this question. Recent reports suggest mitophagy plays an important role in clearing AD-associated protein aggregates [83, 135].

We also observed decreased proteasome activity in ρ0 cells. Decreased proteasome activity may contribute to ρ0 tau accumulation. Consistent with decreased UPS activity, we found increased PARIS protein levels in ρ0 cells. Increased PARIS transcription does not completely explain the observed increases in PARIS protein, as mRNA levels increase by ~40% and protein levels increased 3-fold. Parkin ubiquitinates PARIS, marking it for degradation by the proteasome [207]. PARIS likely accumulates in ρ0 cells due to the decrease in parkin protein coupled with decreased proteasome activity. PARIS represses PGC1α transcription, inhibiting mitochondrial biogenesis pathways [207]. In ρ0 cells, increased PARIS protein levels occur alongside decreased PGC1α mRNA levels. Therefore, PARIS may be partly responsible for the decreased PGC1α mRNA levels in ρ0 cells.

We found decreased levels of mtUPR and erUPR markers upon chronic mtDNA depletion. ATF5, the master regulator of the mammalian mtUPR, decreases in the cytoplasm and nucleus of ρ0 cells. Furthermore, mitochondrial proteases and chaperones regulated by ATF5, including *HSPD1* and *ClpP*, decrease upon chronic mtDNA depletion. Hsp60 and ClpP protein levels also decline. Earlier studies in ρ0 rat hepatoma cells suggested ethidium bromide treatment stimulates mtUPR signaling [220]. However, a subsequent study in human HeLa ρ0 cells found that mtDNA depletion fails to activate the mtUPR [218]. Our findings in SY5Y ρ0 cells agree with and expand upon the findings in HeLa ρ0 cells, showing that mtDNA depletion does not

activate the mtUPR in SY5Y cells. We also examined mtUPR markers following acute mtDNA depletion. We saw no evidence of mtUPR activation during acute mtDNA depletion, suggesting the mtUPR is not responsive to acute or chronic states of respiratory chain incompetence.

Numerous studies in human cells suggest that mitochondrial dysfunction stimulates the ISR [129, 218]. Our findings in SY5Y ρ0 cells agree with prior reports, as chronic mtDNA depletion activated key markers of the ISR. We observed increased eIF2α phosphorylation, increased *DDIT3* transcription, and increased nuclear ATF4 and CHOP protein levels. Furthermore, we found that an integrated stress response inhibitor, ISRIB, decreased nuclear ATF4 and CHOP protein levels in ρ0 cells. ISR inhibition failed to alter tau protein levels, suggesting ISR activation does not cause ρ0 tau accumulation. The ISR can be triggered by multiple stressors, although the ISR's association with ER-stress and the erUPR typically receives the most attention. The erUPR consists of three arms, and mtDNA depletion did not activate the two UPR arms outside of the ISR, as evidenced by decreased XBP1 splicing and no change in *HSPA5* transcription. This suggests that the ISR activation observed in ρ0 cells does not stem from increased ER-stress and PERK activation, but from another eIF2α kinase. Furthermore, PERK inhibition caused no changes in eIF2α phosphorylation (data not shown).

ISR activation likely has many consequences in ρ0 cells. eIF2α phosphorylation typically decreases protein translation rates to reduce proteostatic stress, while ATF4 induction rewires cellular metabolism to adapt to the loss of mitochondrial function [129, 221]. Mitochondrial function contributes to one carbon metabolism and serine production, which serves a role in cellular biosynthesis. In states of respiratory chain dysfunction, ATF4 activation stimulates serine biosynthesis pathways in an apparent attempt to compensate for the loss of mitochondrial-dependent serine synthesis [222]. Chronic induction of CHOP favors apoptosis and cell cycle

arrest. ρ0 cells appear to find a balance in CHOP signaling, as they do not proceed into apoptosis, but they do slow cell cycle progression. Propidium iodide analysis reveals an increased percentage of ρ0 cells in G1 phase and a reduced percentage in S and G2 phases. CHOP expression may contribute to the observed G1 cell cycle arrest [223]. Slowed progression through the cell cycle likely conserves resources for cells struggling to maintain energy levels. Acute EtBr treatment also stimulated CHOP expression, although only at the 7 day time point. This suggests ISR activation and CHOP induction occur following long-term mitochondrial stress.

The differences between mammalian mitochondrial stress responses (MSRs) and those described in yeast and *C. elegans* are beginning to become more clear. Many findings support the existence of an mtISR, or an integrated stress response triggered specifically by mitochondrial dysfunction rather than ER-stress. The mtISR responds to various mitochondrial stressors. The results presented herein confirm that mtDNA depletion activates the mtISR. As for the mtUPR, this pathway canonically becomes activated when misfolded proteins localize to the mitochondria, stimulating mitochondrial chaperone and protease expression in an ATF5-dependent manner. However, mtDNA depletion does not seem to activate this response in human cells. Overall, the mtUPR appears to respond to fewer forms of mitochondrial stress than the mtISR. To further complicate the situation, studies suggest that the mtUPR actually consists of three arms regulated separately by ATF5, SirT3, and AKT.

We found that mtDNA depletion in SY5Y cells activates both SirT3 and AKT. As to whether this response constitutes an mtUPR per se, we remain unsure. The findings could suggest that mtDNA depletion causes mitochondrial proteotoxic stress, which then activates the SirT3 and AKT arms of the mtUPR, without ATF5 activation. However, without further

evidence of mitochondrial proteotoxic stress, we choose to classify this response more broadly as a MSR, since multiple signals outside of unfolded proteins could activate SirT3 and AKT following mtDNA depletion.

SirT3 upregulation and AKT activation likely favor cell survival in the context of mtDNA depletion. Together, AKT phosphorylation and increased SirT3 levels could inhibit numerous apoptotic factors, decrease cellular ROS levels, and increase glucose uptake and glycolytic flux [213, 215]. Multiple studies associate AKT activation with adaptation to mitochondrial stress. mtDNA depletion via EtBr or dideoxycytidine increases AKT1 mRNA, protein, and Ser473 phosphorylation in C2C12 cells. Similar results were found following treatment with the mitochondrial uncoupler, CCCP [224]. Misfolded protein accumulation in the mitochondrial intermembrane space (IMS) activates AKT, stimulating production of the IMS protease HTRA2 and increasing proteasome activity [225]. Meanwhile, SirT3 appears to play a crucial role in reducing ROS levels and proteotoxic stress [226].

Chapter 4: Respiratory chain enzyme sensitivity to mtDNA depletion and SNPs

Introduction

The reasons for AD mitochondrial dysfunction remain unclear, but the mitochondrial cascade hypothesis suggests mtDNA inheritance along with acquired somatic mtDNA mutations determine an individual's baseline mitochondrial function. From there, mitochondrial function declines and, once mitochondrial dysfunction surpasses a functional threshold, disease ensues [100]. COX deficiency occurs in the AD brain as well as systemically throughout an AD patient's body [68, 69]. The AD COX deficiency is relatively specific, as other respiratory chain enzyme activities do not change. AD cybrids recapitulate the observed COX deficiency, suggesting mtDNA inheritance/mutations contribute to this phenomena [73].

Whether acquired mtDNA mutations or inherited mtDNA variants contribute to the COX deficiency remains unclear. Preliminary results from the KUADC cohort provide insight to the AD risk associated with inherited mtDNA variants. Evidence from this cohort suggests haplogroup J increases AD risk relative to haplogroups H and T (unpublished data). The Alzheimer's disease Neuroimaging Initiative (ADNI) cohort also finds haplogroup J to be overrepresented in the AD group. This argues that haplogroup J increases AD risk. Haplogroup J could influence AD risk through multiple mechanisms. Single nucleotide polymorphisms (SNPs) in the mtDNA control region could disrupt mtDNA transcription or replication, leading to decreased mitochondrial transcripts or mtDNA levels. The nucleotide 13708 mutation, which defines haplogroup J, leads to a transition from threonine to alanine in the ND5 protein. This non-synonymous mutation is associated with increased risk of multiple sclerosis and Leber's Hereditary Optic Neuropathy (LHON) [227, 228].

Here, we compare COX and complex I activity in cells depleted of mtDNA to varying degrees. Previous reports show a linear correlation between mtDNA levels and COX activity

[229]. Whether complex I activity follows mtDNA levels so closely remains unclear. If COX activity declines at a greater rate upon mtDNA depletion relative to complex I activity, then mtDNA depletion could reasonably contribute to the specific COX defect observed in AD.

Next, we examined one haplogroup H and one haplogroup J cybrid to learn about haplogroup J's influence on mitochondrial function. Unfortunately, our sample size is not large enough to make broad claims about haplogroup H and J as a whole. The findings from this study, however, will inform future work on haplogroup H and J cybrids. Future studies will examine mitochondrial parameters in a large group of haplogroup H and J cybrids.

Materials and Methods

Methodology relevant to multiple chapters is not repeated in each chapter. Please refer to the materials and methods section of Chapter 2 for techniques common across all chapters (*e.g.* cell culture methods, whole cell lysate preparation, RNA extraction, western blotting, qPCR, etc.)

Cytochrome c oxidase Activity Assay

Cells were grown to 95% confluency in T75 flasks. After removing the media and washing with calcium and magnesium free HBSS (gibco #14025-092), cells were gently scraped in 8 mL of HBSS. The cell suspension was then counted. The cells were pelleted and the supernatant was removed, and cells were resuspended in HBSS at a concentration of 30 million cells per mL. 950 µL 100mM PBS, pH 7.4 and 20 µL of 10 mg/mL β-maltoside (Sigma #D4641) were added to cuvettes and warmed to 30°C in the water bath prior to the assay. A blank reading of this mixture was taken. 30 µL of cell suspension was added to the cuvette, mixed well, and incubated at 30°C for 2 minutes. Reduced cytochrome c (Sigma #C7752) was then added to the cuvette using a Hamilton syringe and mixed well. The absorbance was read at 550 nm at 6 second intervals for 2 minutes. Potassium ferricyanide crystals (Sigma #702587) were added following the first absorbance measurement, and absorbance was read again at 550 nm at 6 second intervals for 2 minutes. For normalization to total protein, 5 µL of cell suspension was loaded into a 96 well plate for a BCA assay. The COX activity, in sec^{-1}, was calculated by subtracting the blank from the absorbance readings, then calculating the log of the absorbance readings and creating a scatter plot with “Time” as the X axis and “Log(Abs)” as the Y axis. The absolute value of the slope represented the COX Vmax activity. The COX Vmax activity was normalized to both citrate synthase activity and total protein.

Citrate Synthase Activity Assay

Following all COX activity assays, citrate synthase activity was measured using the same samples. 936 µL 100 mM Tris pH 8.0, 4 µL of 10% triton X-100 (Sigma #1002841029), and 10 µL of 10mM DTNB (Sigma #D8130) were mixed in a cuvette and warmed to 30°C in the water bath. A blank reading of this mixture was taken. Then, 30 µL cell suspension was added to the cuvette and incubated at 30°C for 2 minutes. 10 µL of 50 mM oxaloacetate (Sigma #07753), made fresh in 10 mM Tris-HCl pH 8.0 and 10 µL of 5 mM acetyl-CoA (Sigma #A2181) were added to the cuvette, and the reaction was mixed well. Absorbance was read at 412 nm at 6 second intervals for 2 minutes. To calculate CS activity, we plotted "Time" as the X-axis and "Absorbance minus blank" on the Y-axis. The slope of this line was multiplied by 60 to get the rate/minute, and then divided by 0.0136 (a constant taking into account the extinction coefficient of DTNB colorimetric reagent at 412 nm and the optical path length of the cuvette). The resulting value represented the CS Vmax activity of the sample in nmol/min. We normalized CS Vmax activity to total protein.

Complex I Activity Assay

Cells were grown to 95% confluency in T180 flasks. After removing the media and washing with PBS, cells were gently scraped in 8 mL of PBS. The cells were then pelleted, the supernatant was aspirated, and pellets were snap frozen in liquid nitrogen and stored at -80°C. For mitochondrial isolation, pellets were thawed on ice. The cell pellet was resuspended in 2.9 mL 10mM Tris pH 7.6 and lysed with 20 strokes in a glass/Teflon homogenizer. Following lysis, 0.6 mL 1.5 mM sucrose was added, and samples were centrifuged at 600x*g* for 10 minutes. The resulting supernatant was centrifuged at 14,000x*g* for 10 minutes. The mitochondrial pellet was resuspended in 100 µL 10mM Tris buffer, snap frozen in liquid nitrogen, and stored at -80°C. On the day of the assay, mitochondrial pellets were thawed on ice, and protein was quantified via

BCA assay. 75 µg of the enriched mitochondrial fraction was loaded per reaction. The 1mL reaction mixture contained 25 mM phosphate, 3.5 g/L BSA, 60 µM DCIP, 70 µM decylubiquinone, and 1 µM antimycin A. The reaction mixture was heated to 37°C in a water bath and 50 µL of mitochondrial-enriched fraction was added. After a 3 minute incubation, 20 µL of 10 mM NADH was added and the absorbance was read at 600 nm with 30 second intervals for 4 minutes. Then, we added 1 µL of 1 mM rotenone and read the absorbance at 600 nm at 30 second intervals for 4 minutes. The slope of the absorbance following rotenone addition was subtracted from the non-rotenone slope to give the rotenone-sensitive complex I activity.

96-well Seahorse Mitochondrial Stress Test

The day before the assay, 40,000 cells were seeded per well in a Seahorse XF96 cell culture plate. Cells were initially seeded in 100µL complete media. The next day, 25 mM glucose, 2 mM glutamine and 1 mM pyruvate were added to mito stress test media. Then, the cells were washed twice in assay media, and finally were brought to a final volume of 180µL in assay media. Cells were degassed at 37°C in a non-CO2 incubator for 45 minutes. Mitochondrial inhibitors were diluted in 3mL assay buffer to the following concentrations (10x): oligomycin (Sigma #75351)= 10 µM, FCCP (Sigma #C2920)= appropriate amount determined through titration experiments, rotenone (Sigma #R8875) and antimycin A (Sigma #A8674) = 5 µM each. The experiment was run on the Seahorse XF96 analyzer using an extracellular flux assay kit and following the mitochondrial stress test protocol.

Results

Acute EtBr treatment reduces ETC subunits, including nuclear encoded subunits

We discovered that 24hr EtBr treatment reduces SY5Y mtDNA levels by ~50%, 3 day treatment reduces mtDNA content by ~75%, and 7 day treatment reduces mtDNA by ~95%. As the mtDNA encodes for numerous ETC subunits, we confirmed successful mtDNA depletion by examining the protein levels of one mtDNA-encoded subunit, MtCO2. We found MtCO2 protein levels decline proportionately with mtDNA levels upon EtBr treatment (Figure 4.1a,b). By 7 days of EtBr treatment and in ρ0 cells, MtCO2 levels fall below the western blot threshold of detection. Next, we measured protein levels of nuclear-encoded ETC subunits. We began by measuring COXIV isoform 1 (COXIVi1) levels, as COXIVi1 is a cytochrome oxidase subunit, like MtCO2. COXIVi1 protein levels declined at a similar rate to mtDNA levels, nearly mirroring the decline in MtCO2 protein levels. Unlike MtCO2 protein levels, however, COXIVi1 protein levels did not fall below the limit of detection in any treatment groups, and COXIVi1 protein was significantly increased in ρ0 cells relative to EtBr 7 day treated cells (Figure 4.1c,d).

Since COXIVi1 is a nuclear-encoded gene, we next examined whether EtBr treatment affects COXIVi1 mRNA levels. We found no changes in COXIVi1 mRNA levels during the EtBr time course, showing decreases in COXIVi1 mRNA levels do not explain the loss of COXIVi1 protein (Figure 4.2). We also examined a nuclear-encoded complex I subunit protein, NADH dehydrogenase (ubiquinone) 1 beta subcomplex 8 (NDUFB8). NDUFB8 protein levels decrease following EtBr treatment, to a greater extent than COXIVi1 protein levels (Figure 4.3a,b). We measured NDUFB8 mRNA levels during the EtBr time course and in ρ0 cells. Acute

mtDNA depletion does not affect NDUFB8 mRNA levels, while chronic mtDNA depletion leads to a slight decrease (Figure 4.4).

Prior reports show that ρ0 cells drastically reduce nuclear-encoded transcription factor A, mitochondrial (TFAM) protein levels [230]. Other reports show TFAM protein levels correlate well with mtDNA levels [231]. We found acute mtDNA depletion decreases TFAM protein levels consistent with decreases in mtDNA levels. Interestingly, ρ0 cells maintain greater TFAM protein levels relative to cells treated with EtBr for 7days (Figure 4.5a,b).

Next, we examined respiratory chain enzyme activity following mtDNA depletion. We found no significant difference between the decline in COX and complex I activity following 24 hours of EtBr treatment (Figure 4.7b). At 24 hours EtBr treatment, mtDNA levels decline to ~52% of control levels, while COX activity declines to ~53% of control levels, and complex I activity declines to ~65% of control levels.

Antibody Name	Dilution	Source	Catalog #
MtCO2	1:2,000	abcam	ab79393
COXIVi1	1:5,000	Cell Signaling	
NDUFB8	1:1,000	abcam	ab110242
TFAM	1:2,000	abcam	ab131607
NDUFV2	1:1,000	abcam	ab96117
OXPHOS Cocktail	1:2,000	abcam	ab110413
p-eIF2α Ser51	1:1,000	abcam	ab32157
eIF2α	1:2,000	Cell Signaling	CST9722
SirT1	1:1,000	Cell Signaling	CST2493
SirT3	1:1,000	Cell Signaling	CST5490

Table 4.1. List of antibodies used in experiments.

Taqman Primer	Catalog #
COX4i1	Hs00971639_m1
NDUFB8	Hs00428204_m1
18s	Hs03003631_g1

Table 4.2. List of Taqman primers used in experiments.

a.

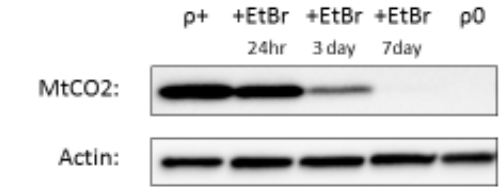
ρ+
+EtBr 24hr
+EtBr 3 day
+EtBr 7day
ρ0
MtCO2:
Actin:

b.

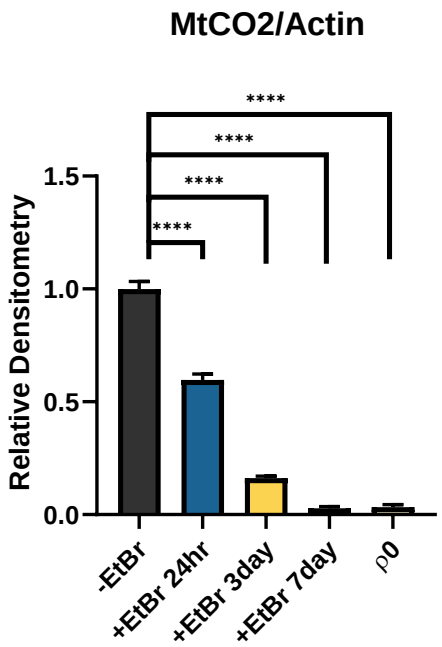
MtCO2/Actin
Relative Densitometry
1.5
1.0
0.5
0.0
****
****
****
****
-EtBr
+EtBr 24hr
+EtBr 3day
+EtBr 7day
ρ0

c.

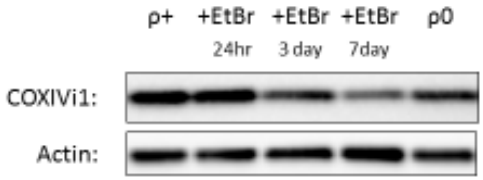
ρ+
+EtBr 24hr
+EtBr 3 day
+EtBr 7day
ρ0
COXIVi1:
Actin:

d.

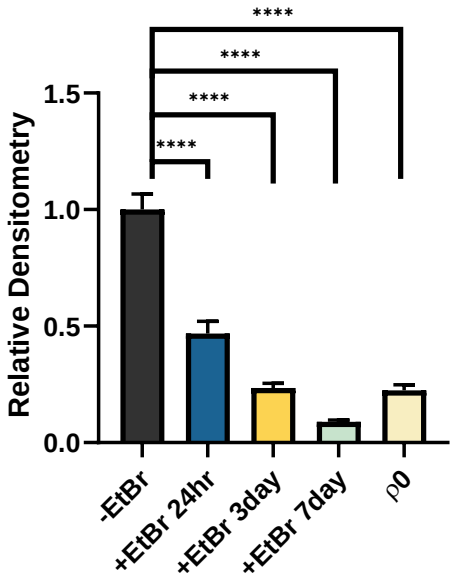
COXIVi1/Actin
Relative Densitometry
1.5
1.0
0.5
0.0
****
****
****
****
-EtBr
+EtBr 24hr
+EtBr 3day
+EtBr 7day
ρ0

Figure 4.1. Mitochondrial and nuclear-encoded COX subunit protein levels decline upon mtDNA depletion. a) Western blot images of EtBr treatment time course, with untreated (ρ+), 24hr treatment, 3day treatment, 7day treatment, and chronic mtDNA depleted (ρ0) whole cell lysates labeled with MtCO2 (mitochondrial encoded complex IV subunit). Actin serves as a loading control. b) Densitometry analysis reveals significant decreases in MtCO2 protein levels with decreasing mtDNA levels. c) Western blot images of EtBr treatment time course, with untreated (ρ+), 24hr treatment, 3day treatment, 7day treatment, and chronic mtDNA depleted (ρ0) whole cell lysates labeled with COXIVi1 (nuclear encoded complex IV subunit). Actin serves as a loading control. d) Densitometry analysis reveals significant decreases in COXIVi1 protein levels with decreasing mtDNA levels. n= 12 per group. $p<0.05$=*, $p<0.01$=**, $p<0.001$=***, $p<0.0001$=****. Error bars represent SEM.

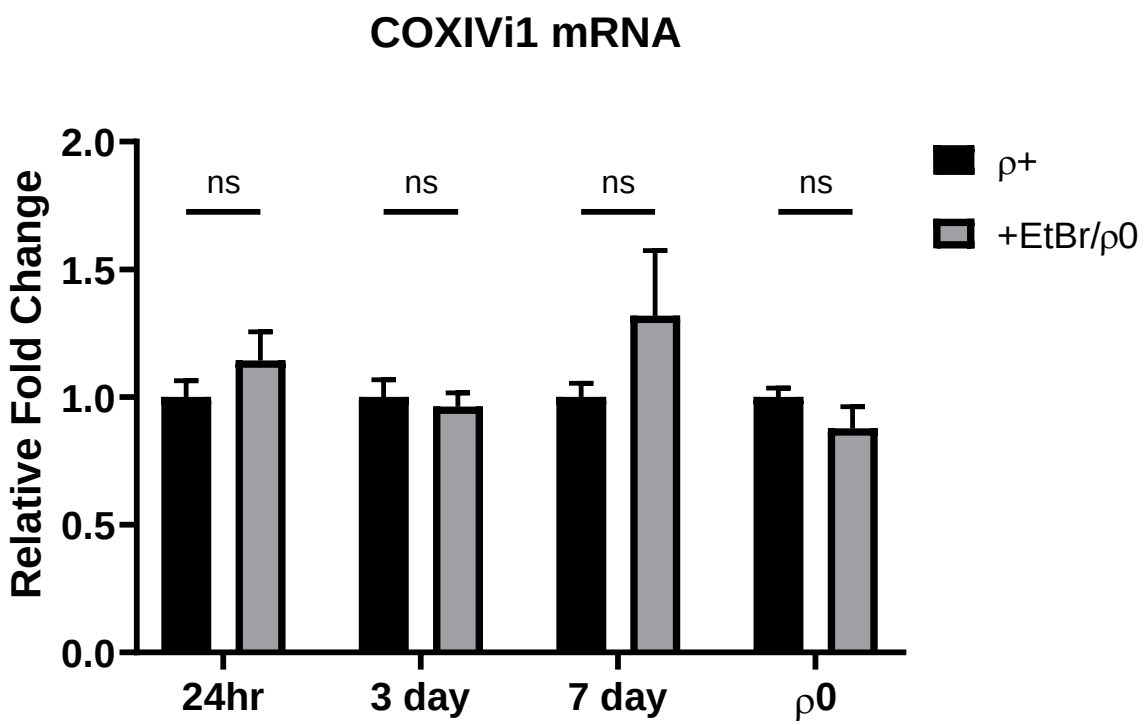
COXIVi1 mRNA
Relative Fold Change
2.0
1.5
1.0
0.5
0.0
ns
ns
ns
ns
24hr
3 day
7 day
ρ0
ρ+
+EtBr/ρ0

Figure 4.2. Nuclear-encoded respiratory chain subunit, COXIVi1, mRNA levels do not change upon mtDNA depletion. qPCR analysis reveals no changes in COXIVi1 mRNA levels during the EtBr treatment time course or in ρ0 cells relative to ρ+. 18s mRNA levels serve as a loading control. n= 12 per group. p<0.05=*, p<0.01=**, p<0.001=***, p<0.0001=****. ns= no significant difference. Error bars represent SEM.

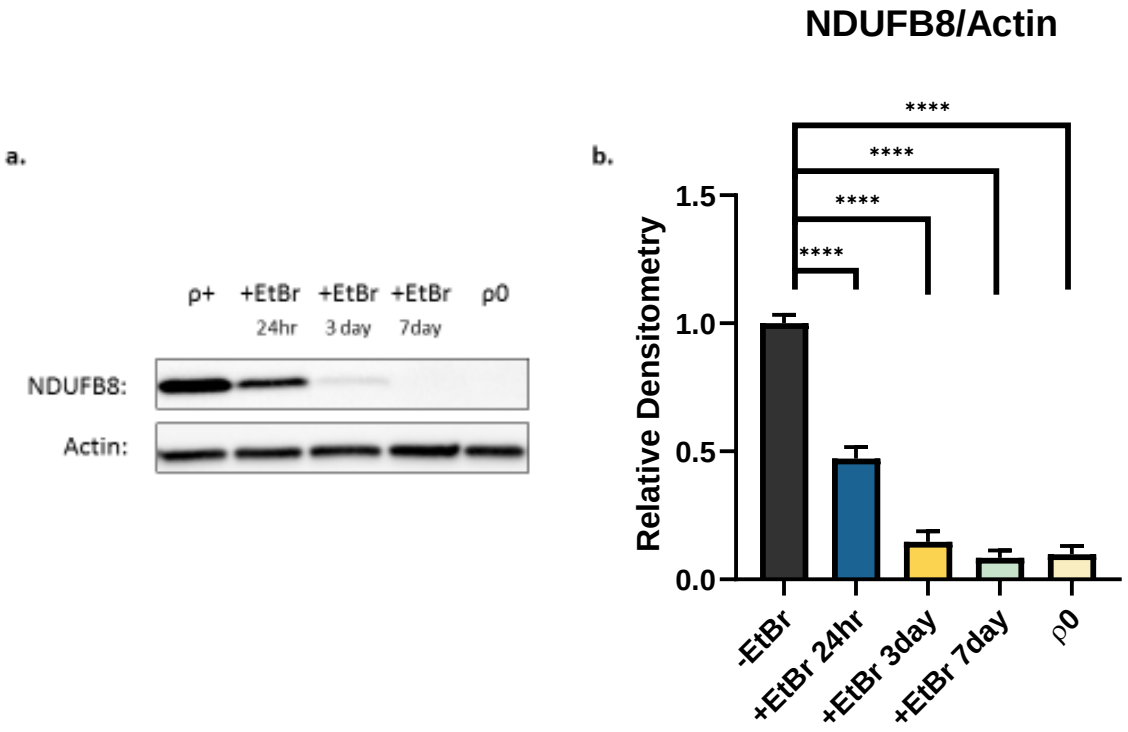
a.
ρ+
+EtBr 24hr
+EtBr 3 day
+EtBr 7day
ρ0
NDUFB8:
Actin:
b.
NDUFB8/Actin
Relative Densitometry
1.5
1.0
0.5
0.0
****
****
****
****
-EtBr
+EtBr 24hr
+EtBr 3day
+EtBr 7day
ρ0

Figure 4.3. Nuclear-encoded complex 1 subunit, NDUFB8, protein levels decline upon mtDNA depletion. a) Western blot images of EtBr treatment time course, with untreated (ρ+), 24hr treatment, 3day treatment, 7day treatment, and chronic mtDNA depleted (ρ0) whole cell lysates labeled with NDUFB8 (nuclear encoded complex I subunit). Actin serves as a loading control. b) Densitometry analysis reveals significant decreases in NDUFB8 protein levels with decreasing mtDNA levels. n= 12 per group. $p<0.05$=*, $p<0.01$=**, $p<0.001$=***, $p<0.0001$=****. Error bars represent SEM.

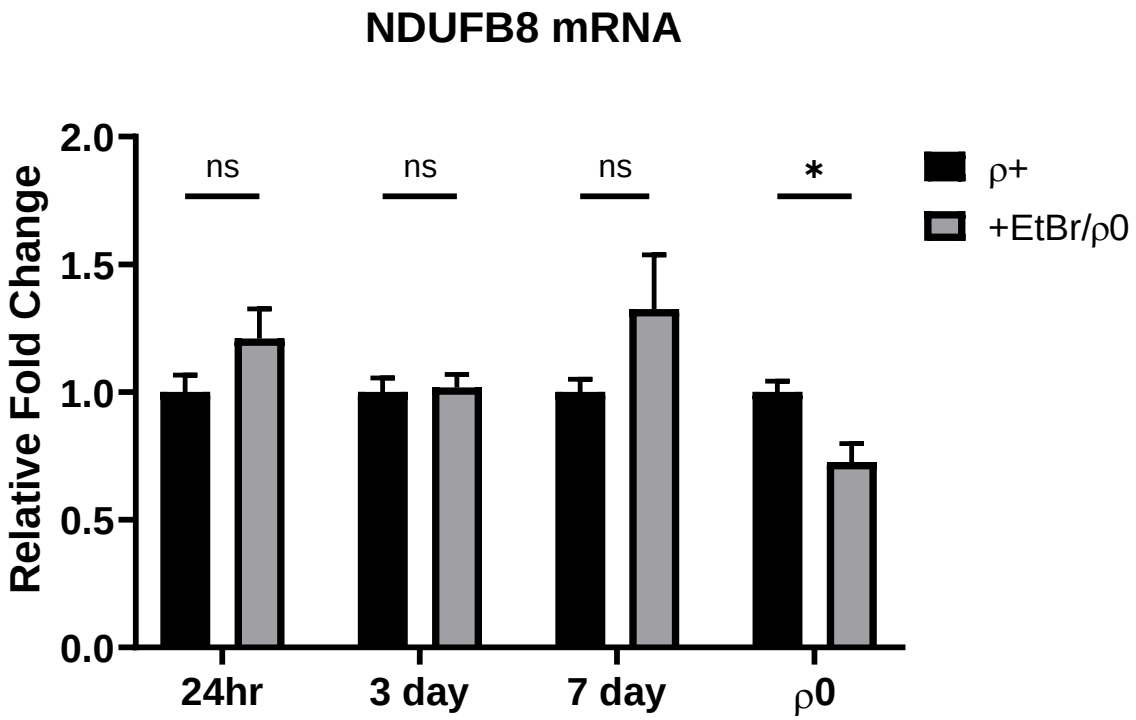
NDUFB8 mRNA
Relative Fold Change
2.0
1.5
1.0
0.5
0.0
ns
ns
ns
*
ρ+
+EtBr/ρ0
24hr
3 day
7 day
ρ0

Figure 4.4. Nuclear-encoded respiratory chain subunit, NDUFB8, mRNA levels do not change upon acute mtDNA depletion, while chronic mtDNA depletion reduces NDUFB8 mRNA levels. qPCR analysis reveals no changes in NDUFB8 mRNA levels during the EtBr treatment time course. NDUFB8 mRNA levels decline in ρ0 cells relative to ρ+. 18s mRNA levels serve as a loading control. n= 12 per group. $p<0.05$=*, $p<0.01$=**, $p<0.001$=***, $p<0.0001$=****. ns= no significant difference. Error bars represent SEM.

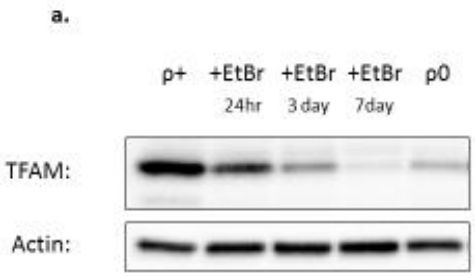
a.
ρ+
+EtBr 24hr
+EtBr 3 day
+EtBr 7day
ρ0
TFAM:
Actin:

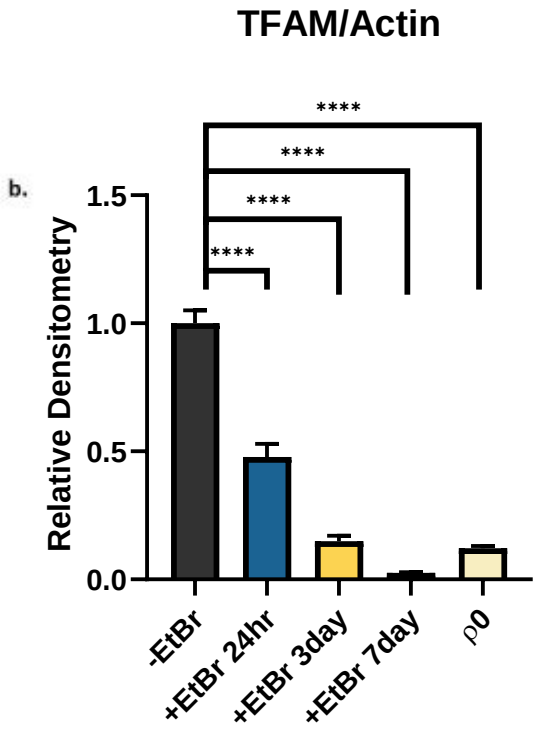
TFAM/Actin
b.
****
****
****
****
Relative Densitometry
1.5
1.0
0.5
0.0
-EtBr
+EtBr 24hr
+EtBr 3day
+EtBr 7day
ρ0

Figure 4.5. Nuclear encoded mitochondrial transcription factor, TFAM, protein levels decline upon mtDNA depletion. a) Western blot images of EtBr treatment time course, with untreated (ρ+), 24hr treatment, 3day treatment, 7day treatment, and chronic mtDNA depleted (ρ0) whole cell lysates labeled with TFAM (nuclear encoded). Actin serves as a loading control. b) Densitometry analysis reveals significant decreases in TFAM protein levels with decreasing mtDNA levels. n= 12 per group. $p<0.05$=*, $p<0.01$=**, $p<0.001$=***, $p<0.0001$=****. Error bars represent SEM.

Acute mtDNA depletion decreases COX activity

Since AD patients display systemic reductions in COX activity without concomitant reductions in complex I, we examined COX activity and complex I activity following mtDNA depletion to determine whether either ETC enzyme complex's acitivity is more sensitive to this intervention [68, 70]. We analyzed COX activity in SY5Y cells following 24hr and 3 day EtBr treatment, which corresponds to ~50% and ~75% mtDNA depletion, respectively. 24hr EtBr treatment significantly decreased COX activity by ~50%, while 3 day ethidium bromide treatment significantly decreased COX activity by ~75% (Figure 4.6). We normalized COX activity to multiple parameters, including citrate synthase (CS) activity and total protein levels. We found similar results regardless of whether we normalized COX activity to CS activity or total protein levels (Figure 4.6a,b). We also found that 24hr and 3 day EtBr treatment do not significantly alter CS activity when normalized to total protein levels, confirming CS activity is a reasonable normalization parameter (Figure 4.6c).

a.

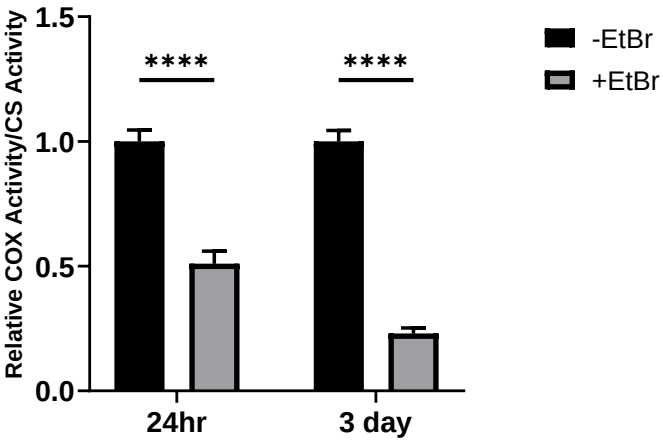
COX Activity/CS Activity
Relative COX Activity/CS Activity
1.5
1.0
0.5
0.0
****
****
24hr
3 day
-EtBr
+EtBr

b.

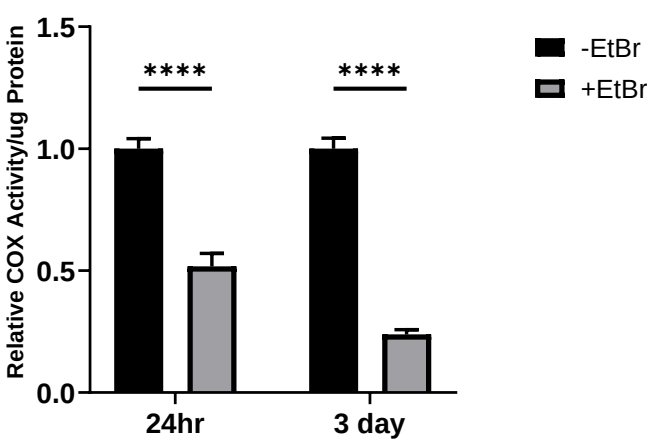
COX Activity/ug Protein
Relative COX Activity/ug Protein
1.5
1.0
0.5
0.0
****
****
24hr
3 day
-EtBr
+EtBr

c.

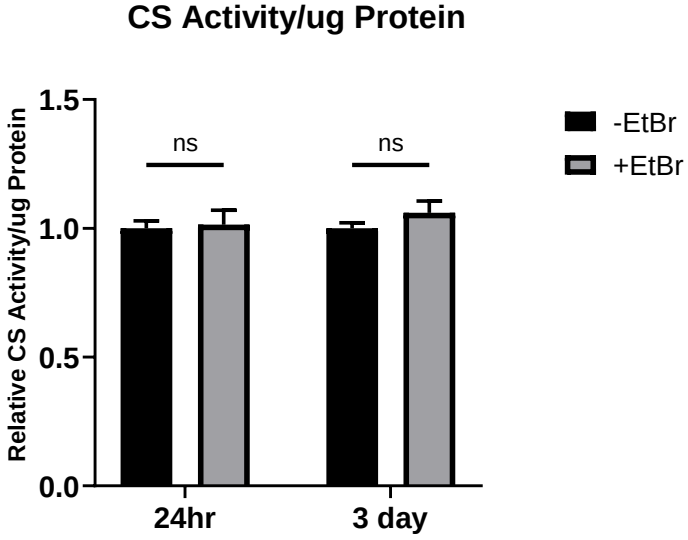
CS Activity/ug Protein
Relative CS Activity/ug Protein
1.5
1.0
0.5
0.0
ns
ns
24hr
3 day
-EtBr
+EtBr

Figure 4.6. Acute mtDNA depletion decreases COX activity. a) SY5Y cells treated with EtBr for 24hr and 3 days show significant decreases in COX activity. Here, COX activity is normalized to CS activity. b) When COX activity is normalized to ug of protein, rather than CS activity, similar decreases in COX activity are observed. c. SY5Y cells treated with EtBr for 24hr and 3 days show no significant difference in CS activity. CS activity is normalized to ug of protein. ns= no significant difference. n= 12 per group. $p<0.05$=*, $p<0.01$=**, $p<0.001$=***, $p<0.0001$=****. Error bars represent SEM.

a.

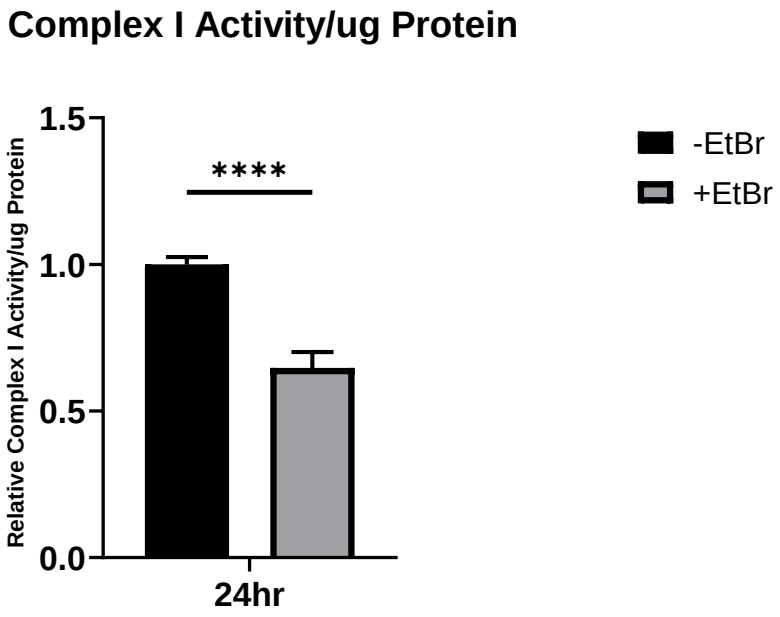
Complex I Activity/ug Protein
Relative Complex I Activity/ug Protein
1.5
1.0
0.5
0.0
****
24hr
-EtBr
+EtBr

b.

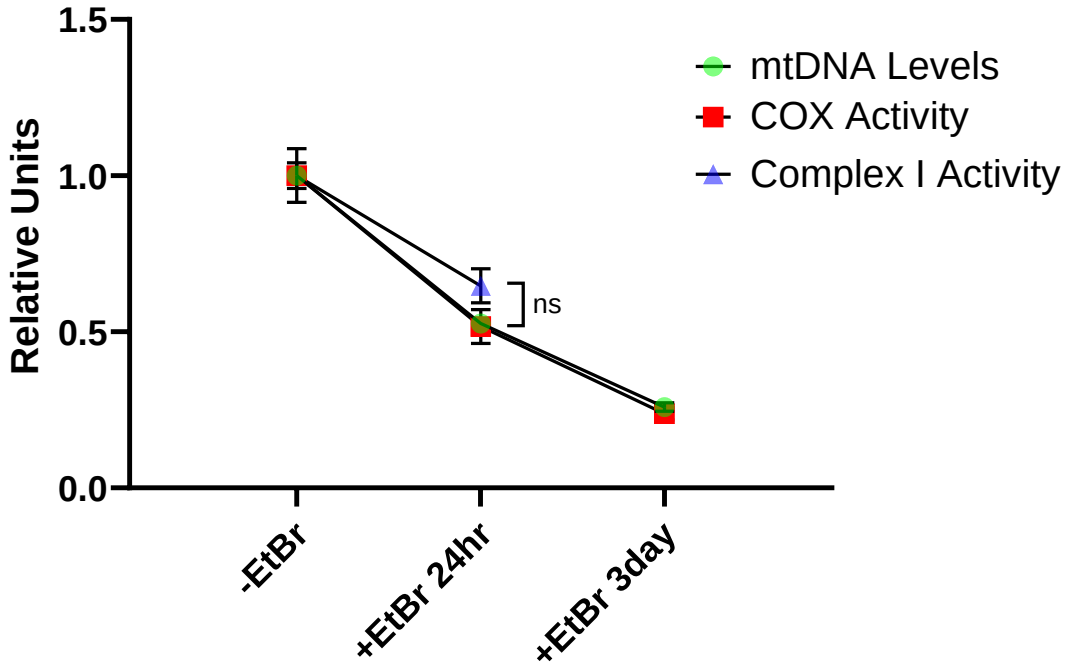
Relative Units
1.5
1.0
0.5
0.0
ns
mtDNA Levels
COX Activity
Complex I Activity
-EtBr
+EtBr 24hr
+EtBr 3day

Figure 4.7. Acute mtDNA depletion decreases Complex I activity. a) SY5Y cells treated with EtBr for 24hr show significant decreases in rotenone-sensitive Complex I activity. Here, Complex I activity is normalized to μg protein. b) Comparison between mtDNA levels, COX activity, and complex I activity following EtBr treatment. n= 12 per group. ns=no significant difference. $p<0.05$=*, $p<0.01$=**, $p<0.001$=***, $p<0.0001$=****. Error bars represent SEM.

A haplogroup J cybrid displays reduced mitochondrial function despite increased mtDNA levels

Initially, we set out to compare mitochondrial function in multiple haplogroup H cybrids to multiple haplogroup J cybrids. In the KU ADC cohort, haplogroup J confers a nearly 2 fold increased risk for developing sporadic AD. We hoped to learn how haplogroup J affects mitochondrial function in these cybrid studies. However, our cybrid cohort had relatively small numbers of haplogroup J cybrids, making it difficult to draw conclusions regarding haplogroup J as a whole. A future study will answer these questions in a more satisfactory manner with a sufficient sample size. We did find drastic differences between one haplogroup J cybrid and one haplogroup H cybrid. Although these findings may not be representative of haplogroup J as a whole and may, instead, stem from private mutations, we believe the findings contribute to our fundamental understanding of mitochondrial biology and ETC function.

First, we measured oxygen consumption and extracellular acidification in the haplogroup J line and the haplogroup H line. We found a significant decrease in the basal OCR of the haplogroup J cybrid, along with a significant increase in haplogroup J cybrid's basal ECAR (Figure 4.8b,d). The representative OCR and ECAR traces show the haplogroup H and J cybrid's oxygen consumption and extracellular acidification over the course of a mitochondrial stress test (MST) (Figure 4.8a,c). During the Seahorse run, four injections occurred in the following order: 1. Oligomycin. 2. FCCP. 3. Rotenone and antimycin A. 4. 2-deoxyglucose. The results suggest a profound defect in ETC function in the haplogroup J cybrid.

We predicted that the haplogroup J cybrid maintains less mtDNA, which would explain the observed decrease in OCR. Upon measuring mtDNA levels in the haplogroup H and J cybrids, we discovered the haplogroup J cybrid maintains more mtDNA than the haplogroup H cybrid (Figure 4.9a). We found no difference in mtDNA synthesis rate between the haplogroup

H and J cybrid, suggesting another mechanism contributes to increased mtDNA levels in the haplogroup J cybrid (Figure 4.9b). We also measured TFAM protein levels, since TFAM contributes to mtDNA replication and we observed increased mtDNA levels. TFAM levels did not change between the haplogroup H and J cybrids (Figure 4.9c,d).

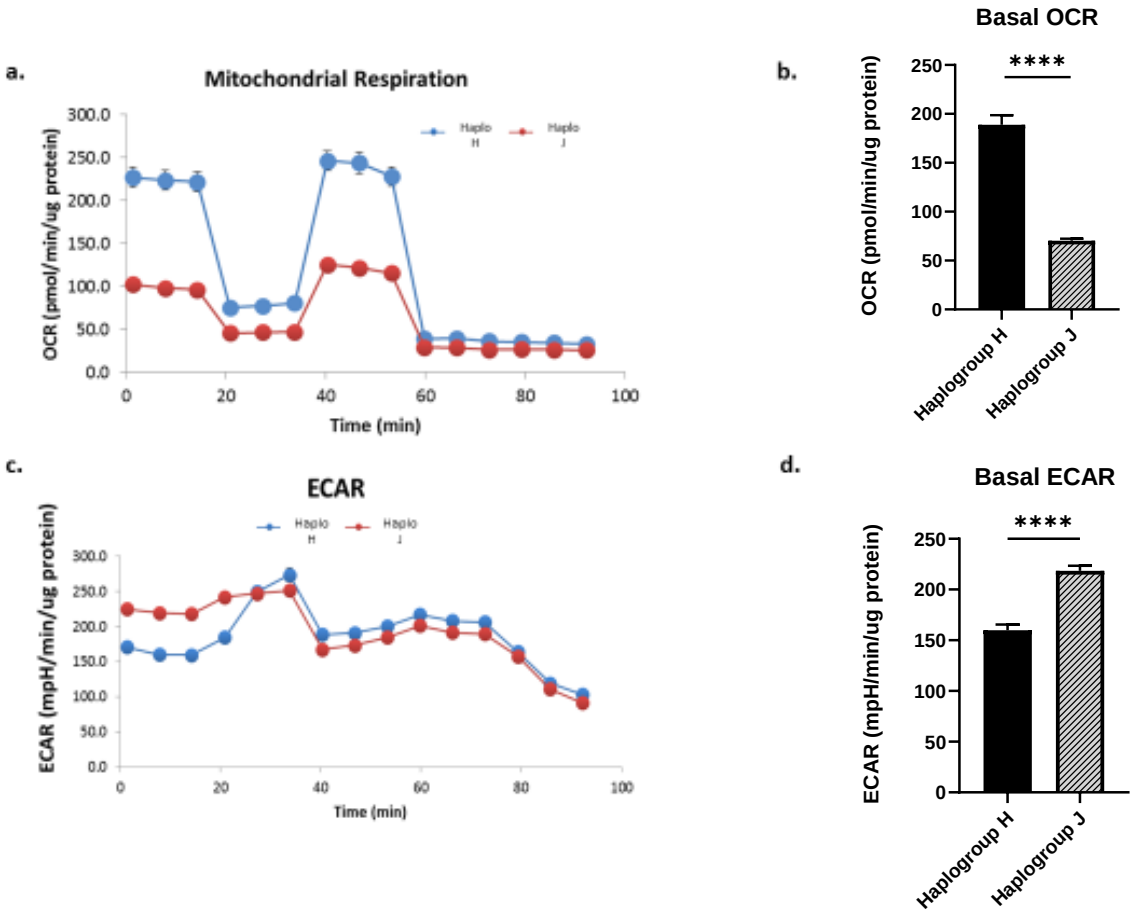
a.
Mitochondrial Respiration
OCR (pmol/min/ug protein)
Time (min)
Haplo H
Haplo J
b.
Basal OCR
****
OCR (pmol/min/ug protein)
Haplogroup H
Haplogroup J
c.
ECAR
ECAR (mpH/min/ug protein)
Time (min)
d.
Basal ECAR
****
ECAR (mpH/min/ug protein)

Figure 4.8. A haplogroup J cybrid shows decreased OCR and increased ECAR relative to a haplogroup H cybrid. a) Oxygen consumption rate (OCR) during a mitochondrial stress test Seahorse in a haplogroup H and haplogroup J cybrid. Injection 1= oligomycin, Injection 2= FCCP, Injection 3= Anitmycin A+Rotenone, Injection 4= 2-deoxyglucose. b) Basal respiration rates derived using the Seahorse analysis program shows significantly decreased basal OCR in the haplogroup J cybrid. c) Extracellular acidification rate (ECAR) during a mitochondrial stress test Seahorse in a haplogroup H and Haplgroup J cybrid. d) Basal ECAR derived using the Seahorse analysis program shows significantly increased basal ECAR in the haplogroup J cybrid. n= 19 per group. $p<0.05$=*, $p<0.01$=**, $p<0.001$=***, $p<0.0001$=****. Error bars represent SEM.

a.

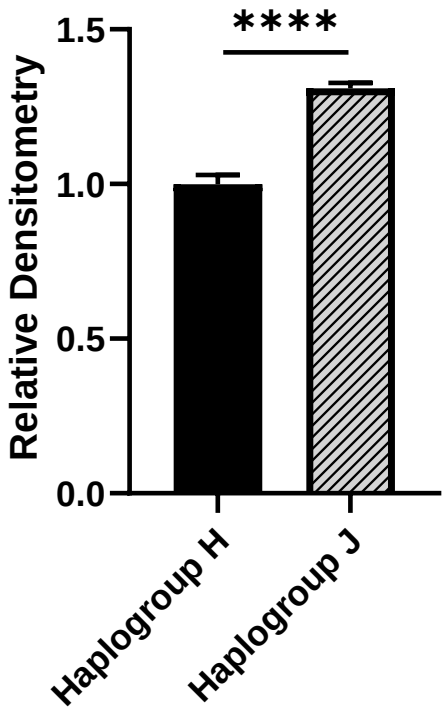
mtDNA/Nuclear DNA Ratio
****
Relative Densitometry
1.5
1.0
0.5
0.0
Haplogroup H
Haplogroup J

b.

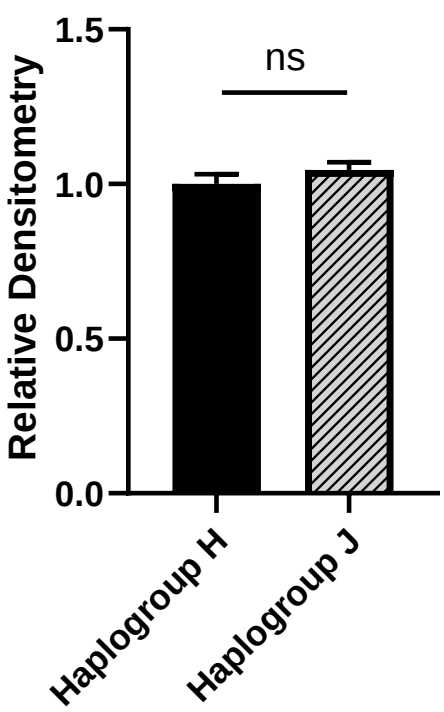
mtDNA Synthesis Rate
ns
Relative Densitometry
1.5
1.0
0.5
0.0
Haplogroup H
Haplogroup J

c.

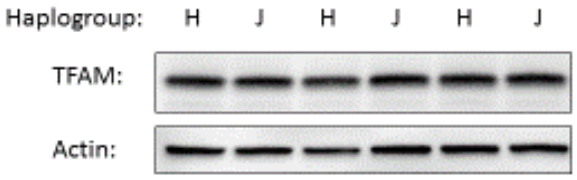
Haplogroup: H J H J H J
TFAM:
Actin:

d.

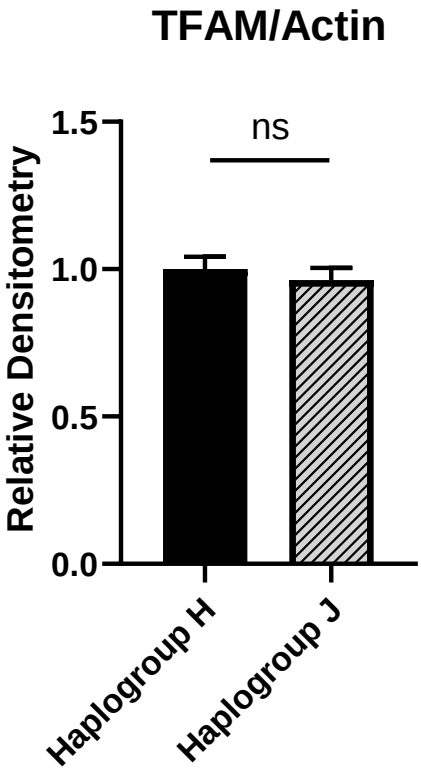
TFAM/Actin
ns
Relative Densitometry
1.5
1.0
0.5
0.0
Haplogroup H
Haplogroup J

Figure 4.9. The haplogroup J cybrid maintains increased mtDNA levels without changing the mtDNA synthesis rate or TFAM protein levels. a) qPCR analysis of haplogroup H and J cybrid DNA utilizing mtDNA specific primers targeting ND1 and nuclear specific primers targeting β2M reveals a specific increase in mtDNA levels in the haplogroup J cybrid. Data represents the ratio of ND1/β2M. b) qPCR analysis of haplogroup H and J cybrid DNA synthesis rate utilizing primers targeting the mtDNA D-loop and ND1. c) Western blot image of whole cell lysates from a haplogroup H and a haplogroup J cybrid labeled with TFAM. d) Densitometry analysis reveals no significant difference in TFAM levels between the haplogroup H cybrid and the haplogroup J cybrid. Data represents the ratio of D-loop/ND1 amplification. n= 12 per group. $p<0.05$=*, $p<0.01$=**, $p<0.001$=***, $p<0.0001$=****. Error bars represent SEM.

Nuclear-encoded complex I protein subunits decrease in the haplogroup cybrid while other ETC complexes are maintained

We measured ETC protein subunit levels in the haplogroup H and J cybrids to see if decreased mitochondrial OCR in the haplogroup J cybrid could stem from ETC protein changes. We first measured COXIVi1, a nuclear-encoded COX subunit, protein levels in haplogroup H and J cybrids. We found no significant difference in COXIVi1 protein levels in haplogroup H and J cybrids (Figure 4.10a,b). Next, we examined MtCO2, a mtDNA-encoded COX subunit, protein levels in the haplogroup H and J cybrids. Similar to COXIVi1, we found no significant difference in MtCO2 protein levels between the haplogroup H and J cybrids (Figure 4.10c,d).

The results suggest that the haplogroup J cybrid's reduced OCR does not stem from a loss of COX subunits. Next, we measured ETC complex I subunit levels. NDUFB8, a nuclear-encoded complex I subunit, protein levels decreased by ~50% in the haplogroup J cybrid relative to the haplogroup H cybrid (Figure 4.11a,c). While NDUFB8 protein levels declined in the haplogroup J cybrid, NDUFB8 mRNA significantly increased in the haplogroup J cybrid (Figure 4.11e). Furthermore, NDUFV2, a nuclear-encoded complex I subunit, protein levels declined ~40% in the haplogroup J cybrid (Figure 4.11b,d). Based on these findings, it appears the haplogroup J cybrid experiences a specific loss of nuclear-encoded complex I subunits, while COX subunits remain unaffected.

Finally, we used an OXPHOS cocktail antibody, capable of simultaneously detecting 5 ETC subunits, each from a different respiratory chain complex. Since we boiled the protein samples, we could not detect the COX subunit, MTCO1. We had already measured NDUFB8 protein levels and observed a decrease in the haplogroup J cybrid, so the NDUFB8 band merely confirmed our earlier results. However, we had not examined any complex III subunits. We

found a significant increase in the complex III subunit, cytochrome b-c1 complex subunit 2, mitochondrial (UQCRC2), in the haplogroup J cybrid (Figure 4.12a,b). This suggests an increased level of intact complex III in the haplogroup J cybrid.

a.

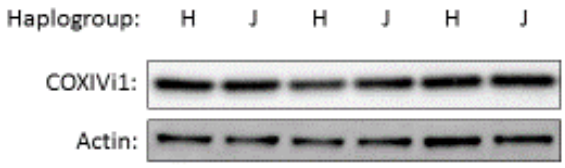
Haplogroup: H J H J H J
COXIVi1:
Actin:

b.

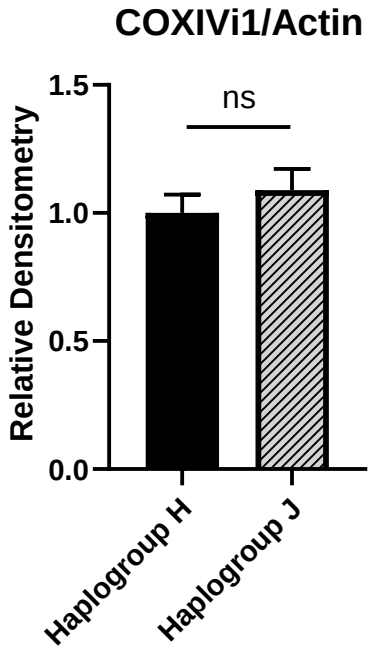
COXIVi1/Actin
ns
Relative Densitometry
1.5
1.0
0.5
0.0
Haplogroup H
Haplogroup J

c.

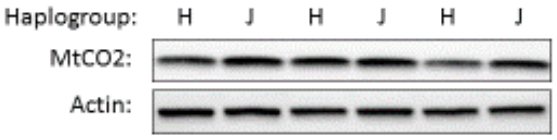
Haplogroup: H J H J H J
MtCO2:
Actin:

d.

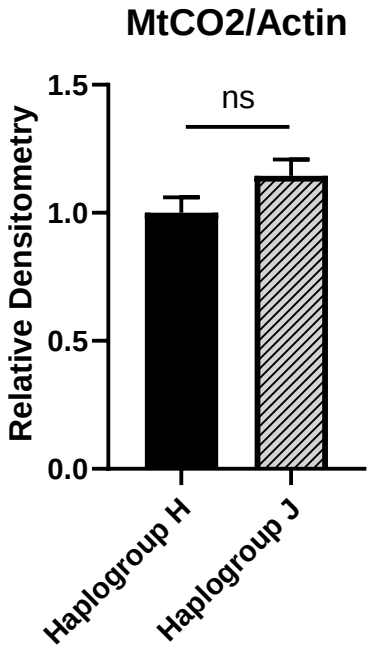
MtCO2/Actin
ns
Relative Densitometry
1.5
1.0
0.5
0.0
Haplogroup H
Haplogroup J

Figure 4.10. The haplogroup J cybrid maintains COX subunit protein levels. a) Western blot image of whole cell lysates from a haplogroup H and a haplogroup J cybrid labeled with COXIVi1 (nuclear encoded, complex IV). b) Densitometry analysis reveals no significant difference in COXIVi1 levels between the haplogroup H cybrid and the haplogroup J cybrid c) Western blot image of whole cell lysates from a haplogroup H and a haplogroup J cybrid labeled with COXIVi1 (nuclear encoded, complex IV). Actin serves as a loading control. d) Densitometry analysis reveals no significant difference in COXIVi1 levels between the haplogroup H cybrid and the haplogroup J cybrid.. n= 12 per group. ns= no significant difference. Error bars represent SEM.

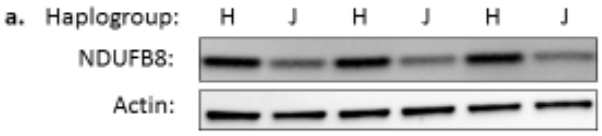
a.
Haplogroup:
H
J
H
J
H
J
NDUFB8:
Actin:

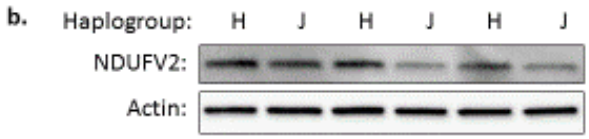
b.
Haplogroup:
H
J
H
J
H
J
NDUFV2:
Actin:

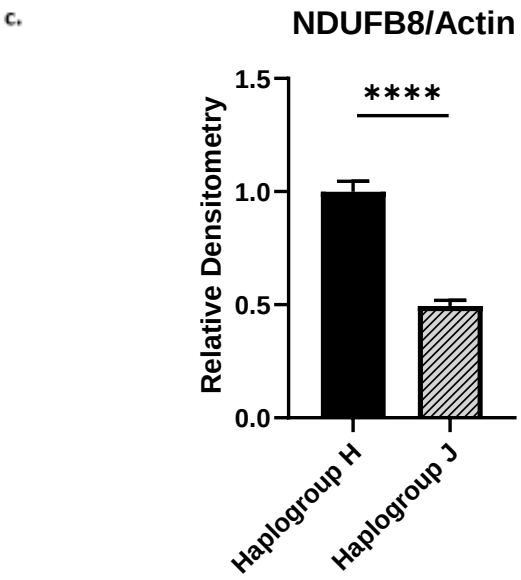
c.
NDUFB8/Actin
Relative Densitometry
1.5
1.0
0.5
0.0
****
Haplogroup H
Haplogroup J

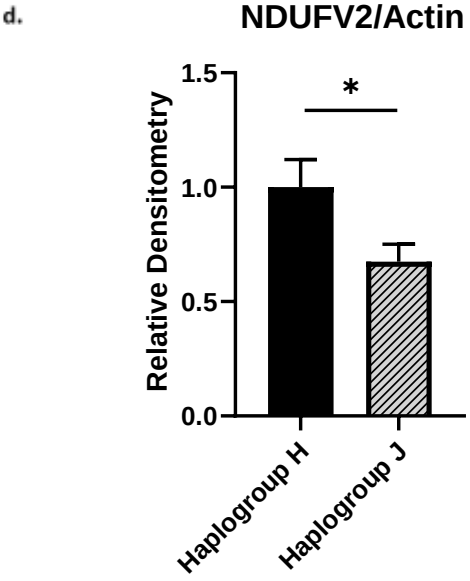
d.
NDUFV2/Actin
Relative Densitometry
1.5
1.0
0.5
0.0
*
Haplogroup H
Haplogroup J

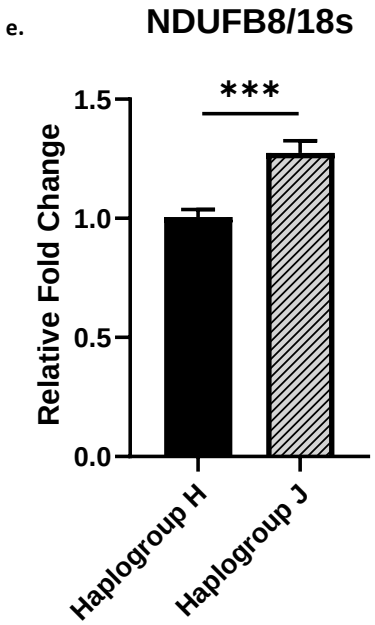
e.
NDUFB8/18s
Relative Fold Change
1.5
1.0
0.5
0.0
***
Haplogroup H
Haplogroup J

Figure 4.11. The haplogroup J cybrid displays reductions in a nuclear-encoded complex I subunit, NDUFB8. a) Western blot image of whole cell lysates from a haplogroup H and a haplogroup J cybrid labeled with NDUFB8 (nuclear-encoded, complex I). Actin serves as a loading control. b) Western blot image of whole cell lysates from a haplogroup H and a haplogroup J cybrid labeled with NDUFV2 (nuclear-encoded, complex I). Actin serves as a loading control. c) Densitometry analysis reveals a significant decrease in NDUFB8 levels in the haplogroup J cybrid relative to the haplogroup H cybrid. d) Densitometry analysis reveals a significant decrease in NDUFV2 levels in the haplogroup J cybrid relative to the haplogroup H cybrid. n= 12 per group. e) qPCR analysis reveals increased NDUFB8 mRNA levels in the haplogroup H cybrid relative to haplogroup J. $p<0.05$=*, $p<0.01$=**, $p<0.001$=***, $p<0.0001$=****. Error bars represent SEM.

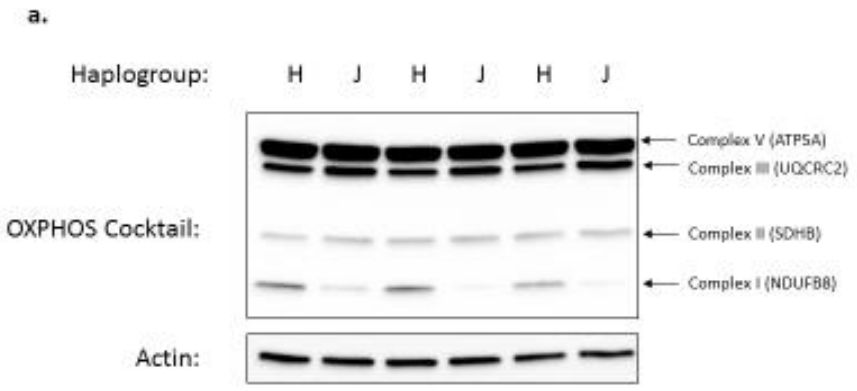
a.
Haplogroup:
H
J
H
J
H
J
OXPHOS Cocktail:
Actin:
Complex V (ATP5A)
Complex III (UQCRC2)
Complex II (SDHB)
Complex I (NDUFB8)

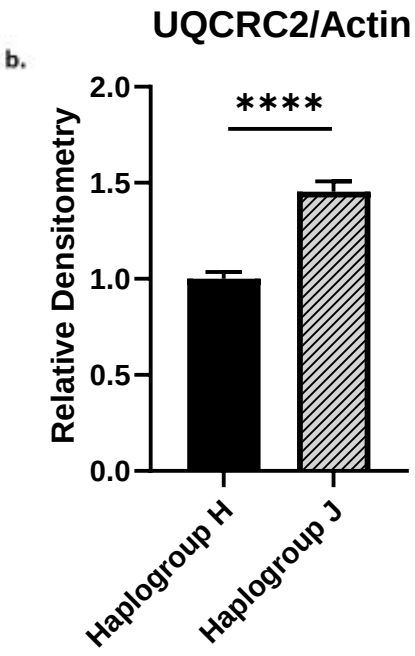
b.
UQCRC2/Actin
Relative Densitometry
2.0
1.5
1.0
0.5
0.0
****
Haplogroup H
Haplogroup J

Figure 4.12. A nuclear-encoded complex III subunit, UQCRC2, increases in the haplogroup J cybrid. a) Western blot image of whole cell lysates from a haplogroup H and a haplogroup J cybrid labeled with an OXPHOS cocktail antibody, which detects a subunit from each ETC complex. Actin serves as a loading control. b) Densitometry analysis reveals significantly increased UQCRC2 levels in the haplogroup J cybrid relative to the haplogroup H cybrid. n= 12 per group. $p<0.05$=*, $p<0.01$=**, $p<0.001$=***, $p<0.0001$=****. Error bars represent SEM.

Mitochondrial defects in the haplogroup J cybrid stimulate retrograde responses

Changes in mitochondrial function activate numerous cellular adaptations in an attempt to maintain homeostasis. We found that mtDNA depletion activates the ISR and alters many cellular signaling pathways. Other reports show similar findings. Since the haplogroup J cybrid displays defective mitochondrial function, we examined retrograde responses in the haplogroup J cybrids. We found increased eIF2α phosphorylation in the haplogroup J cybrid, along with increased CHOP mRNA (Figure 4.13a,b,c). Increased eIF2α phosphorylation and CHOP mRNA suggests ISR activation occurs in the haplogroup J cybrid. SIRT1 protein levels decrease in mtDNA-depleted cells, suggesting SIRT1 plays a role in retrograde responses. Here, we found that SIRT1 protein levels decrease in the haplogroup J cybrid (Figure 4.14a,c). SIRT3 protein levels also change in ρ0 cells, however, no difference in SIRT3 protein levels exists between the haplogroup H and J cybrids (Figure 4.14b,d).

a.

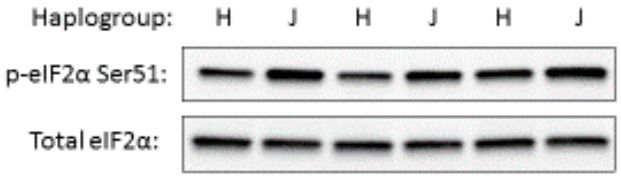
Haplogroup:
H
J
H
J
H
J
p-eIF2α Ser51:
Total eIF2α:

b.

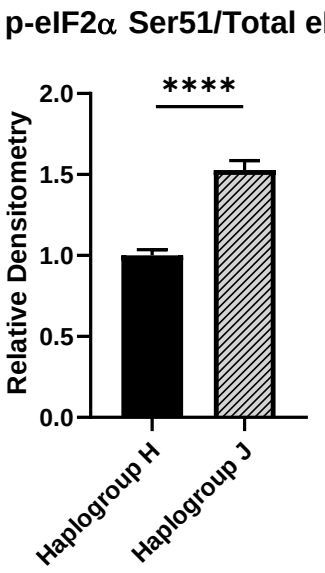
p-eIF2α Ser51/Total eIF2α
****
Relative Densitometry
2.0
1.5
1.0
0.5
0.0
Haplogroup H
Haplogroup J

c.

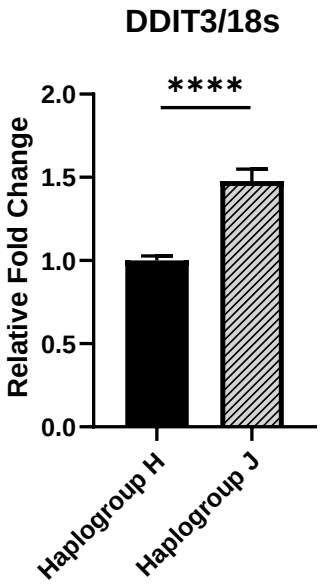
DDIT3/18s
****
Relative Fold Change
2.0
1.5
1.0
0.5
0.0
Haplogroup H
Haplogroup J

Figure 4.13. eIF2α phosphorylation and CHOP mRNA increase in the haplogroup J cybrid. a) Western blot image of whole cell lysates from a haplogroup H and a haplogroup J cybrid labeled with p-eIF2α Ser51 and total eIF2α. b) Densitometry analysis reveals a significant increase in the p-eIF2α/Total eIF2α ratio in the haplogroup J cybrid relative to the haplogroup H cybrid. c) qPCR with DDIT3 (CHOP) primers reveals a significant increase in CHOP mRNA in the haplogroup J cybrid. n= 12 per group. $p<0.05$=*, $p<0.01$=**, $p<0.001$=***, $p<0.0001$=****. Error bars represent SEM.

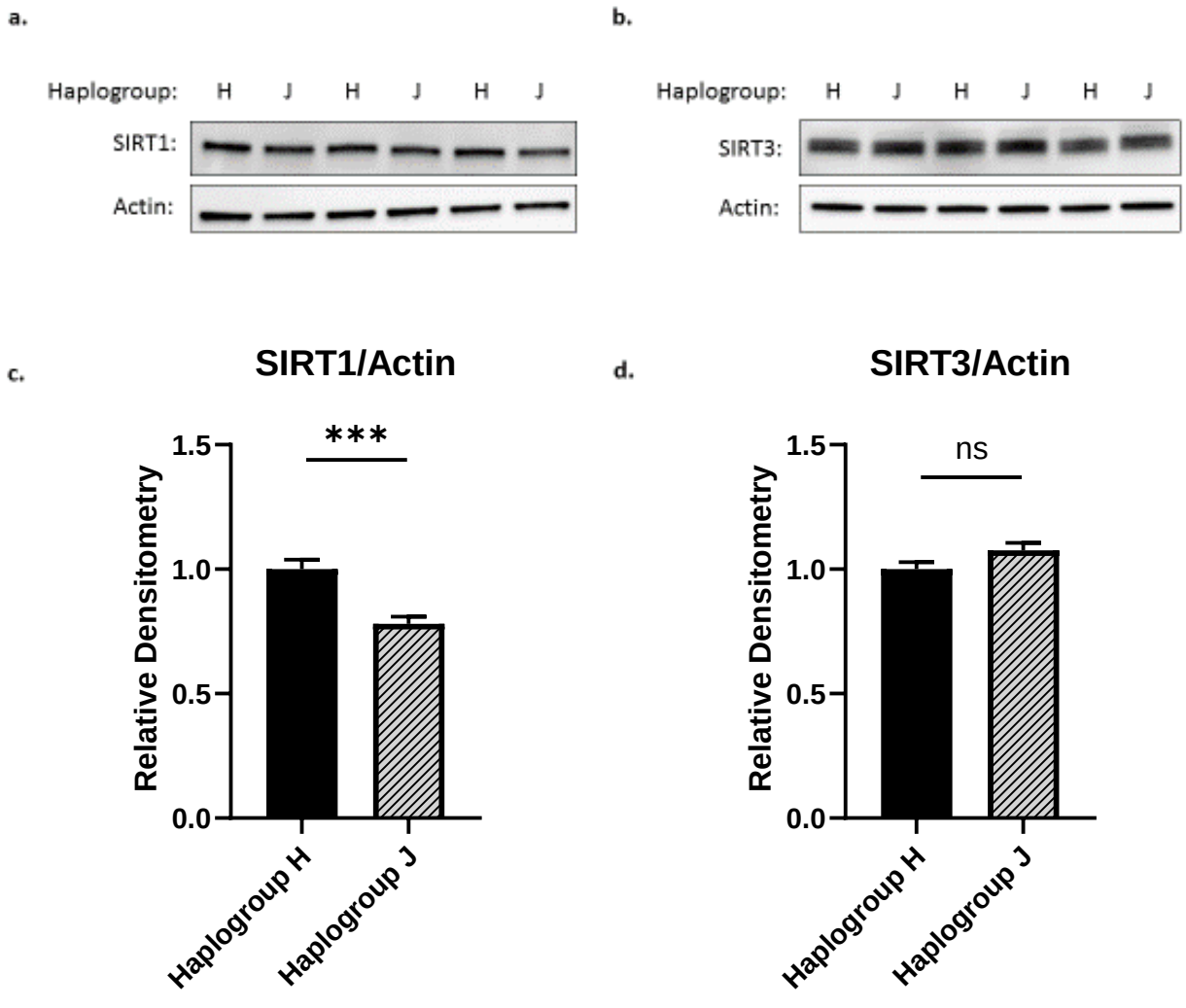
a.
Haplogroup: H J H J H J
SIRT1:
Actin:
b.
Haplogroup: H J H J H J
SIRT3:
Actin:
c.
SIRT1/Actin
***
Relative Densitometry
1.5
1.0
0.5
0.0
Haplogroup H
Haplogroup J
d.
SIRT3/Actin
ns
Relative Densitometry
1.5
1.0
0.5
0.0
Haplogroup H
Haplogroup J

Figure 4.14. SIRT1 protein levels decrease in the haplogroup J cybrid. a) Western blot image of whole cell lysates from a haplogroup H and a haplogroup J cybrid labeled with SIRT1. b) Western blot image of whole cell lysates from a haplogroup H and a haplogroup J cybrid labeled with SIRT3. c) Densitometry analysis reveals a significant increase in SIRT1 protein levels in the haplogroup J cybrid relative to the haplogroup H cybrid. d) Densitometry analysis reveals no significant difference in SIRT3 protein levels in the haplogroup J cybrid relative to the haplogroup H cybrid. n= 12 per group. $p<0.05$=*, $p<0.01$=**, $p<0.001$=***, $p<0.0001$=****. Error bars represent SEM.

Discussion

We observed decreases in nuclear-encoded respiratory chain subunits following mtDNA depletion and in a haplogroup J cybrid line. In both instances, respiratory chain subunit mRNA levels failed to change, suggesting post-transcriptional mechanisms regulate ETC protein levels. mtDNA depletion reduced nuclear-encoded COX and complex I subunit levels. Nuclear complex I subunit levels declined more rapidly following mtDNA depletion than nuclear COX subunits. Based on these results alone, we might hypothesize that complex I activity is more sensitive to mtDNA depletion than COX activity. However, prior reports suggest COX activity declines more rapidly upon mtDNA depletion than complex I activity.

We found that COX activity declines proportionally to mtDNA levels during EtBr treatment. The decreases in COX activity also closely mirror the decline in COXIVi1 protein levels. The mechanism that reduces COXIVi1 protein levels following mtDNA depletion remains unclear. A study in AD brain tissue describes a specific decline in nuclear ETC subunit gene expression in AD brains, while mtDNA-encoded gene expression is maintained [232]. However, we found no change in nuclear-encoded ETC subunit expression during acute mtDNA depletion. In yeast, energetic stress manipulates nuclear-encoded respiratory chain subunits at the translational level. However, this phenomena occurs when the yeast's fuel source is altered, and not following mitochondrial translational inhibition or mtDNA depletion. This suggests cytoplasmic alterations trigger translational changes, while primary mitochondrial deficits do not affect cytoplasmic translation [233].

In human cells, COXIV import into the mitochondria regulates translation of mtDNA-encoded COX subunits [234]. However, here we describe the opposite phenomenon: a primary lesion in mtDNA which causes reductions in nuclear-encoded ETC subunits. Earlier studies in ρ0

cells see similar reductions in COXIV protein levels, and evidence suggests the decline stems from an increased protein turnover rate. The loss of mtDNA-encoded subunits likely destabilizes COX complexes, favoring subunit degradation via mitochondrial proteases. Interestingly, nuclear-encoded COX subunits outside of COXIV decline to a greater extent in ρ0 cells. The authors suggest that this may occur due to a stabilizing interaction that COXIV shares with another nuclear-encoded COX subunit, COXVa. Meanwhile, other nuclear-encoded COX subunits, such as COXVb and COXVIc, interact more directly with mtDNA-encoded subunits and likely experience greater instability in their absence [235].

NDUFB8, a nuclear-encoded complex I subunit, levels also decline rapidly upon SY5Y mtDNA depletion, likely due to complex I destabilization. EtBr reduces NDUFB8 levels more quickly than COXIVi1 levels. Complex I's structure may be more sensitive to mtDNA depletion than COX's structure, or NDUFB8 may be particularly sensitive to mtDNA-encoded subunit loss. We found no significant difference between the relative decline in COX and complex I activity following 24 hours of EtBr treatment. These results suggest that mtDNA depletion does not preferentially affect either respiratory enzyme's activity. Future experiments will measure complex I activity following 3 days of mtDNA depletion, to learn whether complex I or COX shows a preferential sensitivity to more sever declines in mtDNA levels.

We also examined mitochondrial parameters in a haplogroup J cybrid. Unfortunately, we did not have enough haplogroup J cybrids to draw conclusions regarding haplogroup J as a whole. However, we saw a drastic decrease in one haplogroup J cybrid's oxygen consumption relative to one haplogroup H cybrid. We found the haplogroup J cybrid actually possessed more mtDNA than the H cybrid, despite its decreased oxygen utilization. The J cybrid also maintained nuclear and mtDNA-encoded COX subunit levels relative to the H cybrid. However, we

discovered a drastic decrease in nuclear-encoded complex I subunits in the J cybrid. Therefore, we hypothesize the J cybrid displays reduced oxygen consumption due to a decline in complex I function. The J cybrid likely possesses a mtDNA mutation which destabilizes mtDNA-encoded complex I subunits, leading to a concomitant decline in nuclear-encoded subunits. Mitochondrial proteases may mediate the decline in nuclear-encoded complex I subunits, however further work is needed to confirm this hypothesis. Mutations in mtDNA-encoded NADH dehydrogenase (ND) subunits and mtDNA tRNA genes have both been associated with complex I-specific primary mitochondrial disease [236].

Mitochondrial dysfunction in the haplogroup J cybrid stimulates retrograde responses. These cell lines provide further evidence that mitochondrial dysfunction stimulates the ISR, as the J cybrid increased eIF2α phosphorylation and CHOP mRNA levels. SirT1 protein levels also decline in the J cybrid. Decreased SirT1 levels may signal a decreased NAD+:NADH ratio, which would align with a hypothesized decline in the J cybrid's complex I activity [237].

Together, these findings provide information on the coordination between nuclear and mtDNA-encoded ETC subunits. We hypothesize that mtDNA depletion and mtDNA mutation(s) in respiratory chain subunits lead to decreased enzyme complex stability, which stimulates proteolytic degradation of nuclear-encoded subunits. However, more work is necessary to confirm this hypothesis. Furthermore, we found that COX activity displays a strong correlation with mtDNA levels. Future experiments examining complex I activity after mtDNA depletion could address whether mtDNA loss represents a plausible explanation for the AD COX defect.

Chapter 5: Conclusions

Mitochondrial dysfunction triggers AD-like tau alterations

The cellular mechanisms leading to pathological tau alterations in the AD brain remain unknown. Since AD has largely been viewed through the lens of the β-amyloid cascade hypothesis for decades, tau alterations are commonly ascribed to Aβ's cellular influences. Here, we provide evidence for another potential contributor to AD tau pathology, mitochondrial dysfunction. Mitochondrial dysfunction affected tau protein in numerous ways, revealing a clear relationship between mitochondrial function and tau homeostasis.

First, we investigated tau alterations in SY5Y cells experiencing chronic respiratory chain incompetence. Western blots for total tau protein provided the initial observation from which all our other data followed. We observed increased total tau protein levels along with high molecular weight tau protein bands in cells lacking mitochondrial function. We established that the high molecular weight tau bands do not represent non-specific protein species, and tau hyperphosphorylation does not explain their apparent increase in molecular weight. Based on the protein banding pattern observed in mtDNA depleted lysates, we hypothesized the extra bands represent different tau isoforms. We found evidence of altered tau mRNA splicing in ρ0 cells, specifically increased exon 2 inclusion, which is consistent with altered tau isoform ratios.

The most intriguing tau alteration we observed in ρ0 cells was the presence of a tau protein band with an apparent molecular weight above 110 kDa. As monomeric tau in SY5Y cells migrates around 55 kDa, a protein species around 110 kDa could represent a tau oligomer. We did not definitively confirm the identity of this HMW tau band. However, the observation of a HMW tau band led us to measure oligomeric tau levels in respiratory incompetent cells, and we found increased tau oligomers. To follow up on this finding, we decided to measure oligomeric tau levels following acute mtDNA depletion. We found that acute mtDNA depletion

increases tau oligomerization, causing a shift in the ratio of oligomeric tau to total tau. This finding strengthened the relationship between mitochondrial dysfunction and tau oligomerization. Finally, we measured tau oligomerization in AD cybrids. We found increased tau oligomerization in AD cybrids relative to control cybrids. The AD cybrid data ties our findings more closely to AD, establishing that AD-associated mtDNA variants increase tau oligomerization.

We were unable to establish how mitochondrial dysfunction increases tau oligomerization. The epitope recognized by TOC1, the oligomeric tau antibody we used in these studies, depends on a conformational shift in tau's structure. The cause for this conformational shift is unknown, but post-translational modifications could contribute. We examined tau phosphorylation at Ser199 in mtDNA depleted cells to look for a correlation between tau phosphorylation and oligomerization. We found that phosphorylation at Ser199 does not increase with acute mtDNA depletion or in AD cybrids. However, tau protein has many phosphorylation sites which may influence oligomerization, so future work could answer this question more thoroughly. Overall, our work on mitochondrial dysfunction and tau homeostasis did not suggest a strong relationship between mitochondrial defects and tau hyperphosphorylation.

While acute mtDNA depletion and AD cybrids increased the ratio of tau oligomers to total tau, chronic mtDNA depletion increased both tau oligomers and total tau. ρ0 cells also increased tau phosphorylated at Ser199. All of these tau species accumulated to a similar extent, suggesting ρ0 cells have a larger pool of tau, rather than a modified pool of tau. We found no change in total tau mRNA levels in ρ0 cells. Based on these findings, chronic mtDNA depletion appears to affect tau protein stability, likely by altering cellular proteostasis pathways. This naturally led us to the next chapter of the dissertation, which examined the relationship between

mitochondrial dysfunction and cellular proteostasis. The following studies aimed primarily to understand how mtDNA depletion affects proteostasis, with the secondary goal of explaining why tau accumulates in ρ0 cells.

mtDNA depletion alters cellular proteostasis pathways

Because proteostasis pathways become dysfunctional in AD, likely contributing to the hallmark tau and amyloid aggregates, we examined how mitochondrial dysfunction impacts proteostasis. We measured autophagy flux, proteasome activity, UPR activation, and the ISR, and found that mtDNA depletion affected all of these pathways. The findings provided multiple potential explanations for ρ0 tau protein accumulation, although we were unable to pinpoint the major reason for tau protein build-up.

We found increased autophagy flux in ρ0 cells. Major autophagy adaptor proteins, such as p62, NDP52, and optineurin, also increased following chronic mtDNA depletion. This suggests that ρ0 cells move cytoplasmic materials through the lysosomal system at a greater rate. Increased autophagy could benefit ρ0 cells by recycling cellular building blocks, providing energetic substrates to energy-stressed cells. While basal autophagy increases in ρ0 cells, the rate of basal mitophagy remains unclear. NDP52, p62, and optineurin levels all increase in mtDNA-depleted cells, and all can contribute to mitophagy. However, other proteins associated with mitophagy, including BNIP3, Nix, and parkin, become drastically reduced. Mitochondrial turnover occurs at a relatively slow rate, meaning that basal levels of mitophagy are usually quite low. Basal mitophagy rates can, therefore, be difficult to measure. We cannot say whether ρ0 cells change their basal rate of mitophagy relative to ρ+ cells. We can say, however, that lysosomal deacidification does not affect tau protein levels in SY5Y cells. This suggests that tau does not accumulate in ρ0 cells due to compromised autophagy/mitophagy. The major caveat to

this interpretation is that the lysosomal deacidification lasted for six hours, which may not be long enough to capture changes associated with mitophagy.

We observed decreased proteasome activity alongside decreased total ubiquitination in ρ0 cells. Consistent with these findings, we observed decreased levels of parkin, an E3 ubiquitin ligase, and increased PARIS, a protein regulated by ubiquitination and subsequent proteasomal degradation. The proteasome can regulate tau protein levels, thus, decreased proteasome activity could explain increased ρ0 tau levels. In turn, the reduced proteasome activity could be explained by decreased energy production, as proteasome activity requires ATP.

The mtUPR recently emerged as an important aspect of mitochondrial proteostasis. Here, we found that neither chronic nor acute mtDNA depletion activates the mtUPR. ATF5, the master regulator of the mtUPR, declined following mtDNA depletion, as did ATF5 target gene expression. Prior reports suggested that mtDNA depletion activates the mammalian mtUPR, but our results do not agree with these findings. Next, we examined erUPR activity in ρ0 cells. We found decreased XBP1 splicing and HSPA5 mRNA levels in ρ0 cells, suggesting those arms of the erUPR become blunted following mtDNA depletion. However, phosphorylated eIF2α levels increased, alongside ATF4 and CHOP protein levels. The eIF2α-ATF4-CHOP signaling pathway is often referred to as the integrated stress response (ISR), and it helps maintain proteostasis by reducing general rates of protein translation. Our findings suggest mitochondrial dysfunction triggers the ISR, likely independently of ER-stress. This is consistent with other reports suggesting the ISR represents an important mitochondrial stress response. Treating ρ0 cells with an ISR inhibitor reduced nuclear ATF4 and CHOP levels, confirming ISR activation. ISR inhibitors did not affect tau protein levels, however, suggesting ISR activation does not contribute to increased tau protein levels in ρ0 cells.

Finally, we showed that ρ0 cells experience slowed progression through the cell cycle. Slowed cell cycle progression likely conserves resources for a cell struggling to produce energy. The ISR may contribute to cell cycle arrest, as nuclear CHOP stimulates G1-cell cycle arrest.

Coordination of nuclear and mitochondrial-encoded respiratory chain subunit levels and its effect on enzyme activities

AD patients display systemic reductions in COX activity, while other respiratory chain subunit activities remain intact. Cybrid studies show that ρ0 cells repopulated with AD mtDNA recapitulate the COX defect, suggesting mtDNA variants contribute to COX dysfunction in AD. Which mtDNA variants impart specific COX defects remains unclear. We wanted to determine whether mtDNA depletion preferentially affects COX activity relative to complex I activity. We found that COX activity correlates strongly with mtDNA levels. After 24 hours of EtBr treatment, we found no significant difference between the respective decline in COX and complex I activities. Perhaps longer treatment with EtBr will reveal differential declines in enzyme activity, but the current findings suggest mtDNA depletion similarly effects COX and complex I activity.

We also observed that nuclear-encoded COX subunits decline proportionally to mtDNA levels, without a concomitant change in mRNA expression. The same phenomena occurs with nuclear-encoded complex I subunits. The loss of nuclear-encoded subunits upon mtDNA depletion suggests the existence of quality control mechanisms to maintain roughly equivalent levels of nuclear and mitochondrial-encoded subunits. We hypothesize the loss of mtDNA-encoded subunits destabilizes respiratory chain enzyme complexes, favoring nuclear-encoded subunit degradation via mitochondrial proteases. Interestingly, we observed declines in nuclear-encoded complex I subunits in an mtDNA replete cybrid cell line.

We compared mitochondrial function in a haplogroup H and a haplogroup J cybrid cell line. The haplogroup J cybrid line displayed reduced oxygen consumption and increased extracellular acidification, but maintained higher mtDNA levels than the haplogroup H cybrid. Since we found a decreased oxygen consumption rate, we measured levels of respiratory chain subunits in each cybrid. We found no change in COX subunits, however, we found a decline in nuclear-encoded complex I subunits. This suggests the haplogroup J cybrid experiences a complex I-specific deficit. With this knowledge, we hypothesize that mutation(s) in the haplogroup J cybrid's mtDNA affect either mtDNA-encoded complex I subunit production or integration into the enzyme complex, destabilizing complex I and reducing its activity. Future work with haplogroup J cybrids will determine whether the observed alterations stem from private mutations or haplogroup J defining mutations.

Chronic versus acute adaptation to mtDNA depletion

AD manifests over the course of many years. Neurons likely compensate for declining mitochondrial energy production until mitochondrial dysfunction passes a crucial threshold. Here, we found many differences in the cellular response to acute and chronic mtDNA depletion. Whereas acute mitochondrial stressors may activate beneficial retrograde responses, chronic dysfunction may activate maladaptive responses that favor apoptosis. The physiological relevance of differential responses to acute and chronic mitochondrial stress remains unclear, but likely has profound consequences on cellular viability and disease progression.

Study limitations and future directions

ρ0 cells provide an excellent model of mitochondrial dysfunction in a viable cell line, absent the off target effects associated with mitochondrial poisons and other interventions.

However, these cells possess certain drawbacks which are worth mentioning. First, we generated our ρ0 lines through chronic EtBr treatment. EtBr preferentially affects mtDNA, however, it is possible that nuclear DNA changes also occurred during EtBr treatment. Future studies could address this issue by utilizing mtDNA depletion methods which do not rely upon EtBr. Furthermore, these studies represent changes observed in one neuroblastoma cell line. Some key observations in the SY5Y cell line may not replicate in ρ0 cells of a different origin. To address this limitation, studies could look for similar changes in other cell lines. However, the SY5Y cell line is particularly suited for these studies due to its endogenous tau expression, and weak basal ApoE expression, features consistent with neurons. Rather than replicating these findings in other cancer cell lines, it may be more interesting to see the effects of mtDNA depletion in primary neurons. Primary neurons likely rely on oxidative phosphorylation more than neuroblastoma cells. Based on this, it is reasonable to hypothesize that primary neurons may be more sensitive to mtDNA depletion than neuroblastoma cells.

Acute treatment with EtBr may also trigger off target effects. The findings from cells treated acutely with EtBr should be replicated in future studies utilizing other mtDNA depleting agents. The studies of haplogroup H and J cybrids suffered from a small sample size, comparing one haplogroup H cybrid to one haplogroup J cybrid. Future work will assay numerous haplogroup H and J cybrid lines to determine more generalizable haplogroup effects. Finally, the studies herein were *in vitro* analyses. Follow-up studies should utilize rodent models of mitochondrial dysfunction to study mitochondrial effects on cellular proteostasis in the rodent brain.

Summary

AD clinical trials targeting brain energy production have been few and far between. Meanwhile, accumulating evidence suggests mitochondrial dysfunction contributes to neurodegenerative processes. Reduced glucose utilization and profound mitochondrial defects occur in the AD brain, and mtDNA variants associate with increased AD risk. The studies presented herein provide further evidence that mitochondrial dysfunction could play a primary role in AD pathogenesis. We examined how mtDNA levels/variants affect multiple AD-related phenomena, including tau and apoE homeostasis, cellular proteostasis pathways, and respiratory chain enzyme activity. Our findings suggest mtDNA could play a primary role in triggering tau aggregation and disrupting general cellular proteostasis. These findings argue for the increased development of mitochondrial-targeted AD therapeutics, and highlight specific pathways which could be modulated to improve brain energy production.

References

1. Weller, J. and A. Budson, *Current understanding of Alzheimer's disease diagnosis and treatment.* F1000Research, 2018. **7**: p. F1000 Faculty Rev-1161.
2. McKhann, G.M., et al., *The diagnosis of dementia due to Alzheimer's disease: recommendations from the National Institute on Aging-Alzheimer's Association workgroups on diagnostic guidelines for Alzheimer's disease.* Alzheimer's & dementia : the journal of the Alzheimer's Association, 2011. **7**(3): p. 263-269.
3. Bjerke, M. and S. Engelborghs, *Cerebrospinal Fluid Biomarkers for Early and Differential Alzheimer's Disease Diagnosis.* Journal of Alzheimer's disease : JAD, 2018. **62**(3): p. 1199-1209.
4. Grossberg, G.T., G. Tong, A.D. Burke, and P.N. Tariot, *Present Algorithms and Future Treatments for Alzheimer's Disease.* Journal of Alzheimer's disease : JAD, 2019. **67**(4): p. 1157-1171.
5. Sharma, A., M. Bemis, and A.R. Desilets, *Role of Medium Chain Triglycerides (Axona®) in the Treatment of Mild to Moderate Alzheimer's Disease.* American Journal of Alzheimer's Disease & Other Dementias®, 2014. **29**(5): p. 409-414.
6. Croteau, E., C.A. Castellano, M.A. Richard, M. Fortier, S. Nugent, M. Lepage, S. Duchesne, K. Whittingstall, E.E. Turcotte, C. Bocti, T. Fulop, and S.C. Cunnane, *Ketogenic Medium Chain Triglycerides Increase Brain Energy Metabolism in Alzheimer's Disease.* J Alzheimers Dis, 2018. **64**(2): p. 551-561.
7. Wolozin, B., W. Kellman, P. Ruosseau, G.G. Celesia, and G. Siegel, *Decreased Prevalence of Alzheimer Disease Associated With 3-Hydroxy-3-Methyglutaryl Coenzyme A Reductase Inhibitors.* JAMA Neurology, 2000. **57**(10): p. 1439-1443.
8. Jick, H., G.L. Zornberg, S.S. Jick, S. Seshadri, and D.A. Drachman, *Statins and the risk of dementia.* Lancet, 2000. **356**(9242): p. 1627-31.
9. Schultz, B.G., D.K. Patten, and D.J. Berlau, *The role of statins in both cognitive impairment and protection against dementia: a tale of two mechanisms.* Translational neurodegeneration, 2018. **7**: p. 5-5.
10. Zhang, C., Y. Wang, D. Wang, J. Zhang, and F. Zhang, *NSAID Exposure and Risk of Alzheimer's Disease: An Updated Meta-Analysis From Cohort Studies.* Frontiers in aging neuroscience, 2018. **10**: p. 83-83.
11. Szekely, C.A., J.E. Thorne, P.P. Zandi, M. Ek, E. Messias, J.C.S. Breitner, and S.N. Goodman, *Nonsteroidal Anti-Inflammatory Drugs for the Prevention of Alzheimer's Disease: A Systematic Review.* Neuroepidemiology, 2004. **23**(4): p. 159-169.
12. McGeer, P.L. and E.G. McGeer, *NSAIDs and Alzheimer disease: Epidemiological, animal model and clinical studies.* Neurobiology of Aging, 2007. **28**(5): p. 639-647.
13. Li, X., F. Kaida-Yip, and M. Zabel, *NSAID Use and the Prevention of Alzheimer's Disease: A Meta-Analysis (P6.184).* Neurology, 2018. **90**(15 Supplement): p. P6.184.
14. Imbimbo, B.P., V. Solfrizzi, and F. Panza, *Are NSAIDs useful to treat Alzheimer's disease or mild cognitive impairment?* Frontiers in aging neuroscience, 2010. **2**: p. 19.
15. Hardy, J.A. and G.A. Higgins, *Alzheimer's disease: the amyloid cascade hypothesis.* Science, 1992. **256**(5054): p. 184.
16. Goate, A., M.C. Chartier-Harlin, M. Mullan, J. Brown, F. Crawford, L. Fidani, L. Giuffra, A. Haynes, N. Irving, L. James, and et al., *Segregation of a missense mutation in*

the amyloid precursor protein gene with familial Alzheimer's disease. Nature, 1991. **349**(6311): p. 704-6.
17. Murrell, J., M. Farlow, B. Ghetti, and M.D. Benson, *A mutation in the amyloid precursor protein associated with hereditary Alzheimer's disease.* Science, 1991. **254**(5028): p. 97-9.
18. Kelleher, R.J., 3rd and J. Shen, *Presenilin-1 mutations and Alzheimer's disease.* Proceedings of the National Academy of Sciences of the United States of America, 2017. **114**(4): p. 629-631.
19. Scheuner, D., et al., *Secreted amyloid β–protein similar to that in the senile plaques of Alzheimer's disease is increased in vivo by the presenilin 1 and 2 and APP mutations linked to familial Alzheimer's disease.* Nature Medicine, 1996. **2**(8): p. 864-870.
20. Yankner, B.A., L.K. Duffy, and D.A. Kirschner, *Neurotrophic and neurotoxic effects of amyloid beta protein: reversal by tachykinin neuropeptides.* Science, 1990. **250**(4978): p. 279.
21. Kowall, N.W., M.F. Beal, J. Busciglio, L.K. Duffy, and B.A. Yankner, *An in vivo model for the neurodegenerative effects of beta amyloid and protection by substance P.* Proc Natl Acad Sci U S A, 1991. **88**(16): p. 7247-51.
22. Koh, J.Y., L.L. Yang, and C.W. Cotman, *Beta-amyloid protein increases the vulnerability of cultured cortical neurons to excitotoxic damage.* Brain Res, 1990. **533**(2): p. 315-20.
23. Mattson, M.P., B. Cheng, D. Davis, K. Bryant, I. Lieberburg, and R.E. Rydel, *beta-Amyloid peptides destabilize calcium homeostasis and render human cortical neurons vulnerable to excitotoxicity.* J Neurosci, 1992. **12**(2): p. 376-89.
24. Pike, C.J., A.J. Walencewicz, C.G. Glabe, and C.W. Cotman, *In vitro aging of beta-amyloid protein causes peptide aggregation and neurotoxicity.* Brain Res, 1991. **563**(1-2): p. 311-4.
25. Mehta, D., R. Jackson, G. Paul, J. Shi, and M. Sabbagh, *Why do trials for Alzheimer's disease drugs keep failing? A discontinued drug perspective for 2010-2015.* Expert Opin Investig Drugs, 2017. **26**(6): p. 735-739.
26. Harrison, J.R. and M.J. Owen, *Alzheimer's disease: the amyloid hypothesis on trial.* Br J Psychiatry, 2016. **208**(1): p. 1-3.
27. Mullane, K. and M. Williams, *Alzheimer's disease (AD) therapeutics – 1: Repeated clinical failures continue to question the amyloid hypothesis of AD and the current understanding of AD causality.* Biochemical Pharmacology, 2018. **158**: p. 359-375.
28. Selkoe, D.J., *Alzheimer disease and aducanumab: adjusting our approach.* Nature Reviews Neurology, 2019. **15**(7): p. 365-366.
29. Mecocci, P., M. Baroni, U. Senin, and V. Boccardi, *Brain Aging and Late-Onset Alzheimer's Disease: A Matter of Increased Amyloid or Reduced Energy?* J Alzheimers Dis, 2018. **64**(s1): p. S397-s404.
30. Forman, M.S., E.J. Mufson, S. Leurgans, D. Pratico, S. Joyce, S. Leight, V.M. Lee, and J.Q. Trojanowski, *Cortical biochemistry in MCI and Alzheimer disease: lack of correlation with clinical diagnosis.* Neurology, 2007. **68**(10): p. 757-63.
31. Huber, C.M., C. Yee, T. May, A. Dhanala, and C.S. Mitchell, *Cognitive Decline in Preclinical Alzheimer's Disease: Amyloid-Beta versus Tauopathy.* J Alzheimers Dis, 2018. **61**(1): p. 265-281.

32. Cho, H., J.Y. Choi, M.S. Hwang, J.H. Lee, Y.J. Kim, H.M. Lee, C.H. Lyoo, Y.H. Ryu, and M.S. Lee, *Tau PET in Alzheimer disease and mild cognitive impairment.* Neurology, 2016. **87**(4): p. 375-83.
33. Sloane, J.A., M.F. Pietropaolo, D.L. Rosene, M.B. Moss, A. Peters, T. Kemper, and C.R. Abraham, *Lack of correlation between plaque burden and cognition in the aged monkey.* Acta Neuropathol, 1997. **94**(5): p. 471-8.
34. DeKosky, S.T. and S.W. Scheff, *Synapse loss in frontal cortex biopsies in Alzheimer's disease: correlation with cognitive severity.* Ann Neurol, 1990. **27**(5): p. 457-64.
35. Risacher, S.L., W.H. Anderson, A. Charil, P.F. Castelluccio, S. Shcherbinin, A.J. Saykin, A.J. Schwarz, and I. Alzheimer's Disease Neuroimaging, *Alzheimer disease brain atrophy subtypes are associated with cognition and rate of decline.* Neurology, 2017. **89**(21): p. 2176-2186.
36. Hoffman, J.M., K.A. Welsh-Bohmer, M. Hanson, B. Crain, C. Hulette, N. Earl, and R.E. Coleman, *FDG PET imaging in patients with pathologically verified dementia.* J Nucl Med, 2000. **41**(11): p. 1920-8.
37. Nestor, P.J., T.D. Fryer, P. Smielewski, and J.R. Hodges, *Limbic hypometabolism in Alzheimer's disease and mild cognitive impairment.* Annals of Neurology, 2003. **54**(3): p. 343-351.
38. Silverman, D.H.S., et al., *Positron Emission Tomography in Evaluation of DementiaRegional Brain Metabolism and Long-term Outcome.* JAMA, 2001. **286**(17): p. 2120-2127.
39. Mosconi, L., et al., *Multicenter standardized 18F-FDG PET diagnosis of mild cognitive impairment, Alzheimer's disease, and other dementias.* J Nucl Med, 2008. **49**(3): p. 390-8.
40. Mosconi, L., A. Pupi, and M.J. De Leon, *Brain glucose hypometabolism and oxidative stress in preclinical Alzheimer's disease.* Annals of the New York Academy of Sciences, 2008. **1147**: p. 180-195.
41. Smailagic, N., L. Lafortune, S. Kelly, C. Hyde, and C. Brayne, *18F-FDG PET for Prediction of Conversion to Alzheimer's Disease Dementia in People with Mild Cognitive Impairment: An Updated Systematic Review of Test Accuracy.* Journal of Alzheimer's disease : JAD, 2018. **64**(4): p. 1175-1194.
42. Minoshima, S., B. Giordani, S. Berent, K.A. Frey, N.L. Foster, and D.E. Kuhl, *Metabolic reduction in the posterior cingulate cortex in very early Alzheimer's disease.* Annals of Neurology, 1997. **42**(1): p. 85-94.
43. Schrijvers, E.M.C., J.C.M. Witteman, E.J.G. Sijbrands, A. Hofman, P.J. Koudstaal, and M.M.B. Breteler, *Insulin metabolism and the risk of Alzheimer disease: the Rotterdam Study.* Neurology, 2010. **75**(22): p. 1982-1987.
44. Rosendorff, C., M.S. Beeri, and J.M. Silverman, *Cardiovascular risk factors for Alzheimer's disease.* Am J Geriatr Cardiol, 2007. **16**(3): p. 143-9.
45. Whitmer, R.A., E.P. Gunderson, C.P. Quesenberry, Jr., J. Zhou, and K. Yaffe, *Body mass index in midlife and risk of Alzheimer disease and vascular dementia.* Curr Alzheimer Res, 2007. **4**(2): p. 103-9.
46. Frolich, L., D. Blum-Degen, H.G. Bernstein, S. Engelsberger, J. Humrich, S. Laufer, D. Muschner, A. Thalheimer, A. Turk, S. Hoyer, R. Zochling, K.W. Boissl, K. Jellinger, and P. Riederer, *Brain insulin and insulin receptors in aging and sporadic Alzheimer's disease.* J Neural Transm (Vienna), 1998. **105**(4-5): p. 423-38.

47. Cai, H., W.-n. Cong, S. Ji, S. Rothman, S. Maudsley, and B. Martin, *Metabolic dysfunction in Alzheimer's disease and related neurodegenerative disorders.* Current Alzheimer research, 2012. **9**(1): p. 5-17.
48. Phillips, H.S., J.M. Hains, M. Armanini, G.R. Laramee, S.A. Johnson, and J.W. Winslow, *BDNF mRNA is decreased in the hippocampus of individuals with Alzheimer's disease.* Neuron, 1991. **7**(5): p. 695-702.
49. Yeo, G.S., C.C. Connie Hung, J. Rochford, J. Keogh, J. Gray, S. Sivaramakrishnan, S. O'Rahilly, and I.S. Farooqi, *A de novo mutation affecting human TrkB associated with severe obesity and developmental delay.* Nat Neurosci, 2004. **7**(11): p. 1187-9.
50. Simpson, I.A., K.R. Chundu, T. Davies-Hill, W.G. Honer, and P. Davies, *Decreased concentrations of GLUT1 and GLUT3 glucose transporters in the brains of patients with Alzheimer's disease.* Annals of Neurology, 1994. **35**(5): p. 546-551.
51. Barba, I., R. Fernandez-Montesinos, D. Garcia-Dorado, and D. Pozo, *Alzheimer's disease beyond the genomic era: nuclear magnetic resonance (NMR) spectroscopy-based metabolomics.* J Cell Mol Med, 2008. **12**(5a): p. 1477-85.
52. Baslow, M.H., *N-acetylaspartate in the vertebrate brain: metabolism and function.* Neurochem Res, 2003. **28**(6): p. 941-53.
53. Choi, J.K., A. Dedeoglu, and B.G. Jenkins, *Application of MRS to mouse models of neurodegenerative illness.* NMR Biomed, 2007. **20**(3): p. 216-37.
54. Martinez-Bisbal, M.C., E. Arana, L. Marti-Bonmati, E. Molla, and B. Celda, *Cognitive impairment: classification by 1H magnetic resonance spectroscopy.* Eur J Neurol, 2004. **11**(3): p. 187-93.
55. Kantarci, K., S.D. Weigand, R.C. Petersen, B.F. Boeve, D.S. Knopman, J. Gunter, D. Reyes, M. Shiung, P.C. O'Brien, G.E. Smith, R.J. Ivnik, E.G. Tangalos, and C.R. Jack, Jr., *Longitudinal 1H MRS changes in mild cognitive impairment and Alzheimer's disease.* Neurobiol Aging, 2007. **28**(9): p. 1330-9.
56. Mueller, S.G., N. Schuff, and M.W. Weiner, *Evaluation of treatment effects in Alzheimer's and other neurodegenerative diseases by MRI and MRS.* NMR Biomed, 2006. **19**(6): p. 655-68.
57. Volicer, L., P.J. Langlais, W.R. Matson, K.A. Mark, and P.H. Gamache, *Serotoninergic system in dementia of the Alzheimer type. Abnormal forms of 5-hydroxytryptophan and serotonin in cerebrospinal fluid.* Arch Neurol, 1985. **42**(12): p. 1158-61.
58. Kaddurah-Daouk, R., S. Rozen, W. Matson, X. Han, C.M. Hulette, J.R. Burke, P.M. Doraiswamy, and K.A. Welsh-Bohmer, *Metabolomic changes in autopsy-confirmed Alzheimer's disease.* Alzheimer's & dementia : the journal of the Alzheimer's Association, 2011. **7**(3): p. 309-317.
59. Czech, C., P. Berndt, K. Busch, O. Schmitz, J. Wiemer, V. Most, H. Hampel, J. Kastler, and H. Senn, *Metabolite profiling of Alzheimer's disease cerebrospinal fluid.* PloS one, 2012. **7**(2): p. e31501-e31501.
60. Trushina, E. and M.M. Mielke, *Recent advances in the application of metabolomics to Alzheimer's Disease.* Biochimica et biophysica acta, 2014. **1842**(8): p. 1232-1239.
61. Varma, V.R., et al., *Brain and blood metabolite signatures of pathology and progression in Alzheimer disease: A targeted metabolomics study.* PLoS medicine, 2018. **15**(1): p. e1002482-e1002482.
62. He, X., Y. Huang, B. Li, C.X. Gong, and E.H. Schuchman, *Deregulation of sphingolipid metabolism in Alzheimer's disease.* Neurobiol Aging, 2010. **31**(3): p. 398-408.

63. Wong, M.W., N. Braidy, A. Poljak, R. Pickford, M. Thambisetty, and P.S. Sachdev, *Dysregulation of lipids in Alzheimer's disease and their role as potential biomarkers.* Alzheimers Dement, 2017. **13**(7): p. 810-827.
64. Galluzzi, L., O. Kepp, C. Trojel-Hansen, and G. Kroemer, *Mitochondrial control of cellular life, stress, and death.* Circ Res, 2012. **111**(9): p. 1198-207.
65. Wallace, D.C., *A mitochondrial paradigm of metabolic and degenerative diseases, aging, and cancer: a dawn for evolutionary medicine.* Annual review of genetics, 2005. **39**: p. 359-407.
66. Niyazov, D.M., S.G. Kahler, and R.E. Frye, *Primary Mitochondrial Disease and Secondary Mitochondrial Dysfunction: Importance of Distinction for Diagnosis and Treatment.* Mol Syndromol, 2016. **7**(3): p. 122-37.
67. Wallace, D.C. and D. Chalkia, *Mitochondrial DNA genetics and the heteroplasmy conundrum in evolution and disease.* Cold Spring Harbor perspectives in biology, 2013. **5**(11): p. a021220-a021220.
68. Parker, W.D., Jr., C.M. Filley, and J.K. Parks, *Cytochrome oxidase deficiency in Alzheimer's disease.* Neurology, 1990. **40**(8): p. 1302-3.
69. Parker, W.D., Jr. and J.K. Parks, *Cytochrome c oxidase in Alzheimer's disease brain: purification and characterization.* Neurology, 1995. **45**(3 Pt 1): p. 482-6.
70. Mutisya, E.M., A.C. Bowling, and M.F. Beal, *Cortical cytochrome oxidase activity is reduced in Alzheimer's disease.* J Neurochem, 1994. **63**(6): p. 2179-84.
71. Silva, D.F., J.E. Selfridge, J. Lu, L. E, N. Roy, L. Hutfles, J.M. Burns, E.K. Michaelis, S. Yan, S.M. Cardoso, and R.H. Swerdlow, *Bioenergetic flux, mitochondrial mass and mitochondrial morphology dynamics in AD and MCI cybrid cell lines.* Human molecular genetics, 2013. **22**(19): p. 3931-3946.
72. Ghosh, S.S., R.H. Swerdlow, S.W. Miller, B. Sheeman, W.D. Parker, Jr., and R.E. Davis, *Use of cytoplasmic hybrid cell lines for elucidating the role of mitochondrial dysfunction in Alzheimer's disease and Parkinson's disease.* Ann N Y Acad Sci, 1999. **893**: p. 176-91.
73. Swerdlow, R.H., J.K. Parks, D.S. Cassarino, D.J. Maguire, R.S. Maguire, J.P. Bennett, Jr., R.E. Davis, and W.D. Parker, Jr., *Cybrids in Alzheimer's disease: a cellular model of the disease?* Neurology, 1997. **49**(4): p. 918-25.
74. Ojaimi, J., C.L. Masters, C. McLean, K. Opeskin, P. McKelvie, and E. Byrne, *Irregular distribution of cytochrome c oxidase protein subunits in aging and Alzheimer's disease.* Annals of Neurology, 1999. **46**(4): p. 656-660.
75. Cottrell, D.A., E.L. Blakely, M.A. Johnson, P.G. Ince, and D.M. Turnbull, *Mitochondrial enzyme-deficient hippocampal neurons and choroidal cells in AD.* Neurology, 2001. **57**(2): p. 260.
76. Cottrell, D.A., G.M. Borthwick, M.A. Johnson, P.G. Ince, and D.M. Turnbull, *The role of cytochrome c oxidase deficient hippocampal neurones in Alzheimer's disease.* Neuropathology and Applied Neurobiology, 2002. **28**(5): p. 390-396.
77. Baloyannis, S.J., *Mitochondrial alterations in Alzheimer's disease.* J Alzheimers Dis, 2006. **9**(2): p. 119-26.
78. Wang, X., B. Su, H.-g. Lee, X. Li, G. Perry, M.A. Smith, and X. Zhu, *Impaired Balance of Mitochondrial Fission and Fusion in Alzheimer's Disease.* The Journal of Neuroscience, 2009. **29**(28): p. 9090.
79. Zhang, L., et al., *Altered brain energetics induces mitochondrial fission arrest in Alzheimer's Disease.* Scientific Reports, 2016. **6**: p. 18725.

80. Cataldo, A.M., J.L. Barnett, S.A. Berman, J. Li, S. Quarless, S. Bursztajn, C. Lippa, and R.A. Nixon, *Gene expression and cellular content of cathepsin D in Alzheimer's disease brain: evidence for early up-regulation of the endosomal-lysosomal system.* Neuron, 1995. **14**(3): p. 671-80.
81. Nixon, R.A. and D.-S. Yang, *Autophagy failure in Alzheimer's disease--locating the primary defect.* Neurobiology of disease, 2011. **43**(1): p. 38-45.
82. Hirai, K., et al., *Mitochondrial abnormalities in Alzheimer's disease.* J Neurosci, 2001. **21**(9): p. 3017-23.
83. Fang, E.F., et al., *Mitophagy inhibits amyloid-beta and tau pathology and reverses cognitive deficits in models of Alzheimer's disease.* Nat Neurosci, 2019. **22**(3): p. 401-412.
84. Caspersen, C., N. Wang, J. Yao, A. Sosunov, X. Chen, J.W. Lustbader, H.W. Xu, D. Stern, G. McKhann, and S.D. Yan, *Mitochondrial Abeta: a potential focal point for neuronal metabolic dysfunction in Alzheimer's disease.* Faseb j, 2005. **19**(14): p. 2040-1.
85. Devi, L., B.M. Prabhu, D.F. Galati, N.G. Avadhani, and H.K. Anandatheerthavarada, *Accumulation of Amyloid Precursor Protein in the Mitochondrial Import Channels of Human Alzheimer's Disease Brain Is Associated with Mitochondrial Dysfunction.* The Journal of Neuroscience, 2006. **26**(35): p. 9057.
86. Corral-Debrinski, M., T. Horton, M.T. Lott, J.M. Shoffner, M.F. Beal, and D.C. Wallace, *Mitochondrial DNA deletions in human brain: regional variability and increase with advanced age.* Nat Genet, 1992. **2**(4): p. 324-9.
87. Krishnan, K.J., T.E. Ratnaike, H.L.M. De Gruyter, E. Jaros, and D.M. Turnbull, *Mitochondrial DNA deletions cause the biochemical defect observed in Alzheimer's disease.* Neurobiology of Aging, 2012. **33**(9): p. 2210-2214.
88. Corral-Debrinski, M., T. Horton, M.T. Lott, J.M. Shoffner, A.C. McKee, M.F. Beal, B.H. Graham, and D.C. Wallace, *Marked changes in mitochondrial DNA deletion levels in Alzheimer brains.* Genomics, 1994. **23**(2): p. 471-6.
89. Hamblet, N.S. and F.J. Castora, *Elevated levels of the Kearns-Sayre syndrome mitochondrial DNA deletion in temporal cortex of Alzheimer's patients.* Mutat Res, 1997. **379**(2): p. 253-62.
90. Mecocci, P., U. MacGarvey, and M.F. Beal, *Oxidative damage to mitochondrial DNA is increased in Alzheimer's disease.* Ann Neurol, 1994. **36**(5): p. 747-51.
91. Coskun, P.E., M.F. Beal, and D.C. Wallace, *Alzheimer's brains harbor somatic mtDNA control-region mutations that suppress mitochondrial transcription and replication.* Proceedings of the National Academy of Sciences of the United States of America, 2004. **101**(29): p. 10726.
92. Hoekstra, J.G., M.J. Hipp, T.J. Montine, and S.R. Kennedy, *Mitochondrial DNA mutations increase in early stage Alzheimer disease and are inconsistent with oxidative damage.* Ann Neurol, 2016. **80**(2): p. 301-6.
93. Edland, S.D., J.M. Silverman, E.R. Peskind, D. Tsuang, E. Wijsman, and J.C. Morris, *Increased risk of dementia in mothers of Alzheimer's disease cases: evidence for maternal inheritance.* Neurology, 1996. **47**(1): p. 254-6.
94. Heggeli, K.A., J. Crook, C. Thomas, and N. Graff-Radford, *Maternal transmission of Alzheimer disease.* Alzheimer disease and associated disorders, 2012. **26**(4): p. 364-366.

95. Mosconi, L., R. Mistur, R. Switalski, M. Brys, L. Glodzik, K. Rich, E. Pirraglia, W. Tsui, S. De Santi, and M.J. de Leon, *Declining brain glucose metabolism in normal individuals with a maternal history of Alzheimer disease.* Neurology, 2009. **72**(6): p. 513-20.
96. Trimmer, P.A., R.H. Swerdlow, J.K. Parks, P. Keeney, J.P. Bennett, S.W. Miller, R.E. Davis, and W.D. Parker, *Abnormal Mitochondrial Morphology in Sporadic Parkinson's and Alzheimer's Disease Cybrid Cell Lines.* Experimental Neurology, 2000. **162**(1): p. 37-50.
97. Khan, S.M., D.S. Cassarino, N.N. Abramova, P.M. Keeney, M.K. Borland, P.A. Trimmer, C.T. Krebs, J.C. Bennett, J.K. Parks, R.H. Swerdlow, W.D. Parker, Jr., and J.P. Bennett, Jr., *Alzheimer's disease cybrids replicate beta-amyloid abnormalities through cell death pathways.* Ann Neurol, 2000. **48**(2): p. 148-55.
98. Cardoso, S.M., I. Santana, R.H. Swerdlow, and C.R. Oliveira, *Mitochondria dysfunction of Alzheimer's disease cybrids enhances Abeta toxicity.* J Neurochem, 2004. **89**(6): p. 1417-26.
99. Swerdlow, R.H. and S.M. Khan, *A "mitochondrial cascade hypothesis" for sporadic Alzheimer's disease.* Medical Hypotheses, 2004. **63**(1): p. 8-20.
100. Swerdlow, R.H., J.M. Burns, and S.M. Khan, *The Alzheimer's disease mitochondrial cascade hypothesis.* J Alzheimers Dis, 2010. **20 Suppl 2**: p. S265-79.
101. Tomasi, D., G.-J. Wang, and N.D. Volkow, *Energetic cost of brain functional connectivity.* Proceedings of the National Academy of Sciences, 2013. **110**(33): p. 13642.
102. Pereira, C., M.S. Santos, and C. Oliveira, *Mitochondrial function impairment induced by amyloid beta-peptide on PC12 cells.* Neuroreport, 1998. **9**(8): p. 1749-55.
103. Casley, C.S., L. Canevari, J.M. Land, J.B. Clark, and M.A. Sharpe, *Beta-amyloid inhibits integrated mitochondrial respiration and key enzyme activities.* J Neurochem, 2002. **80**(1): p. 91-100.
104. Lustbader, J.W., et al., *ABAD Directly Links Aß to Mitochondrial Toxicity in Alzheimer's Disease.* Science, 2004. **304**(5669): p. 448.
105. Manczak, M., T.S. Anekonda, E. Henson, B.S. Park, J. Quinn, and P.H. Reddy, *Mitochondria are a direct site of Aβ accumulation in Alzheimer's disease neurons: implications for free radical generation and oxidative damage in disease progression.* Human Molecular Genetics, 2006. **15**(9): p. 1437-1449.
106. Pickett, E.K., J. Rose, C. McCrory, C.-A. McKenzie, D. King, C. Smith, T.H. Gillingwater, C.M. Henstridge, and T.L. Spires-Jones, *Region-specific depletion of synaptic mitochondria in the brains of patients with Alzheimer's disease.* Acta Neuropathologica, 2018. **136**(5): p. 747-757.
107. Choi, J., K. Chandrasekaran, T.G. Demarest, T. Kristian, S. Xu, K. Vijaykumar, K.G. Dsouza, N.R. Qi, P.J. Yarowsky, R. Gallipoli, L.G. Koch, G.M. Fiskum, S.L. Britton, and J.W. Russell, *Brain diabetic neurodegeneration segregates with low intrinsic aerobic capacity.* Annals of clinical and translational neurology, 2014. **1**(8): p. 589-604.
108. Manczak, M. and P.H. Reddy, *Abnormal interaction of VDAC1 with amyloid beta and phosphorylated tau causes mitochondrial dysfunction in Alzheimer's disease.* Hum Mol Genet, 2012. **21**(23): p. 5131-46.
109. Gamblin, T.C., F. Chen, A. Zambrano, A. Abraha, S. Lagalwar, A.L. Guillozet, M. Lu, Y. Fu, F. Garcia-Sierra, N. LaPointe, R. Miller, R.W. Berry, L.I. Binder, and V.L. Cryns, *Caspase cleavage of tau: linking amyloid and neurofibrillary tangles in Alzheimer's disease.* Proc Natl Acad Sci U S A, 2003. **100**(17): p. 10032-7.

110. Quintanilla, R.A., T.A. Matthews-Roberson, P.J. Dolan, and G.V. Johnson, *Caspase-cleaved tau expression induces mitochondrial dysfunction in immortalized cortical neurons: implications for the pathogenesis of Alzheimer disease.* J Biol Chem, 2009. **284**(28): p. 18754-66.
111. Atlante, A., G. Amadoro, A. Bobba, L. de Bari, V. Corsetti, G. Pappalardo, E. Marra, P. Calissano, and S. Passarella, *A peptide containing residues 26-44 of tau protein impairs mitochondrial oxidative phosphorylation acting at the level of the adenine nucleotide translocator.* Biochim Biophys Acta, 2008. **1777**(10): p. 1289-300.
112. Heeren, J., T. Grewal, A. Laatsch, N. Becker, F. Rinninger, K.A. Rye, and U. Beisiegel, *Impaired recycling of apolipoprotein E4 is associated with intracellular cholesterol accumulation.* J Biol Chem, 2004. **279**(53): p. 55483-92.
113. Huang, Y., X.Q. Liu, T. Wyss-Coray, W.J. Brecht, D.A. Sanan, and R.W. Mahley, *Apolipoprotein E fragments present in Alzheimer's disease brains induce neurofibrillary tangle-like intracellular inclusions in neurons.* Proc Natl Acad Sci U S A, 2001. **98**(15): p. 8838-43.
114. Nakamura, T., A. Watanabe, T. Fujino, T. Hosono, and M. Michikawa, *Apolipoprotein E4 (1-272) fragment is associated with mitochondrial proteins and affects mitochondrial function in neuronal cells.* Mol Neurodegener, 2009. **4**: p. 35.
115. Blass, J.P., A.C. Baker, L. Ko, and R.S. Black, *Induction of Alzheimer antigens by an uncoupler of oxidative phosphorylation.* Arch Neurol, 1990. **47**(8): p. 864-9.
116. Bruch, J., H. Xu, A. De Andrade, and G. Hoglinger, *Mitochondrial complex 1 inhibition increases 4-repeat isoform tau by SRSF2 upregulation.* PLoS One, 2014. **9**(11): p. e113070.
117. Hoglinger, G.U., A. Lannuzel, M.E. Khondiker, P.P. Michel, C. Duyckaerts, J. Feger, P. Champy, A. Prigent, F. Medja, A. Lombes, W.H. Oertel, M. Ruberg, and E.C. Hirsch, *The mitochondrial complex I inhibitor rotenone triggers a cerebral tauopathy.* J Neurochem, 2005. **95**(4): p. 930-9.
118. Bravo, R., V. Parra, D. Gatica, A.E. Rodriguez, N. Torrealba, F. Paredes, Z.V. Wang, A. Zorzano, J.A. Hill, E. Jaimovich, A.F.G. Quest, and S. Lavandero, *Endoplasmic reticulum and the unfolded protein response: dynamics and metabolic integration.* International review of cell and molecular biology, 2013. **301**: p. 215-290.
119. Grootjans, J., A. Kaser, R.J. Kaufman, and R.S. Blumberg, *The unfolded protein response in immunity and inflammation.* Nature reviews. Immunology, 2016. **16**(8): p. 469-484.
120. Fribley, A., K. Zhang, and R.J. Kaufman, *Regulation of apoptosis by the unfolded protein response.* Methods Mol Biol, 2009. **559**: p. 191-204.
121. Buchberger, A., B. Bukau, and T. Sommer, *Protein Quality Control in the Cytosol and the Endoplasmic Reticulum: Brothers in Arms.* Molecular Cell, 2010. **40**(2): p. 238-252.
122. Kawaguchi, Y., J.J. Kovacs, A. McLaurin, J.M. Vance, A. Ito, and T.-P. Yao, *The Deacetylase HDAC6 Regulates Aggresome Formation and Cell Viability in Response to Misfolded Protein Stress.* Cell, 2003. **115**(6): p. 727-738.
123. Zaarur, N., A.B. Meriin, E. Bejarano, X. Xu, V.L. Gabai, A.M. Cuervo, and M.Y. Sherman, *Proteasome failure promotes positioning of lysosomes around the aggresome via local block of microtubule-dependent transport.* Molecular and cellular biology, 2014. **34**(7): p. 1336-1348.

124. Johnston, J.A., C.L. Ward, and R.R. Kopito, *Aggresomes: A Cellular Response to Misfolded Proteins.* The Journal of Cell Biology, 1998. **143**(7): p. 1883.
125. Jovaisaite, V., L. Mouchiroud, and J. Auwerx, *The mitochondrial unfolded protein response, a conserved stress response pathway with implications in health and disease.* The Journal of Experimental Biology, 2014. **217**(1): p. 137.
126. Yoneda, T., C. Benedetti, F. Urano, S.G. Clark, H.P. Harding, and D. Ron, *Compartment-specific perturbation of protein handling activates genes encoding mitochondrial chaperones.* J Cell Sci, 2004. **117**(Pt 18): p. 4055-66.
127. Nargund, A.M., M.W. Pellegrino, C.J. Fiorese, B.M. Baker, and C.M. Haynes, *Mitochondrial import efficiency of ATFS-1 regulates mitochondrial UPR activation.* Science, 2012. **337**(6094): p. 587-90.
128. Fiorese, C.J., A.M. Schulz, Y.F. Lin, N. Rosin, M.W. Pellegrino, and C.M. Haynes, *The Transcription Factor ATF5 Mediates a Mammalian Mitochondrial UPR.* Curr Biol, 2016. **26**(15): p. 2037-2043.
129. Quirós, P.M., M.A. Prado, N. Zamboni, D. D'Amico, R.W. Williams, D. Finley, S.P. Gygi, and J. Auwerx, *Multi-omics analysis identifies ATF4 as a key regulator of the mitochondrial stress response in mammals.* The Journal of Cell Biology, 2017. **216**(7): p. 2027.
130. Garaeva, A.A., I.E. Kovaleva, P.M. Chumakov, and A.G. Evstafieva, *Mitochondrial dysfunction induces SESN2 gene expression through Activating Transcription Factor 4.* Cell cycle (Georgetown, Tex.), 2016. **15**(1): p. 64-71.
131. D'Amico, D., V. Sorrentino, and J. Auwerx, *Cytosolic Proteostasis Networks of the Mitochondrial Stress Response.* Trends Biochem Sci, 2017. **42**(9): p. 712-725.
132. Wrobel, L., et al., *Mistargeted mitochondrial proteins activate a proteostatic response in the cytosol.* Nature, 2015. **524**: p. 485.
133. Kim, H.-E., A.R. Grant, M.S. Simic, R.A. Kohnz, D.K. Nomura, J. Durieux, C.E. Riera, M. Sanchez, E. Kapernick, S. Wolff, and A. Dillin, *Lipid Biosynthesis Coordinates a Mitochondrial-to-Cytosolic Stress Response.* Cell, 2016. **166**(6): p. 1539-1552.e16.
134. Ruan, L., C. Zhou, E. Jin, A. Kucharavy, Y. Zhang, Z. Wen, L. Florens, and R. Li, *Cytosolic proteostasis through importing of misfolded proteins into mitochondria.* Nature, 2017. **543**(7645): p. 443-446.
135. Du, F., Q. Yu, S. Yan, G. Hu, L.-F. Lue, D.G. Walker, L. Wu, S.F. Yan, K. Tieu, and S.S. Yan, *PINK1 signalling rescues amyloid pathology and mitochondrial dysfunction in Alzheimer's disease.* Brain, 2017. **140**(12): p. 3233-3251.
136. Burman, J.L., S. Pickles, C. Wang, S. Sekine, J.N.S. Vargas, Z. Zhang, A.M. Youle, C.L. Nezich, X. Wu, J.A. Hammer, and R.J. Youle, *Mitochondrial fission facilitates the selective mitophagy of protein aggregates.* The Journal of Cell Biology, 2017. **216**(10): p. 3231.
137. Wood, J.G., S.S. Mirra, N.J. Pollock, and L.I. Binder, *Neurofibrillary tangles of Alzheimer disease share antigenic determinants with the axonal microtubule-associated protein tau (tau).* Proceedings of the National Academy of Sciences, 1986. **83**(11): p. 4040.
138. Kosik, K.S., C.L. Joachim, and D.J. Selkoe, *Microtubule-associated protein tau (tau) is a major antigenic component of paired helical filaments in Alzheimer disease.* Proceedings of the National Academy of Sciences, 1986. **83**(11): p. 4044.

139. Grundke-Iqbal, I., K. Iqbal, Y.C. Tung, M. Quinlan, H.M. Wisniewski, and L.I. Binder, *Abnormal phosphorylation of the microtubule-associated protein tau (tau) in Alzheimer cytoskeletal pathology.* Proceedings of the National Academy of Sciences, 1986. **83**(13): p. 4913.
140. Bancher, C., C. Brunner, H. Lassmann, H. Budka, K. Jellinger, G. Wiche, F. Seitelberger, I. Grundke-Iqbal, K. Iqbal, and H.M. Wisniewski, *Accumulation of abnormally phosphorylated tau precedes the formation of neurofibrillary tangles in Alzheimer's disease.* Brain Res, 1989. **477**(1-2): p. 90-9.
141. Braak, H. and E. Braak, *Neuropathological stageing of Alzheimer-related changes.* Acta Neuropathol, 1991. **82**(4): p. 239-59.
142. Schneider, A., J. Biernat, M. von Bergen, E. Mandelkow, and E.M. Mandelkow, *Phosphorylation that Detaches Tau Protein from Microtubules (Ser262, Ser214) Also Protects It against Aggregation into Alzheimer Paired Helical Filaments.* Biochemistry, 1999. **38**(12): p. 3549-3558.
143. Sun, Q. and T.C. Gamblin, *Pseudohyperphosphorylation causing AD-like changes in tau has significant effects on its polymerization.* Biochemistry, 2009. **48**(25): p. 6002-6011.
144. Ballatore, C., V.M. Lee, and J.Q. Trojanowski, *Tau-mediated neurodegeneration in Alzheimer's disease and related disorders.* Nat Rev Neurosci, 2007. **8**(9): p. 663-72.
145. Carmel, G., E.M. Mager, L.I. Binder, and J. Kuret, *The structural basis of monoclonal antibody Alz50's selectivity for Alzheimer's disease pathology.* J Biol Chem, 1996. **271**(51): p. 32789-95.
146. Jicha, G.A., R. Bowser, I.G. Kazam, and P. Davies, *Alz-50 and MC-1, a new monoclonal antibody raised to paired helical filaments, recognize conformational epitopes on recombinant tau.* J Neurosci Res, 1997. **48**(2): p. 128-32.
147. Ward, S.M., D.S. Himmelstein, J.K. Lancia, Y. Fu, K.R. Patterson, and L.I. Binder, *TOC1: characterization of a selective oligomeric tau antibody.* J Alzheimers Dis, 2013. **37**(3): p. 593-602.
148. Swerdlow, R.H., G.T. Redpath, D.R. Binder, J.N. Davis, 2nd, and S.R. VandenBerg, *Mitochondrial DNA depletion analysis by pseudogene ratioing.* J Neurosci Methods, 2006. **150**(2): p. 265-71.
149. Kirchman, P.A., S. Kim, C.Y. Lai, and S.M. Jazwinski, *Interorganelle signaling is a determinant of longevity in Saccharomyces cerevisiae.* Genetics, 1999. **152**(1): p. 179-90.
150. Miller, S.W., P.A. Trimmer, W.D. Parker, Jr., and R.E. Davis, *Creation and characterization of mitochondrial DNA-depleted cell lines with "neuronal-like" properties.* J Neurochem, 1996. **67**(5): p. 1897-907.
151. Zhang, Z., et al., *Cleavage of tau by asparagine endopeptidase mediates the neurofibrillary pathology in Alzheimer's disease.* Nature Medicine, 2014. **20**: p. 1254.
152. Bukar Maina, M., Y.K. Al-Hilaly, and L.C. Serpell, *Nuclear Tau and Its Potential Role in Alzheimer's Disease.* Biomolecules, 2016. **6**(1): p. 9.
153. Trabzuni, D., et al., *MAPT expression and splicing is differentially regulated by brain region: relation to genotype and implication for tauopathies.* Hum Mol Genet, 2012. **21**(18): p. 4094-103.
154. Smith, C.J., B.H. Anderton, D.R. Davis, and J.M. Gallo, *Tau isoform expression and phosphorylation state during differentiation of cultured neuronal cells.* FEBS Lett, 1995. **375**(3): p. 243-8.

155. Neddens, J., M. Temmel, S. Flunkert, B. Kerschbaumer, C. Hoeller, T. Loeffler, V. Niederkofler, G. Daum, J. Attems, and B. Hutter-Paier, *Phosphorylation of different tau sites during progression of Alzheimer's disease.* Acta neuropathologica communications, 2018. **6**(1): p. 52-52.
156. Patterson, K.R., C. Remmers, Y. Fu, S. Brooker, N.M. Kanaan, L. Vana, S. Ward, J.F. Reyes, K. Philibert, M.J. Glucksman, and L.I. Binder, *Characterization of prefibrillar Tau oligomers in vitro and in Alzheimer disease.* J Biol Chem, 2011. **286**(26): p. 23063-76.
157. Mahley, R.W., K.H. Weisgraber, and Y. Huang, *Apolipoprotein E4: A causative factor and therapeutic target in neuropathology, including Alzheimer's disease.* Proceedings of the National Academy of Sciences, 2006. **103**(15): p. 5644.
158. Roses, A., S. Sundseth, A. Saunders, W. Gottschalk, D. Burns, and M. Lutz, *Understanding the genetics of APOE and TOMM40 and role of mitochondrial structure and function in clinical pharmacology of Alzheimer's disease.* Alzheimers Dement, 2016. **12**(6): p. 687-94.
159. Rissman, R.A., W.W. Poon, M. Blurton-Jones, S. Oddo, R. Torp, M.P. Vitek, F.M. LaFerla, T.T. Rohn, and C.W. Cotman, *Caspase-cleavage of tau is an early event in Alzheimer disease tangle pathology.* The Journal of clinical investigation, 2004. **114**(1): p. 121-130.
160. Ferreira, A. and E.H. Bigio, *Calpain-mediated tau cleavage: a mechanism leading to neurodegeneration shared by multiple tauopathies.* Molecular medicine (Cambridge, Mass.), 2011. **17**(7-8): p. 676-685.
161. Roder, H.M., P.A. Eden, and V.M. Ingram, *Brain Protein Kinase PK40erk Converts TAU into a PHF-like Form as Found in Alzheimer's Disease.* Biochemical and Biophysical Research Communications, 1993. **193**(2): p. 639-647.
162. Gong, C.X., I. Grundke-Iqbal, and K. Iqbal, *Dephosphorylation of Alzheimer's disease abnormally phosphorylated tau by protein phosphatase-2A.* Neuroscience, 1994. **61**(4): p. 765-772.
163. Agholme, L., T. Lindstrom, K. Kagedal, J. Marcusson, and M. Hallbeck, *An in vitro model for neuroscience: differentiation of SH-SY5Y cells into cells with morphological and biochemical characteristics of mature neurons.* J Alzheimers Dis, 2010. **20**(4): p. 1069-82.
164. Boban, M., M. Babić Leko, T. Miškić, P.R. Hof, and G. Šimić, *Human neuroblastoma SH-SY5Y cells treated with okadaic acid express phosphorylated high molecular weight tau-immunoreactive protein species.* Journal of Neuroscience Methods, 2019. **319**: p. 60-68.
165. Buee, L., T. Bussiere, V. Buee-Scherrer, A. Delacourte, and P.R. Hof, *Tau protein isoforms, phosphorylation and role in neurodegenerative disorders.* Brain Res Brain Res Rev, 2000. **33**(1): p. 95-130.
166. Niblock, M. and J.M. Gallo, *Tau alternative splicing in familial and sporadic tauopathies.* Biochem Soc Trans, 2012. **40**(4): p. 677-80.
167. Chen, D., K.W. Drombosky, Z. Hou, L. Sari, O.M. Kashmer, B.D. Ryder, V.A. Perez, D.R. Woodard, M.M. Lin, M.I. Diamond, and L.A. Joachimiak, *Tau local structure shields an amyloid-forming motif and controls aggregation propensity.* Nature Communications, 2019. **10**(1): p. 2493.

168. Couchie, D., C. Mavilia, I.S. Georgieff, R.K. Liem, M.L. Shelanski, and J. Nunez, *Primary structure of high molecular weight tau present in the peripheral nervous system.* Proc Natl Acad Sci U S A, 1992. **89**(10): p. 4378-81.
169. Takeda, S., et al., *Neuronal uptake and propagation of a rare phosphorylated high-molecular-weight tau derived from Alzheimer's disease brain.* Nature Communications, 2015. **6**(1): p. 8490.
170. Gache, Y., F. Ricolfi, J. Guilleminot, G. Theiss, and J. Nunez, *Protein TAU variants present in paired helical filaments (PHFs) of alzheimer brains.* FEBS Letters, 1990. **272**(1): p. 65-68.
171. Shafiei, S.S., M.J. Guerrero-Muñoz, and D.L. Castillo-Carranza, *Tau Oligomers: Cytotoxicity, Propagation, and Mitochondrial Damage.* Frontiers in aging neuroscience, 2017. **9**: p. 83-83.
172. Merezhko, M., C.A. Brunello, X. Yan, H. Vihinen, E. Jokitalo, R.L. Uronen, and H.J. Huttunen, *Secretion of Tau via an Unconventional Non-vesicular Mechanism.* Cell Rep, 2018. **25**(8): p. 2027-2035.e4.
173. Katsinelos, T., M. Zeitler, E. Dimou, A. Karakatsani, H.M. Muller, E. Nachman, J.P. Steringer, C. Ruiz de Almodovar, W. Nickel, and T.R. Jahn, *Unconventional Secretion Mediates the Trans-cellular Spreading of Tau.* Cell Rep, 2018. **23**(7): p. 2039-2055.
174. Sherer, T.B., P.A. Trimmer, J.K. Parks, and J.B. Tuttle, *Mitochondrial DNA-depleted neuroblastoma (Rho°) cells exhibit altered calcium signaling.* Biochimica et Biophysica Acta (BBA) - Molecular Cell Research, 2000. **1496**(2): p. 341-355.
175. Tepper, K., J. Biernat, S. Kumar, S. Wegmann, T. Timm, S. Hubschmann, L. Redecke, E.M. Mandelkow, D.J. Muller, and E. Mandelkow, *Oligomer formation of tau protein hyperphosphorylated in cells.* J Biol Chem, 2014. **289**(49): p. 34389-407.
176. Nübling, G., J. Levin, B. Bader, L. Israel, K. Bötzel, S. Lorenzl, and A. Giese, *Limited cleavage of tau with matrix-metalloproteinase MMP-9, but not MMP-3, enhances tau oligomer formation.* Experimental Neurology, 2012. **237**(2): p. 470-476.
177. Nübling, G., B. Bader, J. Levin, J. Hildebrandt, H. Kretzschmar, and A. Giese, *Synergistic influence of phosphorylation and metal ions on tau oligomer formation and coaggregation with α-synuclein at the single molecule level.* Molecular Neurodegeneration, 2012. **7**(1): p. 35.
178. Szabados, T., C. Dul, K. Majtényi, J. Hargitai, Z. Pénzes, and R. Urbanics, *A chronic Alzheimer's model evoked by mitochondrial poison sodium azide for pharmacological investigations.* Behavioural Brain Research, 2004. **154**(1): p. 31-40.
179. Mahley, R.W. and Y. Huang, *Apolipoprotein e sets the stage: response to injury triggers neuropathology.* Neuron, 2012. **76**(5): p. 871-885.
180. Cheng, J., B.J. North, T. Zhang, X. Dai, K. Tao, J. Guo, and W. Wei, *The emerging roles of protein homeostasis-governing pathways in Alzheimer's disease.* Aging cell, 2018. **17**(5): p. e12801-e12801.
181. Nandi, D., P. Tahiliani, A. Kumar, and D. Chandu, *The ubiquitin-proteasome system.* J Biosci, 2006. **31**(1): p. 137-55.
182. Perry, G., R. Friedman, G. Shaw, and V. Chau, *Ubiquitin is detected in neurofibrillary tangles and senile plaque neurites of Alzheimer disease brains.* Proc Natl Acad Sci U S A, 1987. **84**(9): p. 3033-6.
183. Mori, H., J. Kondo, and Y. Ihara, *Ubiquitin is a component of paired helical filaments in Alzheimer's disease.* Science, 1987. **235**(4796): p. 1641-4.

184. Ii, K., H. Ito, K. Tanaka, and A. Hirano, *Immunocytochemical co-localization of the proteasome in ubiquitinated structures in neurodegenerative diseases and the elderly.* J Neuropathol Exp Neurol, 1997. **56**(2): p. 125-31.
185. Castegna, A., M. Aksenov, M. Aksenova, V. Thongboonkerd, J.B. Klein, W.M. Pierce, R. Booze, W.R. Markesbery, and D.A. Butterfield, *Proteomic identification of oxidatively modified proteins in alzheimer's disease brain. part I: creatine kinase BB, glutamine synthase, and ubiquitin carboxy-terminal hydrolase L-1.* Free Radical Biology and Medicine, 2002. **33**(4): p. 562-571.
186. Keck, S., R. Nitsch, T. Grune, and O. Ullrich, *Proteasome inhibition by paired helical filament-tau in brains of patients with Alzheimer's disease.* J Neurochem, 2003. **85**(1): p. 115-22.
187. Keller, J.N., K.B. Hanni, and W.R. Markesbery, *Impaired proteasome function in Alzheimer's disease.* J Neurochem, 2000. **75**(1): p. 436-9.
188. Sha, Y., L. Rao, C. Settembre, A. Ballabio, and N.T. Eissa, *STUB1 regulates TFEB-induced autophagy–lysosome pathway.* The EMBO Journal, 2017. **36**(17): p. 2544-2552.
189. Grumati, P. and I. Dikic, *Ubiquitin signaling and autophagy.* J Biol Chem, 2018. **293**(15): p. 5404-5413.
190. Zatloukal, K., C. Stumptner, A. Fuchsbichler, H. Heid, M. Schnoelzer, L. Kenner, R. Kleinert, M. Prinz, A. Aguzzi, and H. Denk, *p62 Is a Common Component of Cytoplasmic Inclusions in Protein Aggregation Diseases.* The American Journal of Pathology, 2002. **160**(1): p. 255-263.
191. Kirkin, V., et al., *A Role for NBR1 in Autophagosomal Degradation of Ubiquitinated Substrates.* Molecular Cell, 2009. **33**(4): p. 505-516.
192. Pickford, F., E. Masliah, M. Britschgi, K. Lucin, R. Narasimhan, P.A. Jaeger, S. Small, B. Spencer, E. Rockenstein, B. Levine, and T. Wyss-Coray, *The autophagy-related protein beclin 1 shows reduced expression in early Alzheimer disease and regulates amyloid beta accumulation in mice.* J Clin Invest, 2008. **118**(6): p. 2190-9.
193. Nixon, R.A., J. Wegiel, A. Kumar, W.H. Yu, C. Peterhoff, A. Cataldo, and A.M. Cuervo, *Extensive involvement of autophagy in Alzheimer disease: an immuno-electron microscopy study.* J Neuropathol Exp Neurol, 2005. **64**(2): p. 113-22.
194. Hoozemans, J.J., R. Veerhuis, E.S. Van Haastert, J.M. Rozemuller, F. Baas, P. Eikelenboom, and W. Scheper, *The unfolded protein response is activated in Alzheimer's disease.* Acta Neuropathol, 2005. **110**(2): p. 165-72.
195. Unterberger, U., R. Hoftberger, E. Gelpi, H. Flicker, H. Budka, and T. Voigtlander, *Endoplasmic reticulum stress features are prominent in Alzheimer disease but not in prion diseases in vivo.* J Neuropathol Exp Neurol, 2006. **65**(4): p. 348-57.
196. Beck, J.S., E.J. Mufson, and S.E. Counts, *Evidence for Mitochondrial UPR Gene Activation in Familial and Sporadic Alzheimer's Disease.* Current Alzheimer research, 2016. **13**(6): p. 610-614.
197. Hernandez-Ortega, K., P. Garcia-Esparcia, L. Gil, J.J. Lucas, and I. Ferrer, *Altered Machinery of Protein Synthesis in Alzheimer's: From the Nucleolus to the Ribosome.* Brain Pathol, 2016. **26**(5): p. 593-605.
198. Ding, Q., W.R. Markesbery, Q. Chen, F. Li, and J.N. Keller, *Ribosome Dysfunction Is an Early Event in Alzheimer's Disease.* The Journal of Neuroscience, 2005. **25**(40): p. 9171.

199. Liu, W., et al., *PINK1 defect causes mitochondrial dysfunction, proteasomal deficit and alpha-synuclein aggregation in cell culture models of Parkinson's disease.* PLoS One, 2009. **4**(2): p. e4597.
200. Domingues, A.F., D.M. Arduíno, A.R. Esteves, R.H. Swerdlow, C.R. Oliveira, and S.M. Cardoso, *Mitochondria and ubiquitin-proteasomal system interplay: Relevance to Parkinson's disease.* Free Radical Biology and Medicine, 2008. **45**(6): p. 820-825.
201. Salminen, A., K. Kaarniranta, A. Haapasalo, M. Hiltunen, H. Soininen, and I. Alafuzoff, *Emerging role of p62/sequestosome-1 in the pathogenesis of Alzheimer's disease.* Prog Neurobiol, 2012. **96**(1): p. 87-95.
202. Padman, B.S., T.N. Nguyen, L. Uoselis, M. Skulsuppaisarn, L.K. Nguyen, and M. Lazarou, *LC3/GABARAPs drive ubiquitin-independent recruitment of Optineurin and NDP52 to amplify mitophagy.* Nature Communications, 2019. **10**(1): p. 408.
203. Nguyen, T.N., B.S. Padman, and M. Lazarou, *Deciphering the Molecular Signals of PINK1/Parkin Mitophagy.* Trends in Cell Biology, 2016. **26**(10): p. 733-744.
204. Hatano, Y., et al., *Novel PINK1 mutations in early-onset parkinsonism.* Annals of Neurology, 2004. **56**(3): p. 424-427.
205. Narendra, D.P., S.M. Jin, A. Tanaka, D.F. Suen, C.A. Gautier, J. Shen, M.R. Cookson, and R.J. Youle, *PINK1 is selectively stabilized on impaired mitochondria to activate Parkin.* PLoS Biol, 2010. **8**(1): p. e1000298.
206. Ding, W.X. and X.M. Yin, *Mitophagy: mechanisms, pathophysiological roles, and analysis.* Biol Chem, 2012. **393**(7): p. 547-64.
207. Shin, J.H., H.S. Ko, H. Kang, Y. Lee, Y.I. Lee, O. Pletinkova, J.C. Troconso, V.L. Dawson, and T.M. Dawson, *PARIS (ZNF746) repression of PGC-1alpha contributes to neurodegeneration in Parkinson's disease.* Cell, 2011. **144**(5): p. 689-702.
208. Muaddi, H., M. Majumder, P. Peidis, A.I. Papadakis, M. Holcik, D. Scheuner, R.J. Kaufman, M. Hatzoglou, and A.E. Koromilas, *Phosphorylation of eIF2α at serine 51 is an important determinant of cell survival and adaptation to glucose deficiency.* Molecular biology of the cell, 2010. **21**(18): p. 3220-3231.
209. Junjappa, R.P., P. Patil, K.R. Bhattarai, H.-R. Kim, and H.-J. Chae, *IRE1α Implications in Endoplasmic Reticulum Stress-Mediated Development and Pathogenesis of Autoimmune Diseases.* Frontiers in Immunology, 2018. **9**(1289).
210. Baumeister, P., S. Luo, W.C. Skarnes, G. Sui, E. Seto, Y. Shi, and A.S. Lee, *Endoplasmic reticulum stress induction of the Grp78/BiP promoter: activating mechanisms mediated by YY1 and its interactive chromatin modifiers.* Mol Cell Biol, 2005. **25**(11): p. 4529-40.
211. Hart, J.R. and P.K. Vogt, *Phosphorylation of AKT: a mutational analysis.* Oncotarget, 2011. **2**(6): p. 467-476.
212. Huang, X., G. Liu, J. Guo, and Z. Su, *The PI3K/AKT pathway in obesity and type 2 diabetes.* International journal of biological sciences, 2018. **14**(11): p. 1483-1496.
213. Gonzalez, E. and T.E. McGraw, *The Akt kinases: isoform specificity in metabolism and cancer.* Cell cycle (Georgetown, Tex.), 2009. **8**(16): p. 2502-2508.
214. Saporita, A.J., M. Schluter, D. MacIvor, J. Mistry, and J. Hwang, *Abstract 4611: Interrogation of PI3K signaling via multiplex detection of differential phosphorylation of specific Akt isoforms.* Cancer Research, 2016. **76**(14 Supplement): p. 4611.
215. Ansari, A., M.S. Rahman, S.K. Saha, F.K. Saikot, A. Deep, and K.-H. Kim, *Function of the SIRT3 mitochondrial deacetylase in cellular physiology, cancer, and neurodegenerative disease.* Aging cell, 2017. **16**(1): p. 4-16.

216. Crider, D.G., L.J. García-Rodríguez, P. Srivastava, L. Peraza-Reyes, K. Upadhyaya, I.R. Boldogh, and L.A. Pon, *Rad53 is essential for a mitochondrial DNA inheritance checkpoint regulating G1 to S progression.* The Journal of Cell Biology, 2012. **198**(5): p. 793.
217. Mineri, R., N. Pavelka, E. Fernandez-Vizarra, P. Ricciardi-Castagnoli, M. Zeviani, and V. Tiranti, *How Do Human Cells React to the Absence of Mitochondrial DNA?* PLOS ONE, 2009. **4**(5): p. e5713.
218. Michel, S., M. Canonne, T. Arnould, and P. Renard, *Inhibition of mitochondrial genome expression triggers the activation of CHOP-10 by a cell signaling dependent on the integrated stress response but not the mitochondrial unfolded protein response.* Mitochondrion, 2015. **21**: p. 58-68.
219. Zhang, H., M. Bosch-Marce, L.A. Shimoda, Y.S. Tan, J.H. Baek, J.B. Wesley, F.J. Gonzalez, and G.L. Semenza, *Mitochondrial autophagy is an HIF-1-dependent adaptive metabolic response to hypoxia.* J Biol Chem, 2008. **283**(16): p. 10892-903.
220. Martinus, R.D., G.P. Garth, T.L. Webster, P. Cartwright, D.J. Naylor, P.B. Hoj, and N.J. Hoogenraad, *Selective induction of mitochondrial chaperones in response to loss of the mitochondrial genome.* Eur J Biochem, 1996. **240**(1): p. 98-103.
221. Celardo, I., S. Lehmann, A.C. Costa, S.H. Loh, and L. Miguel Martins, *dATF4 regulation of mitochondrial folate-mediated one-carbon metabolism is neuroprotective.* Cell Death Differ, 2017. **24**(4): p. 638-648.
222. Bao, X.R., et al., *Mitochondrial dysfunction remodels one-carbon metabolism in human cells.* eLife, 2016. **5**: p. e10575.
223. Jauhiainen, A., C. Thomsen, L. Strombom, P. Grundevik, C. Andersson, A. Danielsson, M.K. Andersson, O. Nerman, L. Rorkvist, A. Stahlberg, and P. Aman, *Distinct cytoplasmic and nuclear functions of the stress induced protein DDIT3/CHOP/GADD153.* PLoS One, 2012. **7**(4): p. e33208.
224. Guha, M., J.-K. Fang, R. Monks, M.J. Birnbaum, and N.G. Avadhani, *Activation of Akt is essential for the propagation of mitochondrial respiratory stress signaling and activation of the transcriptional coactivator heterogeneous ribonucleoprotein A2.* Molecular biology of the cell, 2010. **21**(20): p. 3578-3589.
225. Papa, L. and D. Germain, *Estrogen receptor mediates a distinct mitochondrial unfolded protein response.* Journal of Cell Science, 2011. **124**(9): p. 1396.
226. Papa, L. and D. Germain, *SirT3 regulates the mitochondrial unfolded protein response.* Molecular and cellular biology, 2014. **34**(4): p. 699-710.
227. Johns, D.R. and J. Berman, *Alternative, simultaneous complex I mitochondrial DNA mutations in Leber's hereditary optic neuropathy.* Biochem Biophys Res Commun, 1991. **174**(3): p. 1324-30.
228. Kalman, B., F.D. Lublin, and H. Alder, *Mitochondrial DNA mutations in multiple sclerosis.* Mult Scler, 1995. **1**(1): p. 32-6.
229. Rocher, C., J.-W. Taanman, D. Pierron, B. Faustin, G. Benard, R. Rossignol, M. Malgat, L. Pedespan, and T. Letellier, *Influence of mitochondrial DNA level on cellular energy metabolism: implications for mitochondrial diseases.* Journal of Bioenergetics and Biomembranes, 2008. **40**(2): p. 59.
230. Lu, B., J. Lee, X. Nie, M. Li, Y.I. Morozov, S. Venkatesh, D.F. Bogenhagen, D. Temiakov, and C.K. Suzuki, *Phosphorylation of human TFAM in mitochondria impairs*

DNA binding and promotes degradation by the AAA+ Lon protease. Molecular cell, 2013. **49**(1): p. 121-132.

231. Ekstrand, M.I., M. Falkenberg, A. Rantanen, C.B. Park, M. Gaspari, K. Hultenby, P. Rustin, C.M. Gustafsson, and N.-G. Larsson, *Mitochondrial transcription factor A regulates mtDNA copy number in mammals.* Human Molecular Genetics, 2004. **13**(9): p. 935-944.
232. Mastroeni, D., O.M. Khdour, E. Delvaux, J. Nolz, G. Olsen, N. Berchtold, C. Cotman, S.M. Hecht, and P.D. Coleman, *Nuclear but not mitochondrial-encoded oxidative phosphorylation genes are altered in aging, mild cognitive impairment, and Alzheimer's disease.* Alzheimer's & dementia : the journal of the Alzheimer's Association, 2017. **13**(5): p. 510-519.
233. Couvillion, M.T., I.C. Soto, G. Shipkovenska, and L.S. Churchman, *Synchronized mitochondrial and cytosolic translation programs.* Nature, 2016. **533**: p. 499.
234. Richter-Dennerlein, R., S. Oeljeklaus, I. Lorenzi, C. Ronsör, B. Bareth, A.B. Schendzielorz, C. Wang, B. Warscheid, P. Rehling, and S. Dennerlein, *Mitochondrial Protein Synthesis Adapts to Influx of Nuclear-Encoded Protein.* Cell, 2016. **167**(2): p. 471-483.e10.
235. Marusich, M.F., B.H. Robinson, J.-W. Taanman, S.J. Kim, R. Schillace, J.L. Smith, and R.A. Capaldi, *Expression of mtDNA and nDNA encoded respiratory chain proteins in chemically and genetically-derived Rho0 human fibroblasts: a comparison of subunit proteins in normal fibroblasts treated with ethidium bromide and fibroblasts from a patient with mtDNA depletion syndrome.* Biochimica et Biophysica Acta (BBA) - Molecular Basis of Disease, 1997. **1362**(2): p. 145-159.
236. Swalwell, H., D.M. Kirby, E.L. Blakely, A. Mitchell, R. Salemi, C. Sugiana, A.G. Compton, E.J. Tucker, B.-X. Ke, P.J. Lamont, D.M. Turnbull, R. McFarland, R.W. Taylor, and D.R. Thorburn, *Respiratory chain complex I deficiency caused by mitochondrial DNA mutations.* European journal of human genetics : EJHG, 2011. **19**(7): p. 769-775.
237. Hong, J., B.W. Kim, H.J. Choo, J.J. Park, J.S. Yi, D.M. Yu, H. Lee, G.S. Yoon, J.S. Lee, and Y.G. Ko, *Mitochondrial complex I deficiency enhances skeletal myogenesis but impairs insulin signaling through SIRT1 inactivation.* J Biol Chem, 2014. **289**(29): p. 20012-25.